CUKUROVA UNIVERSITY

INSTITUTE OF NATURAL AND APPLIED SCIENCES

MSc THESIS

The Development of Self-Healing Functions of Composite Structures via Microvascular Channels

Eray KOŞTUR

Mechanical Engineering Department

February, 2024

CUKUROVA UNIVERSITY

INSTITUTE OF NATURAL AND APPLIED SCIENCES

MSc THESIS APPROVAL

The Development of Self-Healing Functions of Composite Structures via Microvascular Channels

Eray KOŞTUR

Mechanical Engineering Department

This Master's Thesis was evaluated by the following Jury Members on 16/02/2024 and was approved by unanimity / ~~majority of votes~~.

Jury : Prof. Dr. Necdet GEREN (Advisor) ……

: Prof. Dr. Melih BAYRAMOĞLU ……

: Assoc. Prof. Dr. Çağrı UZAY ……

This Thesis was written in the Department of Mechanical Engineering, Institute of Natural and Applied Sciences.
Thesis Number:

Prof. Dr. Sadık DİNÇER
Director
Institute of Natural and Applied Sciences

This work was supported by the BAP.
Project ID: FYL-2022-14609

Note: The usage of the presented specific declarations, tables, figures, and photographs either in this thesis or in any other reference without citation is subject to "The law of Arts and Intellectual Products" number of 5846 of Turkish Republic

CONTENTS

ABSTRACT I
ÖZ II
EXTENDED ABSTRACT III
GENİŞLETİLMİŞ ÖZET VII
ACKNOWLEDGEMENTS XI
LIST OF TABLES XII
LIST OF FIGURES XIII
1. INTRODUCTION 1
1.1. An Overview of Composites 3
1.1.1. Common Applications of Polymer Composites 6
1.1.2. Failures of Composites 9
1.2. Introduction to Self-Healing 11
1.2.1. Self-Healing Mechanisms 14
1.2.2. Non-autonomous Self-Healing 15
1.2.3. Autonomous Self-Healing 16
1.2.4. Healing Performance Assessment 19
1.2.5. Self-Healing Applications in Polymer Composites 20
2. PREVIOUS STUDIES 23
2.1. Self-Healing via Vascular Systems 23
2.1.1. Sacrificial Fibers and Scaffolds Methods 23
2.1.2. Electrostatic Discharge Method 28
2.1.3. Laser Direct-write Method 28
2.1.4. Hollow Fiber Method 29
2.1.5. Other Studies 29
2.2. Aim of The Study 31
3. MATERIAL AND METHOD 33
3.1. Materials 33
3.1.1. Carbon Fabric 33
3.1.2. Polymer Matrix 33
3.1.3. Self-Healing Catalyst 34
3.1.4. Self-Healing Agent 35
3.1.5. Consumables 36
3.2. Method 37
3.2.1. Manufacturing of Composite Structures 39
3.2.2. Manufacturing of Microvascular Channels 44

3.2.3. Determining The Effect of Channels on The Strength of Composite Structure 49
3.2.4. Morphological Characterization Methods..... 53
3.2.5. Preliminary Inspection of Self-Healing in Microvascular Channels..... 53
3.2.6. Self-Healing Characterization with Compact Tension Test..... 54
4. RESULTS AND DISCUSSION 59
4.1. Discovery of Novel Microvascular Channel Production 59
4.1.1. Material Selection for Channel Formation..... 60
4.1.2. Selection of the Way of Channel Wall Coating 62
4.2. Inspection of Channel Structure Inside Composite Laminate..... 63
4.2.1. Inspection via Thermal Camera 63
4.2.2. Micro CT Inspection 64
4.3. Mechanical Performance of Composites Including Microvascular Channels 66
4.4. Uniformity of Catalyst in Composite Laminate..... 74
4.5. Self-Healing of Composite..... 74
5. CONCLUSION..... 81
REFERENCES 85
CURRICCULUM VIATE 97

CUKUROVA UNIVERSITY
INSTITUTE OF NATURAL AND APPLIED SCIENCES

MSc THESIS

The Development of Self-Healing Functions of Composite Structures via Microvascular Channels

Eray KOŞTUR

Advisor: Prof. Dr. Necdet GEREN

Department of Mechanical Engineering

ABSTRACT

Carbon fiber-reinforced polymer (CFRP) composites having high specific strength and modulus, are highly convenient for aerospace and automotive applications which require light-weight and high strength. Nevertheless, the usage of CFRP is limited by their low crack resistance and poor off-axis strength causing material damage as a result of static and dynamic effects over its service time. Besides, prediction of the failure due to local damages are not reliable so far. This study aims to provide the composite structure with its self-healing feature through a novel microvascular channel mechanism while preserving its mechanical properties and as a result, to repair micro-sized cracks that occur in its structure. The effect of various channel configurations on mechanical properties of structure was evaluated with mechanical tests. 5-ethylidene-2-norbornene (5E2N) used as the self-healing agent was injected into microvascular channels and the reaction triggered by the Grubbs' catalyst which is distributed into matrix is determined in different conditions, as the crack propagates through the channels. The crack propagation test is performed for different healing times and approaches. Healing efficiencies were observed up to 136% and 149% for practiced approaches.

Keywords: Self-healing, Self-repairing polymers, Microvascular systems, Composites, Crack propagation

ÇUKUROVA ÜNİVERSİTESİ
FEN BİLİMLERİ ENSTİTÜSÜ

YÜKSEK LİSANS TEZİ

Kompozit Yapıların Kendini İyileştirme Fonksiyonlarının Mikrovasküler Kanallar Aracılığıyla Geliştirilmesi

Eray KOŞTUR

Danışman: Prof. Dr. Necdet GEREN

Makine Mühendisliği Anabilim Dalı

ÖZ

Yüksek özgül mukavemet ve modüle sahip karbon fiber takviyeli polimer (CFRP) kompozitler, hafiflik ve yüksek mukavemet gerektiren havacılık ve otomotiv uygulamaları için oldukça uygundur. Bununla birlikte, servis süresi boyunca statik ve dinamik etkilerin bir sonucu olarak malzeme hasarına neden olan düşük çatlak direnci ve zayıf eksen dışı mukavemeti nedeniyle CFRP'nin kullanımı sınırlıdır. Ayrıca yerel hasarlardan kaynaklanan arızaların tahmini şu ana kadar güvenilir değildir. Bu çalışma, kompozit yapının, mekanik özelliklerini korurken yeni bir mikrovasküler kanal mekanizması aracılığıyla kendi kendini iyileştirme özelliğini kazanmasını ve bunun sonucunda yapısında oluşan mikro boyuttaki çatlakların onarılmasını amaçlamaktadır. Farklı kanal konfigürasyonlarının yapının mekanik özelliklerine etkisi mekanik testlerle değerlendirilmiştir. Onarıcı ajan olarak kullanılan 5-etiliden-2-norbornen (5E2N), mikrovasküler kanallara enjekte edilmiş ve çatlak kanallar boyunca ilerledikçe matriks içerisine dağılan Grubbs' katalizörünün tetiklediği reaksiyon farklı koşullarda belirlenmiştir. Çatlak ilerleme testi, farklı iyileşme süreleri ve yaklaşımlar için gerçekleştirilmiştir. Uygulanan yaklaşımlarda %136 ve %149'a kadar iyileşme verimliliği gözlemlenmiştir.

Anahtar Kelimeler: Kendi kendini onarma, Kendi kendini onaran polimerler, Mikrovasküler sistemler, Kompozitler, Çatlak ilerlemesi

EXTENDED ABSTRACT

Carbon fiber-reinforced polymer (CFRP) composites with high specific strength (σ_f/ρ) and modulus (E/ρ) properties are highly convenient for applications which require lightweight and high-strength materials such as aerospace, defence, and automotive industries. Especially, in the aerospace industry, CFRPs constitute the vast majority of the total weight of structural members on recent aircraft. Nowadays, CFRP is implemented in main load-carrying structures like, sandwich panel skins, fuselages and wing planks to reduce weight and hence the fuel consumption.

In contrast with the excellent properties of CFRP composites, use is limited due to disadvantages such as low crack resistance and poor off-axis strength. Also, some of the most common problems in these structures are the prediction of failure due to local damages is not reliable so far and detection of micro-sized damages is very difficult. This is because they occur at relatively low impact energies and there are usually no visible signs of damage on the surfaces of the structure. These micro-cracks may cause catastrophic failures as a result of static and dynamic effects over the lifetime of the structure. Therefore, it is very important and necessary to control the damages while they are still micron-sized, to prevent larger damages and to increase the life of the structure.

Recently, composite structures with self-healing properties have become increasingly important in order to eliminate the above-mentioned disadvantages of CFRP composites. Self-healing in fiber-reinforced composites refers to the ability of these materials to autonomously repair damage or cracks that may occur over their lifetime. This feature largely eliminates the drawbacks of composite materials and significantly increases the performance, durability and reliability of the structure. Nowadays, many studies have been carried out using different methods for composite structures with self-healing properties and the size of the global self-healing materials market is expected to reach high levels.

In this study, the self-healing mechanisms of composite structures are studied to inhibit and eliminate damage as soon as it occurs at the microscale. Generally, microcapsules and micro-vascular channels are used for autonomous healing mechanisms of composites. In the self-healing mechanism performed with microcapsules, when the crack breaks the capsule, the self-healing mechanism is triggered autonomously where the repairing agent in the capsule reacts with the catalysts in the structure and healing is achieved. On the other hand, the application of self-healing composite structures through microvascular channels involves the inclusion of small channels containing healing agents and catalysts within the composite material. When a crack occurs in the channels, the self-healing mechanism is triggered, the healing agent mixes with the catalyst and a healing reaction occurs.

The self-healing method with microvascular channels stands out with advantages such as providing continuous healing potential by creating a wide and continuous network within the structure, allowing the use of different healing materials at the same time, and having no limitation

on the number of healings for the same location. There are many microvascular channel formation methods available in the literature such as hollow glass fibers, metallic tubes, direct ink writing, laser processing, fugitive inks, sacrificial fibers, step moulding technique etc. Their use for rapid and large-scale production of fiber-reinforced composites with complex vascular structures is limited.

In this thesis, a novel, rapid and cheap microvascular channel production method was invented to develop a composite structure having self-healing features that can autonomously repair micro-sized cracks while preserving its mechanical properties.

High-strength aerospace-grade carbon fabric with an areal weight of 193 g/m^2 as reinforcement material, Araldite® LY 5052 epoxy resin and Aradur® 5052 hardener as matrix material, 1st Generation Grubbs' Catalyst® M102 as self-healing catalyst and 5-Ethylidene-2-Norbornene (5E2N) as self-healing agent were used in this study. The 5E2N was preferred as the healing agent due to its shorter reaction time with the Grubbs' catalyst and its ability to operate in wide temperature ranges. For the microvascular channel formation process, aluminium wire, galvanized steel wire and polyamide monofilaments were selected as candidate core materials that could be removed after the curing process of the CFRP composite. Five samples having the same diameter and length for each kind of material were placed in the composite structure during the composite production. After the curing process of the composite, the core material was removed. During the removal step, removal forces were measured to determine the suitable material for the microvascular channel formation process. The shear stresses during the removal of polyamide monofilament, aluminium wire and galvanized steel wire are determined as 0.11 MPa, 0.39 MPa and 0.59 MPa, respectively. From these results, polyamide monofilament was selected as channel formation material. This can be due to the high thermal expansion coefficient of polyamide which expand during curing and shrink after the cooling of the CFRP.

In present studies available in the literature, the healing agent and catalyst, in liquid form, are filled into separate microvascular channels and the crack is expected to reach these two separate channels in order to activate the self-healing mechanism, thus healing is obtained. However, this can accelerate the progression of the crack to grow further, and the strength of the composite structure may be adversely affected because, for every channel containing the healing agent, there must be a channel containing the catalyst. Because of these disadvantages, in this project, the catalyst is dispersed in the matrix and only the restorative agent is present in the microvascular channels. The challenge, in this case, was to keep the restorative agent within the channels without inadvertently reacting before cracks formed.

A coating was applied to the channel walls to prevent the reaction from occurring spontaneously within the channel before crack formation. This process was carried out by coating the polyamide monofilaments used in the creation of microvascular channels with various materials (mold release wax, pure epoxy, etc.) and leaving these materials on the channel walls within the composite structure. Scanning Electron Microscope (SEM) analyses were conducted to observe the

layer on channel walls. Also, the healing agent was injected into channels, and it was examined whether the healing reaction occurred or not, by conducting SEM analyses. At the end of these examinations, neat epoxy was selected to coat the walls of microvascular channels.

Grubbs' catalyst was mixed with epoxy polymer by using a 3 Roll Mill machine for homogeneous distribution. A uniform distribution is observed as a result of Energy Dispersive Spectrometry (EDS) analyses.

In order to observe channel continuity and clarity, inspections were conducted by using a thermal camera and micro-computed tomography (μCT). First, the composite structure including an interconnected channel was produced by above mentioned method. Then, hot water was injected into the microvascular channels and heat distribution in the channels was observed via a thermal camera. Additionally, clearance and state of the microvascular channels inside the composite structures were detected by μCT scanning.

According to the ASTM D790 standard, 3-Point Bending Tests were carried out to obtain the effect of microvascular channels on the flexural strength of composite material. Therefore, channels were placed in a composite structure in the longitudinal direction for 6 different configurations. According to followed standard, the size of the sample was determined as 120x40 mm, and 5 specimens for each configuration were needed so, a total of 30 specimens were produced. The top surfaces of laminates were corrugated due to the placement of the core material to create microvascular channels, because thickness of the laminate is not enough to compensate the corrugation. This situation caused a shape factor effect on the laminate specimens. In order to evaluate the results correctly, the second moment of area (I) values were determined by scanning the cross-sectional areas with a Hexagon RS6 3D scanner. Then, microscopic shape factors were defined for each configuration and force and stiffness values obtained from the 3-point bending tests were modified to eliminate the effect of microscopic shape factor. As a result, it is observed that microvascular channels do not have a significant negative effect on the flexural strength of the composite structure.

A compact tension test, according to the ASTM D5045 standards, was performed to observe the behaviour of the self-healing mechanism during crack propagation. Therefore, test specimens were manufactured based on standards. Force and crack tip opening displacement (CTOD) values were measured and plotted. The tests were carried out for two different approaches and different healing times in order to determine the optimum healing conditions while comparing efficiencies. In the first approach, channels were filled with healing agent and load was applied till micro cracks occurred. Then load was released, and a certain period was waited for the self-healing mechanism to activate. In the second approach, microvascular channels were fed continuously, and the load was applied till the fracture was detected where the crack was in the macro scale. Then load was released, and a certain period was waited for the self-healing mechanism to activate. It was observed that, after the first 30 minutes, the polymerization reaction started. Hence, the tests were carried out for healing

times of 30, 60, 120 and 150 minutes. Also, specimens without channels and with empty channels were tested for comparison. In total, tests were repeated for 10 different scenarios.

In order to compare the healing ability, healing efficiency values were evaluated based on Mode-I strain release rate (G_I) which is measured in terms of energy per unit area required to propagate a crack. The definition of healing efficiency was simplified as the ratio of area under the load-displacement curve of the healed specimen (ΔU_{healed}) to the area under the load-displacement curve of the virgin specimen (ΔU_{virgin}) for the same crack length and specimen width.

According to the obtained results, it was observed that healing efficiency increases as the healing time increases for both approaches. It was found that healing efficiencies could reach up to 136% in the first approach and 149% in the second approach.

Also, the crack zone was scanned with a stereo microscope to see the situation of the crack with and without a healing mechanism.

GENİŞLETİLMİŞ ÖZET

Yüksek özgül mukavemet (σf/ρ) ve modül (E/ρ) özelliklerine sahip karbon fiber takviyeli polimer (CFRP) kompozitler, havacılık, savunma ve otomotiv endüstrileri gibi hafif ve yüksek mukavemetli malzemeler gerektiren uygulamalar için oldukça uygundur. Özellikle havacılık endüstrisinde CFRP'ler, güncel uçaklardaki yapısal elemanların toplam ağırlığının büyük çoğunluğunu oluşturmaktadır. Günümüzde ağırlığı ve dolayısıyla yakıt tüketimini azaltmak için sandviç panel kaplamaları, gövdeler ve kanat kalasları gibi ana yük taşıyan yapılarda CFRP uygulanmaktadır.

CFRP kompozitlerin mükemmel özelliklerinin aksine, düşük çatlak direnci ve zayıf eksen dışı mukavemet gibi dezavantajları nedeniyle kullanımı sınırlıdır. Ayrıca bu yapılarda en sık karşılaşılan sorunlardan biri de lokal hasarlardan kaynaklanan hasar tahmininin şu ana kadar güvenilir olmaması ve mikro boyuttaki hasarların tespitinin çok zor olmasıdır. Bunun nedeni, nispeten düşük darbe enerjilerinde meydana gelmeleri ve genellikle yapının yüzeylerinde görünür bir hasar belirtisinin bulunmamasıdır. Bu mikro çatlaklar yapının ömrü boyunca statik ve dinamik etkiler sonucu büyük hasarlara neden olabilir. Bu nedenle hasarların henüz mikron boyutundayken kontrol altına alınması, daha büyük hasarların önlenmesi ve yapının ömrünün uzatılması açısından çok önemli ve gereklidir.

Son zamanlarda, CFRP kompozitlerin yukarıda belirtilen dezavantajlarını ortadan kaldırmak amacıyla kendi kendini iyileştirme özelliğine sahip kompozit yapılar giderek önem kazanmaktadır. Fiber takviyeli kompozitlerde kendi kendini iyileştirme, bu malzemelerin kullanım ömrü boyunca meydana gelebilecek hasar veya çatlakları bağımsız olarak onarma yeteneğini ifade eder. Bu özellik, kompozit malzemelerin dezavantajlarını büyük ölçüde ortadan kaldırır ve yapının performansını, dayanıklılığını ve güvenilirliğini önemli ölçüde artırır. Günümüzde kendi kendini iyileştirme özelliğine sahip kompozit yapılara yönelik farklı yöntemler kullanılarak birçok çalışma yapılmakta olup, küresel kendi kendini onaran malzeme pazarının büyüklüğünün yüksek seviyelere ulaşması beklenmektedir.

Bu çalışmada mikro ölçekte hasarın, oluştuğu anda engellenmesi ve ortadan kaldırılması için kompozit yapıların kendi kendini iyileştirme mekanizmaları incelenmiştir. Kompozitlerin otonom iyileşme mekanizmaları için genellikle mikro kapsüller ve mikro-vasküler kanallar kullanılmaktadır. Mikro kapsüllerle gerçekleştirilen kendi kendini iyileştirme mekanizmasında, çatlak kapsülü kırdığında, kapsül içindeki tamir maddesinin yapıdaki katalizörlerle reaksiyona girmesiyle kendi kendini iyileştirme mekanizması otonom olarak tetiklenir ve iyileşme sağlanır. Kendi kendini onaran kompozit yapıların mikrovasküler kanallar aracılığıyla uygulanması ise kompozit malzeme içerisine iyileştirici ajanlar ve katalizörler içeren küçük kanalların dahil edilmesini içermektedir. Kanallarda çatlak oluştuğunda kendi kendini iyileştirme mekanizması tetiklenir, iyileştirici ajan katalizör ile karışır ve iyileşme reaksiyonu meydana gelir.

Bu tez çalışmasında, mekanik özelliklerini korurken mikro boyutlu çatlakları otonom olarak onarabilen, kendi kendini iyileştirme özelliğine sahip kompozit bir yapı geliştirmek için yeni, hızlı ve ucuz bir mikrovasküler kanal üretim yöntemi icat edildi.

Bu çalışmada takviye malzemesi olarak 193 g/m2 ağırlığına sahip yüksek mukavemetli havacılık sınıfı karbon kumaş, matris malzemesi olarak Araldite® LY 5052 epoksi reçine ve Aradur® 5052 sertleştirici, kendini onarma mekanizmasında katalizör olarak 1. Nesil Grubbs' Catalyst® M102 ve onarıcı ajan olarak 5-Etiliden-2-Norbornen (5E2N) kullanılmıştır. Grubbs katalizörü ile reaksiyon süresinin daha kısa olması ve geniş sıcaklık aralıklarında çalışabilmesi nedeniyle onarıcı ajan olarak 5E2N tercih edildi. Mikrovasküler kanal oluşturma işlemi için CFRP kompozitin kürleme işleminden sonra çıkarılabilecek maça malzemelerine aday olarak alüminyum tel, galvanizli çelik tel ve poliamid monofilamentler seçildi. Kompozit üretimi sırasında kompozit yapıya her malzeme türü için aynı çap ve uzunlukta beşer numune yerleştirildi. Kompozitin kürleme işleminden sonra yerleştirilen malzemeler çıkarıldı. Çıkarma adımı sırasında, mikrovasküler kanal oluşum süreci için uygun materyali belirlemek amacıyla, çıkarma kuvvetleri ölçüldü. Poliamid monofilament, alüminyum tel ve galvanizli çelik telin çıkarılması sırasındaki kayma gerilmeleri sırasıyla 0,11 MPa, 0,39 MPa ve 0,59 MPa olarak belirlenmiştir. Bu sonuçlardan kanal oluşturma materyali olarak poliamid monofilament seçilmiştir. Bunun nedeni, kürleme sırasında genişleyen ve laminatın soğutulmasından sonra büzüşen poliamidin yüksek termal genleşme katsayısından kaynaklanabilir.

Mevcut çalışmalarda sıvı haldeki iyileştirici ajan ve katalizör ayrı mikrovasküler kanallara doldurularak kendi kendini iyileştirme mekanizmasını aktive etmek için çatlağın bu iki ayrı kanala ulaşması beklenir ve böylece iyileşme sağlanır. Ancak bu durum çatlağın daha da büyümesine neden olabilir ve iyileştirici ajan içeren her kanal için katalizör içeren de bir kanal olması gerektiğinden, kompozit yapının mukavemeti olumsuz etkilenebilir. Bu dezavantajlardan dolayı bu projede katalizör, matriks içerisinde dağılmış durumda olup, mikrovasküler kanallarda sadece onarıcı ajan bulunmaktadır. Bu durumdaki zorluk, onarıcı ajanı, çatlaklar oluşmadan önce kasıtsız reaksiyona girmeden kanallar içinde tutmaktır.

Kanal içerisinde reaksiyonun kendiliğinden oluşmasını engellemek için kanal duvarlarına kaplama uygulanmıştır. Bu işlem, mikrovasküler kanalların oluşturulmasında kullanılan poliamid monofilamentlerin çeşitli malzemelerle (kalıp ayırıcı vaks, saf epoksi vb.) kaplanması ve bu kaplama malzemelerinin kompozit yapı içerisindeki kanal duvarlarında bırakılmasıyla gerçekleştirildi. Kanal duvarlarındaki katmanı gözlemlemek için Taramalı Elektron Mikroskobu (SEM) analizleri yapıldı. Ayrıca kanallara iyileştirici ajan enjekte edildi ve SEM analizleri yapılarak iyileşme reaksiyonunun oluşup oluşmadığı incelendi. Bu incelemeler sonunda mikrovasküler kanalların duvarlarını kaplamak için saf epoksi seçildi.

Grubbs katalizörü, homojen dağılım için 3 Roll Mill makinesi kullanılarak epoksi polimer ile karıştırıldı. Enerji Dağılımı Spektrometresi (EDS) analizleri sonucunda düzgün bir dağılım gözlenmektedir.

Kanal devamlılığını ve netliğini gözlemlemek amacıyla termal kamera ve mikro bilgisayarlı tomografi (μCT) kullanılarak incelemeler yapıldı. Yukarıda bahsedilen yöntemle öncelikle birbirine bağlı kanal içeren kompozit yapı üretildi. Daha sonra mikrovasküler kanallara sıcak su enjekte edilerek termal kamera aracılığıyla kanallardaki ısı dağılımı gözlemlendi. Ek olarak, kompozit yapıların içindeki mikrovasküler kanalların açıklığı ve durumu μCT taramasıyla tespit edildi.

Mikrovasküler kanalların kompozit malzemenin bükülme mukavemeti üzerindeki etkisini bulmak için ASTM D790 standardına göre 3 Nokta Eğme Testleri yapılmıştır. Bu nedenle, kompozit yapıya 6 farklı konfigürasyonda kanallar boylamasına yönde yerleştirildi. Takip edilen standarda göre numune boyutu 120x40 mm olarak belirlenmiş ve her konfigürasyon için 5 adet numune olmak üzere toplam 30 adet numune üretilmiştir. Laminatların mikrovasküler kanallara sahip üst yüzeyleri dalgalı olduğundan şekil faktörü etkisine neden olmaktadır. Sonuçların doğru değerlendirilebilmesi için kesit alanları Hexagon RS6 3D tarayıcı ile taranarak atalet momenti (I) değerleri belirlendi. Daha sonra her konfigürasyon için mikroskobik şekil faktörleri tanımlandı ve 3 nokta eğme testlerinden elde edilen kuvvet ve sağlamlık (stiffness) değerleri, mikroskobik şekil faktörünün etkisini ortadan kaldıracak şekilde değiştirildi. Sonuç olarak mikrovasküler kanalların kompozit yapının eğilme dayanımına önemli bir etkisinin olmadığı görülmüştür.

Çatlak ilerlemesi sırasında kendi kendini iyileştirme mekanizmasının davranışını gözlemlemek amacıyla, ASTM D5045 standartlarına göre kompakt çekme testi yapıldı. Bu nedenle test numuneleri standartlara uygun olarak üretildi. Kuvvet ve çatlak ucu açılma yer değiştirmesi (CTOD) değerleri ölçülmüş ve grafikler oluşturulmuştur. Verimlilikleri karşılaştırırken optimum iyileştirme koşullarını belirlemek amacıyla testler iki farklı yaklaşım ve farklı iyileşme süreleri için gerçekleştirildi. İlk yaklaşımda kanallar iyileştirici madde ile doldurularak mikro çatlaklar oluşana kadar yük uygulandı. Daha sonra yük serbest bırakıldı ve kendi kendini iyileştirme mekanizmasının devreye girmesi için belli bir süre beklendi. İkinci yaklaşımda mikrovasküler kanallar sürekli olarak beslendi ve çatlağın makro ölçekte olduğu yerde kırık tespit edilene kadar yük uygulandı. Daha sonra yük serbest bırakıldı ve kendi kendini iyileştirme mekanizmasının devreye girmesi için belli bir süre beklendi. İlk 30 dakikadan sonra polimerizasyon reaksiyonunun başladığı gözlendi. Bu nedenle testler 30, 60, 120 ve 150 dakikalık iyileşme süreleri için gerçekleştirildi. Ayrıca karşılaştırma amacıyla kanalsız ve boş kanallı numuneler de test edildi. Toplamda 10 farklı senaryo için testler tekrarlandı.

İyileşme yeteneğini karşılaştırmak amacıyla, iyileştirme verimliliği değerleri, bir çatlağın yayılması için gereken birim alan başına enerji cinsinden ölçülen Mod-I gerinim salınım hızına (GI) dayalı olarak değerlendirildi. İyileştirme verimliliğinin tanımı, aynı çatlak uzunluğu ve numune genişliği için iyileştirilmiş numunenin kuvvet-yer değiştirme eğrisi altındaki alanın (ΔU_{healed})

işlenmemiş numunenin kuvvet-yer değiştirme eğrisi altındaki alana (ΔU_{virgin}) oranı olarak basitleştirildi.

Elde edilen sonuçlara göre her iki yaklaşımda da iyileşme süresi arttıkça iyileşme veriminin de arttığı gözlemlendi. İyileşme verimlerinin ilk yaklaşımda %136'ya, ikinci yaklaşımda ise %149'a kadar çıkabildiği tespit edildi.

Ayrıca çatlak bölgesi stereo mikroskopla taranarak, iyileşme mekanizması içeren ve içermeyen yapılarda meydana gelen çatlakların durumları gözlemlendi.

ACKNOWLEDGEMENTS

I would first like to express my deep appreciation of gratitude to my supervisor Prof. Dr. Necdet GEREN who enabled me to undertake this amazing project with his invaluable mentorship. Prof. GEREN's office door and phone were always open to me whenever I encountered a challenging situation or sought clarification regarding my research or writing. He consistently respected my authorship of the paper, but readily provided guidance whenever he believed it was beneficial.

Furthermore, I would like to express my sincere gratitude to Dr. Merve ÖZKUTLU DEMİREL as my co-advisor in this thesis.

Also, I would like to extend my heartfelt appreciation to Prof. Dr. Melih BAYRAMOĞLU and Assoc. Prof. Dr. Çağrı UZAY as the jury members of my thesis.

Furthermore, I would like to extend my gratitude to the Turkish Aerospace (TUSAS) University-Industry Collaboration Support Program and Unit of Scientific Research Projects (BAP) department for providing financial support for this study with a project named as 2021-BAP-22.

I thank my colleagues in TUSAS who motivated and encouraged me in this thesis.

I express my profound and heartfelt appreciation to the people who hold significant importance in my life, my family and friends, for their unwavering belief in me. I am grateful to a special person, my fiancé Dt. Ebru T., for her enduring and unwavering affection, assistance, and support.

I would like to dedicate this thesis to my mother who is no longer alive but has taught me everything that I know to survive. Thank you, mom! I couldn't do it without your ambition.

In the memory of Asuman KOŞTUR…

LIST OF TABLES

Table 3.1. Physical and mechanical properties of carbon fabric (*Toho Tenax Impregnated Strand Test Method. Based on JIS R7601 or DIN 29965) 33
Table 3.2. Chemical and physical properties of epoxy resin and its hardener..... 34
Table 3.3. Physical and mechanical properties of the matrix 34
Table 3.4. The chemical properties of the catalyst (Grubbs' Catalyst® M102)..... 34
Table 3.5. The chemical properties of the healing agent (5-Ethylidene-2-Norbornene) 35
Table 3.6. The properties of consumables 37
Table 3.7. The configurations of positions of channels in the CFRP composite laminates..... 47
Table 3.8. The designations for specimens used in compact tension tests 56
Table 4.1. Properties of commercial candidate materials for the sacrificial fiber method determined with CES software 60
Table 4.2. Pull-out resistance force measurements for 200 mm specimen length and average shear stress values during pulling out of different materials 61
Table 4.3. The pull-out and shear fracture forces of polyamide monofilaments of different diameters for 1-meter length..... 61
Table 4.4. Averages of fracture force, deflection and stiffness values of specimens in different configurations and their standard deviation values..... 69
Table 4.5. Scanned cross-sections and second moment of area (I) values of each configuration ... 71
Table 4.6. Averages of specific fracture force, specific stiffness and shape factor values of specimens in different configurations..... 72
Table 4.7. Averages of force, strain energy and healing efficiency values of specimens in different scenarios for both Approach 1 and Approach 2..... 77

LIST OF FIGURES

Figure 1.1. History of composite usage in commercial transport aircrafts (Smith, 2013; Trilaksono et al. 2014) 1
Figure 1.2. Schematic demonstrations of autonomous self-healing processes 2
Figure 1.3. Types of composites according to shape of reinforcement 3
Figure 1.4. Plot of specific modulus (E/ρ) against specific strength (σ_f /ρ) (Ashby, 2011a) 4
Figure 1.5. Plot of Young's modulus (E) against density (ρ), on log scales with constant E/ρ, E1/2/ρ, and E1/3/ρ guidelines. (Ashby, 2011a) 5
Figure 1.6. Fracture toughness against yield strength for engineering materials (Kaw, 2006) 5
Figure 1.7. Tail of Airbus A310-300 6
Figure 1.8. Bell-Boeing V-22 Osprey military tiltrotor 7
Figure 1.9. Composite structures in the space shuttle (Kaw, 2006) 7
Figure 1.10. Reinforced mirror-antenna reflectors with different layouts of the ribs (Reznik et al., 2015) 8
Figure 1.11. Corvette Rear Fiberglass Monospring 8
Figure 1.12. Typical failure modes observed in composites (Garrett, 2016) 9
Figure 1.13. Types of crack opening modes (Siddique et al., 2021) 11
Figure 1.14. Classification of self-healing systems (Mobaraki et al., 2020a) 12
Figure 1.15. Damage recovery stages in self-healing materials (Ramesh et al., 2020) 14
Figure 1.16. Schematic explanation of disruption and reformation of polymer nanocomposite with gold nanoparticle inclusive (Vaiyapuri et al., 2013) 15
Figure 1.17. Autonomous self-healing methods: a) capsule based, b) microvascular based, c) intrinsic approach (Blaiszik et al., 2010) 16
Figure 1.18. Schematic illustration of self-healing via capsules (Xue et al., 2019) 17
Figure 1.19. Schematic illustration of vascular self-healing mechanism (Kahar et al., 2021) 18
Figure 1.20. Self-healing applications in aircrafts (LeCompte) 20
Figure 2.1. Fabrication of scaffolds. (a) With 3D printer (Therriault et al., 2003); (b) biomimicking pattern with 3D printer (W. Wu et al., 2011); (c) self-propagated photopolymer (Jacobsen et al., 2007) 23
Figure 2.2. Degradation of PLA fiber (Esser-Kahn et al., 2011) 24
Figure 2.3. Self-healing process of a composite including 3D fabricated vascular system (Patrick et al., 2014) 25
Figure 2.4. Compression strength recovery (Norris, Meadway, et al., 2011) 26
Figure 2.5. An illustration of the steps in the PDMS construct fabrication process (Bellan et al., 2009) 26

Figure 2.6. Building micro-fluidics inside hydrogel with soft lithography (Golden and Tien, 2007) 27
Figure 2.7. Schematic illustration of the microreplication process from natural leaf to synthetic materials (He et al., 2013) 27
Figure 2.8. Electrostatic discharge to fabricate vascular patterns (Huang et al., 2009) 28
Figure 2.9. Schematic demonstration of the self-healing concept using hollow fibers (Ramesh et al., 2020) 29
Figure 2.10. Schematic demonstration of step-molding technique (Saeed et al. 2016) 29
Figure 2.11. Graphical abstract of nano-reinforced polymeric healing agents for vascular self-healing composites (Bekas et al., 2017) 30
Figure 2.12. Healing efficiency vs healing agent system (Bekas et al., 2017) 30
Figure 2.13. Channel forming method with four step braiding 31
Figure 3.1. Dimensional measurements with (a) Optical and (b) SEM micrographs of 1st Generation Grubbs' catalyst 35
Figure 3.2. The reaction times of the 5E2N and DCP monomers with Grubbs' catalyst 36
Figure 3.3. The comparison of properties of different monomers (Aïssa et al., 2012) 36
Figure 3.4. Flowchart demonstrating a systematic approach for building of novel self-healing mechanism for CFRP composite laminates 38
Figure 3.5. Outline of composite laminate production with vacuum bagging method (Vacuum Systems for Composite Manufacturing) 39
Figure 3.6. MDF molds manufactured for the hand lay-up and oven-curing operations 40
Figure 3.7. The general configuration of 3-Roll Mill Machine 40
Figure 3.8. The mixing process of Grubbs' catalyst with 3-Roll Mills 41
Figure 3.9. Preparation for the hand lay-up and vacuum bagging operations 41
Figure 3.10. Hand lay-up operation of CFRP composite laminate 42
Figure 3.11. Vacuum bagging operation 42
Figure 3.12. Molds in the curing oven under the vacuum atmosphere 43
Figure 3.13. The specimen cutting with a CNC router 43
Figure 3.14. a) Polyamide monofilament, b) aluminium wire and c) galvanized steel wire placed in the composite structure for pulling force measurements 45
Figure 3.15. Measurements of shear forces of different monofilaments tried in pull-out method 45
Figure 3.16. The interconnected channel configuration for thermal camera monitoring 46
Figure 3.17. A special frame containing parallel monofilament wires for the channel configuration to keep the distances between channels at a constant gap 46
Figure 3.18. The representation of the channel coating method 48
Figure 3.19. a) Injection of 5E2N monomer into channels and b) CFRP laminate after injection 49

Figure 3.20. Different types of specimens of 5E2N were injected into the microvascular channels 49
Figure 3.21. Performing the ASTM D790 Three-Point Bending Test for different microvascular channel configurations..... 49
Figure 3.22. The cross-sectional images of different configurations..... 50
Figure 3.23. The representation of the 10% - 40% portion of the load-deflection curve for the slope calculations..... 52
Figure 3.24. a) The technical drawing and b) a picture of the CFRP composite specimen manufactured based on ASTM D5045 to use in compact tension tests..... 55
Figure 3.25. The demonstration of loads applied to the specimen to initiate crack propagation..... 55
Figure 4.1. SEM images of a) uncoated b) wax-coated and c) epoxy-coated microvascular channels 62
Figure 4.2. SEM images of a) uncoated b) wax-coated and c) epoxy-coated microvascular channels after 5E2N agent injected into channels 63
Figure 4.3. Thermal camera images of hot water injected composite laminates containing interconnected microvascular channels 64
Figure 4.4. 3D scanned images obtained from μCT inspection of specimens including a) no channels, c) three channels, e) five channels, g) uncoated channels which are healed after 5E2N is injected. X-ray scan images obtained from μCT inspection of specimens including b) no channels, d) three channels, f) five channels, h) uncoated channels which are healed after 5E2N is injected 65
Figure 4.5. Load–extension curves as a result of 3-point bending tests conducted for specimens in E00 configuration 66
Figure 4.6. Load–extension curves as a result of 3-point bending tests conducted for specimens in 1710D configuration..... 67
Figure 4.7. Load–extension curves as a result of 3-point bending tests conducted for specimens in 1710U configuration..... 67
Figure 4.8. Load–extension curves as a result of 3-point bending tests conducted for specimens in 2610D configuration..... 68
Figure 4.9. Load–extension curves as a result of 3-point bending tests conducted for specimens in 1705D configuration..... 68
Figure 4.10. Load–extension curves as a result of 3-point bending tests conducted for specimens in E1710D configuration 69
Figure 4.11. Bar charts of a) fracture forces and b) stiffness values in different configurations based on 3-point bending test results..... 70
Figure 4.12. Bar charts of a) specific fracture forces and b) specific stiffness values in different configurations irrespective of the shape factor effect..... 73

Figure 4.13. Visualization of the distribution of Ru atoms with EDS analyses in a cross-sectional area of 800µm x 650µm taken from the composite structure 74
Figure 4.14. Schematically visualization of situation inside the structure during the compact tension tests in relation to the Force-CTOD curve 75
Figure 4.15. Force – CTOD curves of the solid, virgin and self-healing agent injected specimens according to Approach 1 76
Figure 4.16. Force – CTOD curves of the solid, virgin and self-healing agent injected specimens according to Approach 2 77
Figure 4.17. Development of healing efficiency over time according to Approach 1 78
Figure 4.18. Development of healing efficiency over time according to Approach 2 79
Figure 4.19. a) Distant view and b) close-up images of the crack zone where the agent was not injected, c) distant view and d) close-up images of the crack zone where the agent was injected 80

1. INTRODUCTION

Since they have high specific strength (σf/ρ) and modulus (E/ρ) properties, carbon fiber-reinforced polymer (CFRP) composites are highly convenient for applications which require light weight and high strength (Kaw, 2006). These properties make composites a preferred choice in sectors such as aerospace, automotive, construction, marine, energy, and many others.

In the aerospace industry, CFRPs account for half of the overall weight of the structural members on aircraft, leading to a 20% reduction in the weight of these structural members (Maria, 2013). More recently, CFRP is implemented to main load-carrying structures like, sandwich panel skins, fuselages and wing planks (Ibrahim, 2014). Application of CFRPs will reduce the fuel consumption and contribute to the reduction of CO_2 emission of aircrafts (Scelsi et al., 2011). In the past fifty years, the aerospace industry has witnessed a continuous growth in the size and flight range of transport aircraft. Consequently, there has been a corresponding rise in the utilization of composite materials in this sector. This can be attributed to the significant advantage offered by these materials in terms of strength-to-weight ratio (Trilaksono et al. 2014). Figure 1.1 indicates the increasing rates of composite usage and the applications of composite structures in commercial transport aircraft over time.

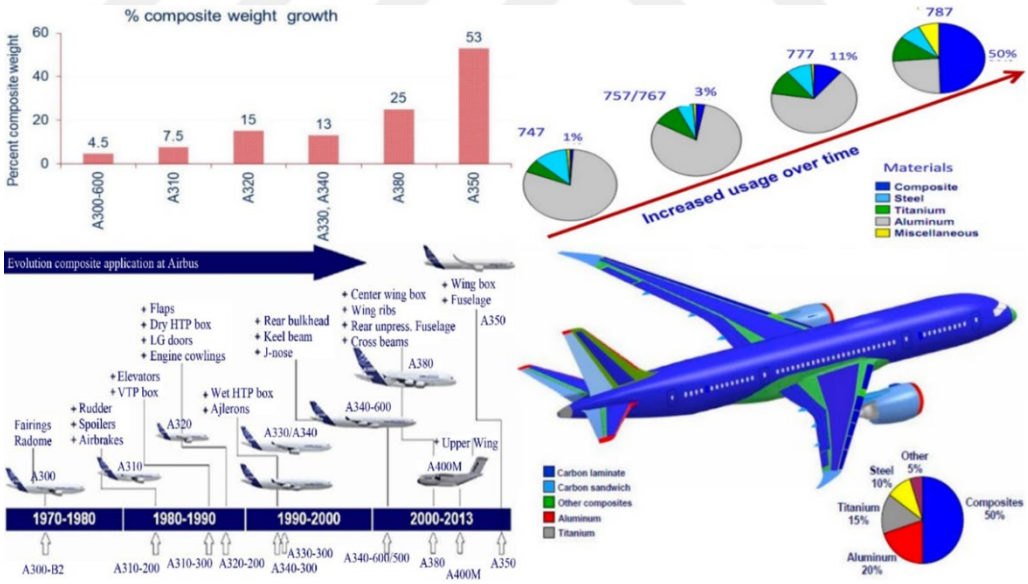


Figure 1.1. History of composite usage in commercial transport aircrafts (Smith, 2013; Trilaksono et al. 2014)

Due to their unequalled properties and versatility, composite materials are crucial in numerous industries. They offer benefits such as high strength-to-weight ratio, resistance to fatigue and corrosion, design flexibility and durability. Composites are suitable for applications in harsh environments, chemical processing, manufacturing, and storage. They also lead to reduced maintenance costs and contribute to energy efficiency and sustainability. However, the usage of

CFRP is limited by their low crack resistance, and poor off-axis strength. Besides, prediction of the failure due to local damages is not reliable so far (Boroujeni et al., 2014). Composite failure is influenced by several factors such as loading, fiber properties, resin properties, stacking sequence, residual stresses, and environmental degradation. Since, the behaviour of multi-directional laminates against failure is not definite it is difficult to accurately predict ultimate failure. Various forms of failure must be evaluated in order to assess the strength of a laminate. Through-thickness failure is more difficult to predict depending on the overall situation of stress or strain in the matrix (Tan et al., 2008; Takeda, 2002; Trilaksono et al., 2014; Wang et al., 2006). It is important to prioritize the improvement of safety and reliability in composite materials that exhibit intricate failure mechanisms.

To overcome these disadvantages of CFRP composites, self-healing is gaining importance. The ability of composite materials to heal damage or cracks which may develop autonomously during their lifetime is referred to as self-healing mechanism. By possessing this characteristic, composite structures are able to effectively overcome their limitations and enhance the overall performance, durability, and reliability. Numerous investigations have been conducted utilizing various methods to develop composite structures that possess self-healing properties.

Autonomous healing in polymer composites is usually facilitated through the use of microcapsules and micro-vascular channels (Figure 1.2). In microcapsules, the mechanism is activated when a crack ruptures the capsule, and healing is accomplished when the repairing agent in the capsule reacts with the catalysts in the structure. Microvascular structures incorporate small channels that contain healing agents and catalysts within the composite material. When a crack emerges, the healing substance merges with the catalyst and healing reaction initiates (Ekeocha et al., 2021).

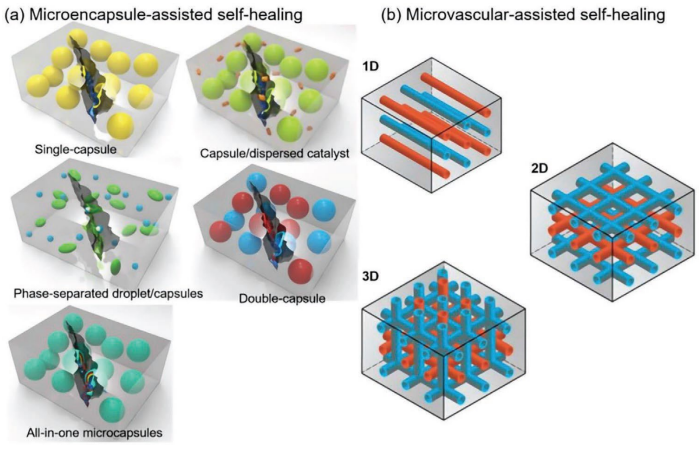


Figure 1.2. Schematic demonstrations of autonomous self-healing processes

In this study, self-healing on polymer composites via microvascular channels was investigated and the characteristics of composite having healing mechanism were observed.

1.1. An Overview of Composites

A composite material is formed by combining two or more materials, which are not soluble in each other, resulting in creation of a new material with enhanced properties. The two main components are the matrix and reinforcement, which work together to produce a material with enhanced mechanical, thermal, or other performance attributes. Composites are designed to take advantage of the strengths of each component, resulting in a material that surpasses the properties of individual materials alone. The matrix surrounds and connects the reinforcement materials. The reinforcement is responsible for providing the composite material with its enhanced mechanical properties. Common reinforcement materials include fibers, particles, or flakes (Figure 1.3). Depending on the material of matrix, such as polymer matrix, metal matrix, ceramic matrix, and carbon-carbon, composite materials can be classified (Kaw, 2006).

A lamina refers to a single layer or ply of a composite material, usually comprising reinforcing fibers that are embedded in a matrix material. A laminate consists of multiple layers, known as laminae, which can have either identical or varying orientations and materials. The macro-mechanics of a lamina determine the mechanical properties of whole laminate such as stiffness, flexibility and strength. Composite materials have advantages over monolithic materials due to their structure and anisotropic mechanical response (Altenbach et al., 2004).

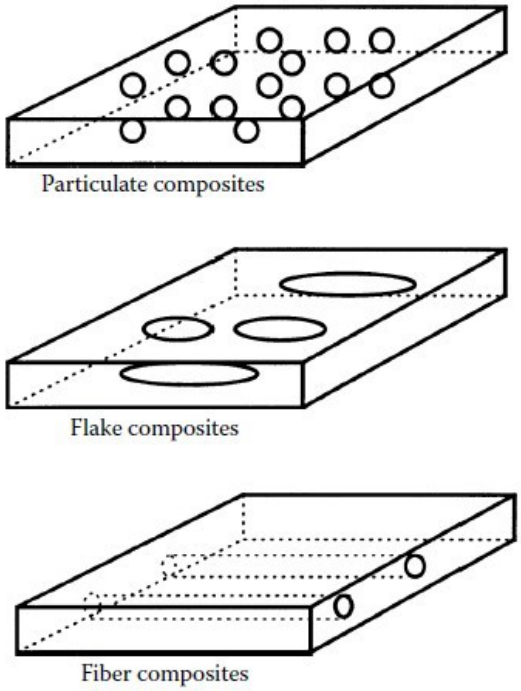


Figure 1.3. Types of composites according to shape of reinforcement

Today's advanced technologies cannot always be met by monolithic metals or their alloys. Composites, like carbon/epoxy, are the sole materials that meet these requirements. In many cases, the utilization of composites is more effective in reducing the overall mass of the structural system,

such as an aircraft, while maintaining the rigidity and durability of its constituent parts. Despite the potentially higher expenses associated with composite materials, the decrease in the quantity of components in an assembly and the resulting fuel savings render them a more lucrative option (Mijovic, 1995).

In order to define advantages of composites, some parameters are considered. For example, the lightest tie for a specific tensile load and deflection limit has the highest E/ρ value, which is called specific modulus. Similarly, it should have high specific strength value (σ_{ult}/ρ) in order to be light and strong. Composite materials have high ratios of these two parameters, resulting in a reduction in mass which reduces the costs of material and energy. Figure 1.4 represents the specific modulus against specific strength of materials.

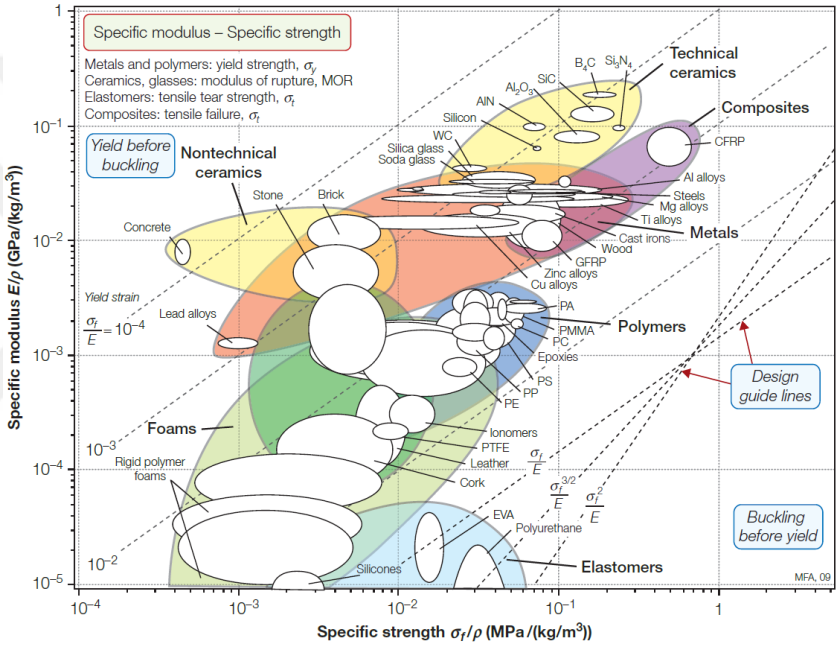


Figure 1.4. Plot of specific modulus (E/ρ) against specific strength (σ_f /ρ) (Ashby, 2011a)

Parameters to evaluate the superiority of composites in comparison to metals are not limited with specific strength and specific modulus. The lightest column that can withstand a specific compressive load without buckling is selected based on the highest $E^{1/2}/\rho$ value. Even, the lightest panel that can withstand a specific pressure with minimum deflection is determined according to the highest $E^{1/3}/\rho$ value (Ashby, 1989). Composites exhibit superior advantages for these parameters in contrast to metals as indicated in Figure 1.5. Fracture resistance, impact resistance, fatigue life and creep are the other parameters to be considered while comparing the performance of composites (Kaw, 2006).

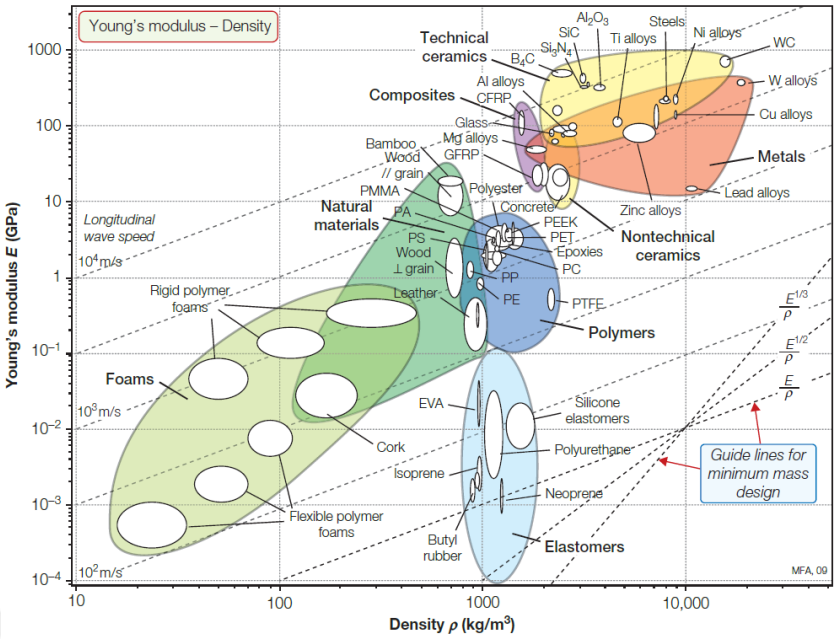


Figure 1.5. Plot of Young's modulus (E) against density (ρ), on log scales with constant E/ρ, E1/2/ρ, and E1/3/ρ guidelines. (Ashby, 2011a)

Although they have many advantages over metals, composites have some drawbacks such as high fabrication costs and complex mechanical characterization. To reduce costs, improvements in manufacturing techniques are needed. Composite structures pose a greater challenge in terms of mechanical characterization compared to metals, as they require a larger number of material parameters. The repair of composites is a complex procedure, and critical defects in composites may remain unnoticed. Composites do not have high fracture toughness in contrast to metals. The plot of fracture toughness against yield strength for engineering materials are indicated in Figure 1.6. From the figure, metals demonstrate a significant combination of fracture toughness and strength.

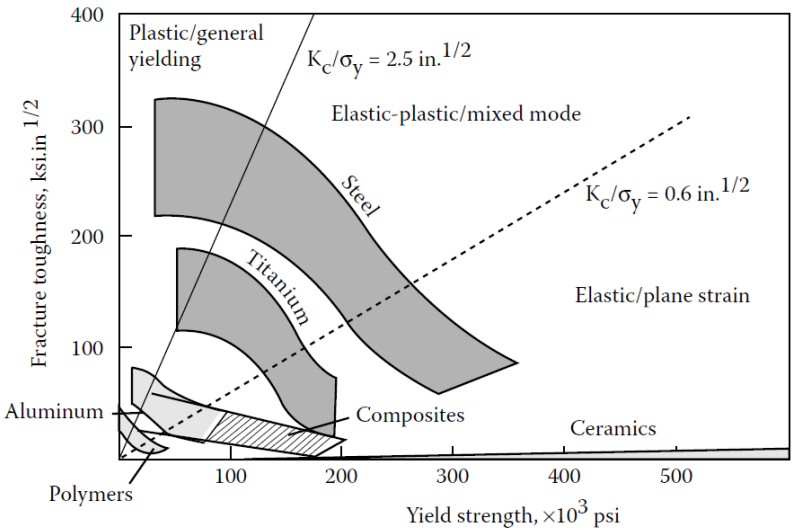


Figure 1.6. Fracture toughness against yield strength for engineering materials (Kaw, 2006)

Polymer matrix composites (PMCs) are widely utilized advanced composites because they are cost-effective, have impressive strength, and are easy to manufacture. However, they have disadvantages, including limited operating temperatures, high coefficients of thermal and moisture expansion, as well as relatively low elastic properties. Mostly utilized fibers are carbon, Kevlar, graphite and glass; polymers are epoxy, polyester, phenolics, urethane, and polyamide. Epoxy is the most favoured PMC matrix, finding extensive application in the aerospace industry. This is primarily due to its exceptional strength, low viscosity, minimal flow rates, negligible volatility during the curing process, and minimal shrinkage rates. It is available in over 20 grades, allowing for customization to meet specific processing requirements.

1.1.1. Common Applications of Polymer Composites

Polymer matrix composites find extensive applications in numerous industries, from tennis racquets to space shuttles. The utilization of polymer composites in the military aviation sector has spearheaded the achievement of weight reduction in comparison to metal components. In commercial airlines like Boeing, composites are predominantly employed in secondary structures, such as rudders and elevators, which are constructed using graphite/epoxy. Additionally, landing gear doors are crafted using Kevlar-graphite/epoxy. However, there are instances where composites are utilized in a primary structure. The integration of composites in primary structures is exemplified by the tail fin of the Airbus A310-300 and the all-composite Lear Fan 2100 aircraft. The tail fin constructed using a graphite/epoxy and aramid honeycomb combination (Figure 1.7), not only achieved a weight reduction of 300 kg but also simplified the manufacturing process by reducing the number of components from 2000 to 100.



Figure 1.7. Tail of Airbus A310-300

Helicopters and tiltrotors (Figure 1.8) use rotor blades made of graphite/epoxy and glass/epoxy materials, ushering in a remarkable increase in blade lifespan of more than 100% when

compared to metals. Moreover, these advanced blade materials significantly facilitate achieving higher top speeds.



Figure 1.8. Bell-Boeing V-22 Osprey military tiltrotor

On the other hand, composites are desirable material for space applications due to their strength and dimensional stability. Graphite/epoxy was selected due to its ability to reduce weight and minimize mechanical and thermal deflections (Figure 1.9). The utilization of lightweight materials instead of traditional metal alloys results in increased payload capacities, which can incur expenses of up to $2208 per kilogram (Schwartz, 1984).

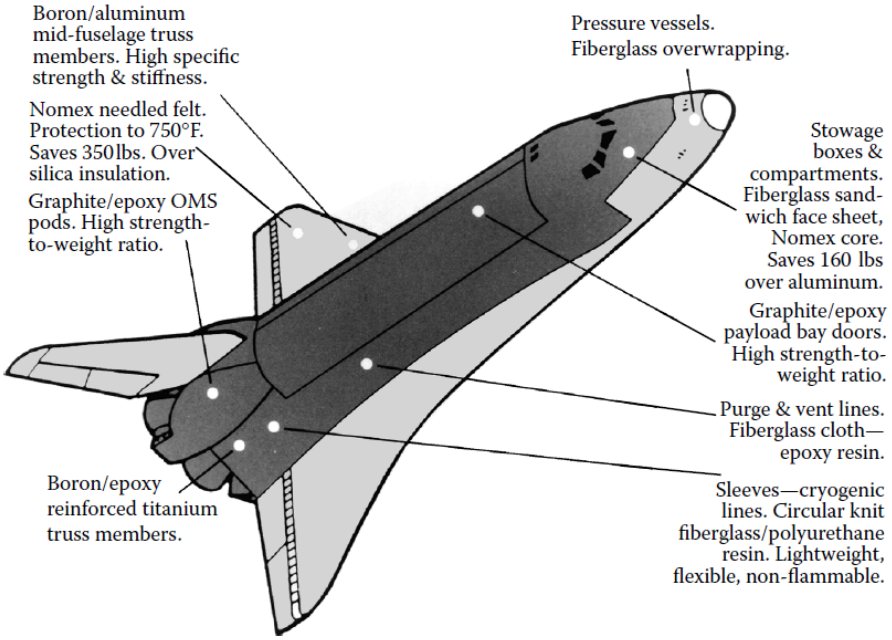


Figure 1.9. Composite structures in the space shuttle (Kaw, 2006)

Figure 1.10 depicts a high-gain antenna, reinforced with fibers, specifically designed for the purpose of being used in space stations. This antenna utilizes sandwiches composed of an aluminium

honeycomb core combined with graphite/epoxy facings. In satellite systems, antenna struts and ribs employ graphite/epoxy having remarkable specific stiffness due to their capacity to fulfil the dimensional stability prerequisites caused by significant temperature variations experienced in space (Reznik et al., 2015).

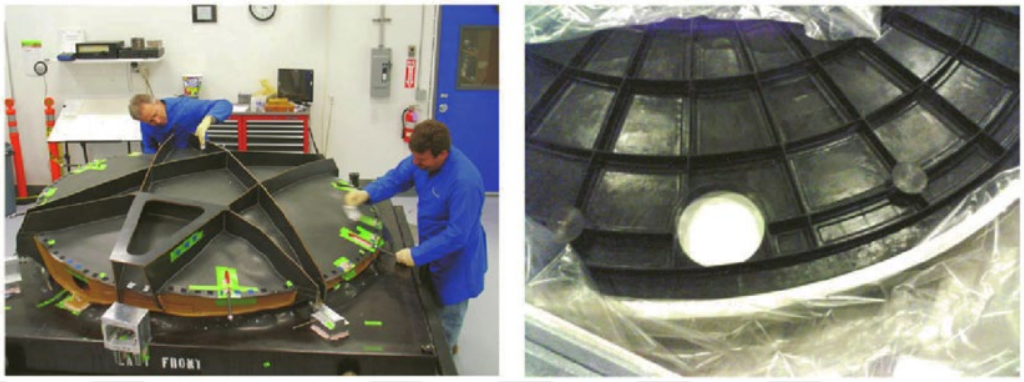


Figure 1.10. Reinforced mirror-antenna reflectors with different layouts of the ribs (Reznik et al., 2015)

In the automotive industry, the Corvette's fiberglass body and composite leaf springs are examples of polymer matrix composites in automotive applications. Composite leaf springs as depicted in Figure 1.11 offer a smoother ride, rapid response to road shock, reduced risk of sudden and severe damage, exceptional ability to withstand corrosion and a fatigue life exceeding five times that of steel (Pruez et al., 2013). Weight has increased by over 20% due to increased engine power in today's automobiles. Carbon composite bodies have the potential to achieve a significant weight reduction of up to 50% while still ensuring the necessary safety standards are met (Neil, 2004).

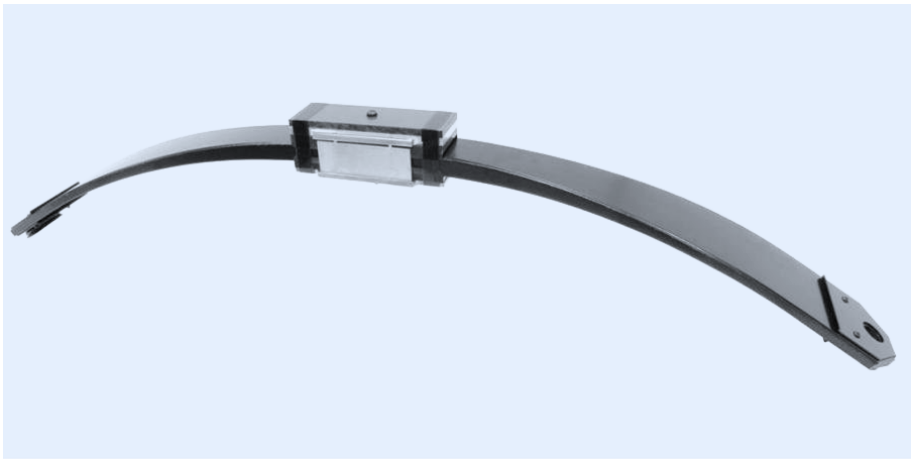


Figure 1.11. Corvette Rear Fiberglass Monospring

There is a growing trend in utilizing composite materials for sports equipment. Bicycles employ a hybrid construction technique that combines graphite/epoxy composites with aluminium tubing and S-glass reinforced urethane foam, increasing specific modulus and reducing frame mass

by 25% (Lessard et al., 1995). Also, carbon/polyamide composite wheels exhibit reduced weight and superior impact resistance compared to aluminium wheels. Composites are commonly used in tennis, racquetball, and ice hockey for improved rigidity and reduced risk of elbow injury (C. Sun, 1995). Glass/polyester composite ski poles exhibit superior strength and reduced weight in comparison to traditional poles.

In addition to all these, composite materials find utility in various sectors including the marine industry, medical devices and commercial components such as pressure vessels, garden tools, bridges, boats, X-ray tables, etc.

1.1.2. Failures of Composites

Ductile materials experience failure as a result of undergoing plastic deformation, while brittle materials such as ceramics rupture catastrophically. Composite structures can fail in various ways, such as delamination, fiber breakage, matrix cracking and fiber-matrix debonding (Figure 1.12). Multiple modes of failure can occur simultaneously, depending on factors such as material properties, fiber architecture, and environmental conditions.

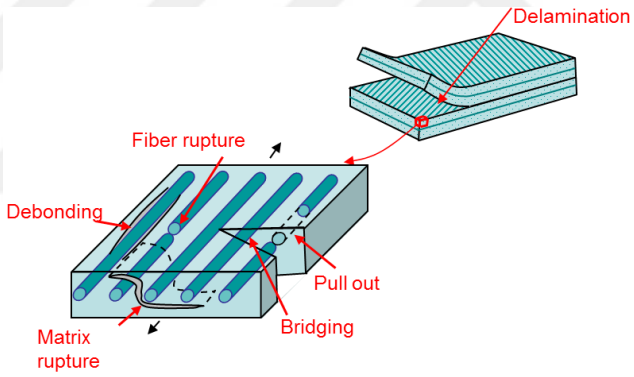


Figure 1.12. Typical failure modes observed in composites (Garrett, 2016)

The presence of a failure mode can vary based on factors such as strain energy release, flaw distribution, interface toughness, and matrix properties. Fiber structures allow for customized strength and stiffness in a preferred direction, but the matrix component can fail under mechanical loading in another direction (Daniel and Mccormick, 2007).

In composites, failure can occur in various ways, including interlaminar delamination, cracking between and along the fibers, as well as excessive shear. When matrix cracking takes place, fibers have the potential to undergo failure through fracturing near the crack initiation point. Fiber fracture is the most probable failure mode, in cases where the matrix possesses toughness and ductility, or if there is a residue present in a fiber. If mechanical loads exceed the strength of the fiber, fiber fracture occurs leading to catastrophic failure. This changes the load path and increases the susceptibility of surrounding fibers to fracture. A matrix with high fracture toughness and a suitable

bond with the fibers reduces the amount of strain energy released when fiber fractures (Gdoutos et al., 2000).

Fiber debonding occurs when cracks align with the fibers, causing them to disconnect from the matrix. This disrupts the chemical bond between the fiber and matrix, resulting in the formation of new surfaces that enhance both fracture toughness and strain energy. Furthermore, the critical impact energy of the laminate can be enhanced through its potential increase. Additionally, debonding can raise the laminate critical impact energy by reducing the strength of the interface, which encourages delamination. This allows for the release of more elastic strain energy (Agarwal et al., 2006).

Delamination is a common and significant issue in evaluating the durability and damage tolerance of composite laminates. Unlike other failure modes like matrix cracking or fiber fracture, delamination cannot be seen from the surface, making external damage inspection insufficient. This weakness has led to extensive research on understanding delamination initiation and propagation (Ding, 1999). Aerospace components are engineered to withstand mechanical stresses that are lower than their failure thresholds when subjected to operational loads in order to tackle this specific problem. (Williams and Pavan, 2000). Thinner laminates tend to experience delamination on the bottom side during impact, while thicker laminates show matrix crushing on the top surface. When delamination occurs, a significant quantity of strain energy is released, particularly in ductile and toughened matrices. The simultaneous occurrence of delamination, fiber fracture and matrix cracking also release a substantial amount of strain energy (Gdoutos et al., 2000).

The plies in a laminate stick together because of the curing of the matrix. They stay together because of the shear stresses acting between them. If these bonds weaken, delamination occurs, causing the plies to separate and move freely. Materials that possess a reduced interlaminar shear strength are prone to experiencing delamination. The strength is influenced by the resin's ductility and toughness, as well as the chemical bond it creates. The matrix assumes a crucial function in determining delamination, interlaminar shear strength, and fracture toughness (Garrett, 2016).

There are several elements that contribute to the determination of the fracture toughness of composites. These include the volume fraction of fibers, the alignment of the fibers, as well as the strength and flexibility of both the fibers and matrix. However, the toughness of the resin is paramount, as it absorbs energy and releases strain during failure (Ding, 1999). Russell and Street (1987) have shown that enhancing the toughness of the resin improves the interlaminar fracture toughness in laminates.

There are several main causes for delamination: poor bonding during the curing process, manufacturing defects or inclusions, low ILSS, impact loading, and edge effects (Daniel and Mccormick, 2007). If the resin bonding between layers is not done properly during the curing process, it may not be strong enough to handle the intended loads. Similarly, if there are defects or inclusions from manufacturing or mishandling, the probability of delamination or premature failure

increases. Moreover, composites with lower ILSS are more prone to delamination, which results to reduced stiffness and damage tolerance (Russell and Street, 1987). Composites that are not designed to withstand impact loading face a significant vulnerability to interlaminar delamination. This risk persists even with low-velocity impacts, as delamination and debonding may start from the impact area and propagate across multiple layers (Garrett, 2016).

In laminated composites, delamination can occur in three different modes of interlaminar fracture. Mode-I is known as the opening mode or peel mode, whereas mode-II is the in-plane shear mode or sliding shear mode. Also, mode-III is identified as the out of-plane shear mode or twisting shear mode, as depicted in Figure 1.13. Mode-I fracture leads to the separation of laminates mainly as a result of the applied tensile stress. Whereas mode-II fracture leads to the sliding/shearing of laminates when subjected to shear stress that acts parallel to the crack plane. Lastly, mode-III fracture leads to the tearing of laminates as a consequence of shear stress applied parallel to the crack plane (Mohapatra, 2009; Siddique et al., 2021).

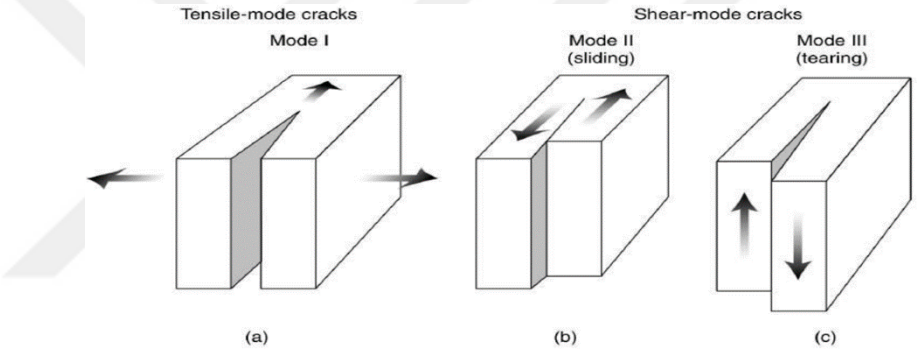


Figure 1.13. Types of crack opening modes (Siddique et al., 2021)

The critical strain energy release rate, denoted by the symbol G, is widely accepted as the measure of the total energy needed to start delamination in a material. This value varies depending on the specific mode of delamination. Therefore, three different G values exist: G_{Ic}, G_{IIc}, and G_{IIIc} which correspond to mode-I, mode-II, and mode-III failure, respectively (Siddique et al., 2021).

Proper inspection and maintenance practices are crucial to detect and repair any signs of deterioration or damage throughout the service life of composite components.

1.2. Introduction to Self-Healing

Materials like polymers, ceramics, metals and their composites are subjected to experiencing various forms of damage caused by mechanical, thermal, chemical, radiational or combination of these factors over their entire lifetime. These damage factors cause microcracks in the surface of structure which is leading to sudden rupture and catastrophic failures. In such cases, it may not be reliable to repair the same material and reproduce it with the intended effectiveness (Ramesh et al., 2020). Therefore, engineers and scientists have been researching on fabricating materials in which

ability to heal and renew its function with autonomous or nonautonomous actions as shown in Figure 1.14 (Mauldin and Kessler, 2013).

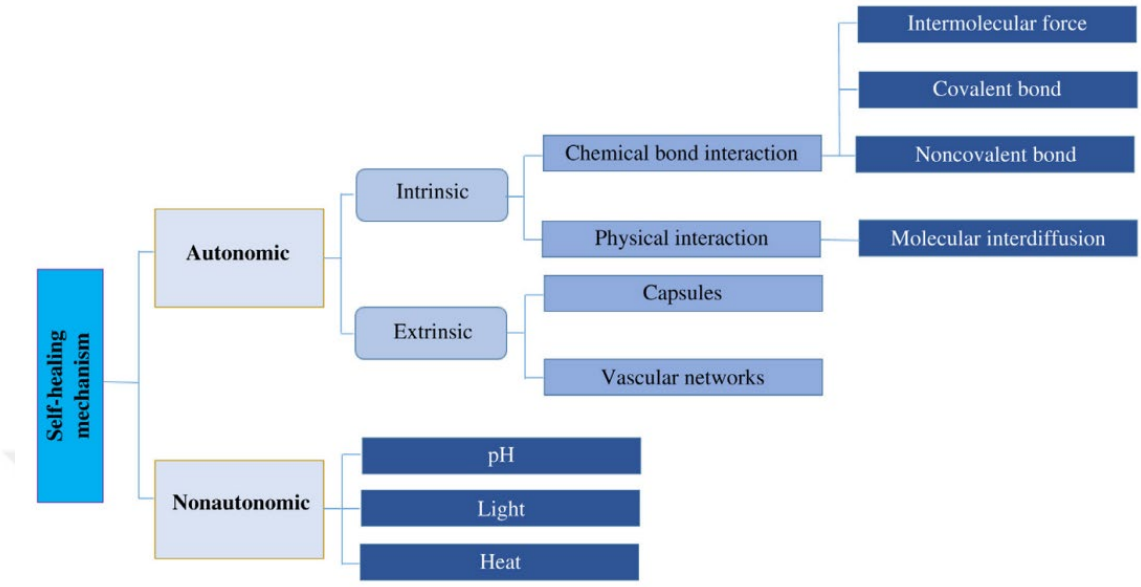


Figure 1.14. Classification of self-healing systems (Mobaraki et al., 2020a)

The self-healing concept mimics the healing in biological systems like clotting process on human skin and the regrowth of a lizard's tail. These processes are accomplished by the transfer of necessary biochemicals to the damaged area in biological ways. There are many research have been carried out on designing artificial materials that possess self-healing properties, drawing inspiration from natural systems.

The first investigation of self-healing has made by Malinskii et al. (1970) with polyvinyl alcohol specimens. Then, in the 1980s, thousands of studies began to be conducted on self-healing in polymers, copolymers, and elastomers (Wool, 1980; Wool and O'Connor, 1981). After these developments the self-repairing behaviour of the crack formed in the cement matrices has been studied by Dry in 1994. In 2001, White et al. made a remarkable contribution to the exploration of self-healing materials, ushering a new era in their development. Since then, there has been a substantial increase in scientific publications focusing on self-healing materials, indicating the extensive research conducted in this field from that time until the present. Numerous methods have been developed and keep going under development in order to fabricate materials having self-healing ability. Bergman and Wudl (2007), identified the self-healing treatment in polymers and their mechanisms in detail. Drawing from the field of crack healing of relevant polymer-polymer interfaces, Wool (2008), sought to establish a comprehensive failure theory and healing approach for polymers. Wu et al. (2008), presented a study on the fundamental structural and functional principles underlying the fracture structure and healing mechanisms in polymeric systems. Besides these there have been publications on the self-healing mechanisms in polymers and composites (Youngblood

and Sottos, 2008). Aïssa et al. (2012), Toohey et al. (2007), Trask et al. (2007), Esser-Kahn et al. (2011), Patrick et al. (2014) have provided novel point of views on self-healing in fiber reinforced composites (FRC).

Materials that have the extraordinary capability to restore their structural integrity without showing any visible signs of damage are known as self-healing materials (Ramesh et al., 2020). One of the remarkable characteristics of such materials is their ability to regenerate their functionality following damage caused by external factors (Hager et al., 2010). Basically, this entails the recovery of mechanical strength and other material properties as a consequence of material failure or fracture. Inherently, artificial materials lack the ability for self-healing. Instead, self-healing properties are incorporated into man-made materials through the utilization of external sources or agents. For specific materials, even micro voids can be filled up and the desired properties can be restored. The healing agents inside fiber reinforced polymer composite structures, provide bonding and seal the cracks that is occurred by contacting of monomer with the catalyst end up with polymerization reaction (White et al., 2001).

Different materials, including polymers, metals, paints, and coatings, possess unique self-healing mechanisms that are inherent to their microstructure. Detection of micro cracks in composite materials is very hard to see and notice by the human eye. There are various approaches such as embedding piezoelectric sensors, optical fibers and magnetostrictive materials, have been made which are incorporated into the structure for the detection of damage (Thostenson and Chou, 2006). By using these approaches, the degree of damage and its influences needs to be determined in non-destructive manner. Regarding to the degree of damage, to repair the material or remove it from the service are available options which are very expensive, complicated, time consuming and requiring easy access.

The self-healing polymers and other such materials possess the ability to significantly regain their load carrying capacity by healing the micro cracks occurred anywhere in the material after damage. All in all, these materials are reliable as they eliminate high costs and time-consuming processes of active damage detection or external repair by extending the life of the structures autonomically. Because of their significant advantages, numerous applications of this materials can be found in the fields of aeronautics and space, electronics, electrical and so on. Despite all, there are some limitations including modifications in original properties, crack healing dynamics and functionality and cost factors.

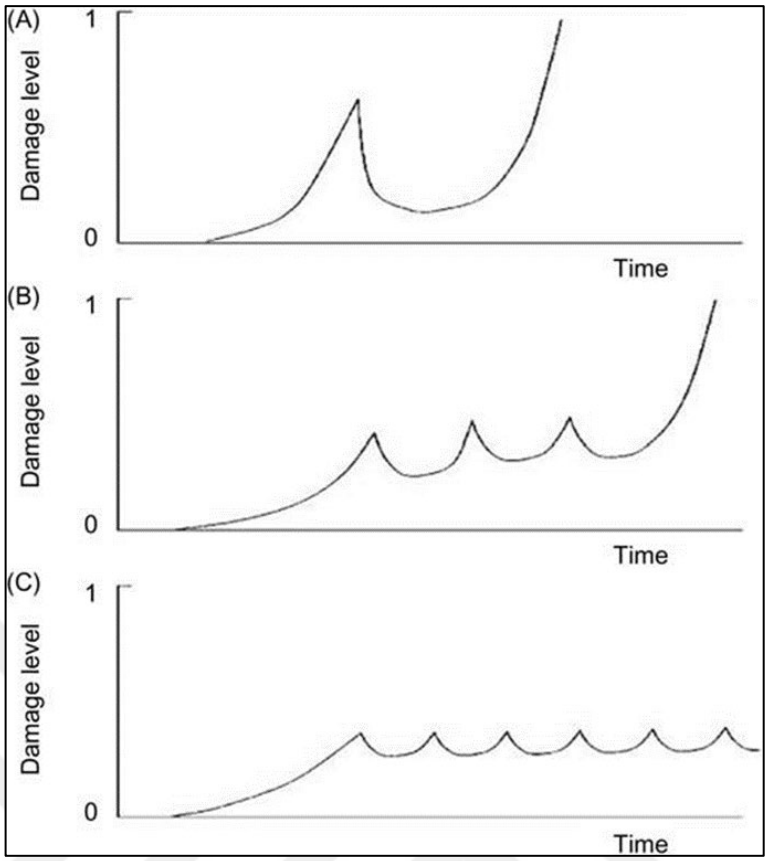


Figure 1.15. Damage recovery stages in self-healing materials (Ramesh et al., 2020)

Damage management constructs the basis of self-healing approach. The time-dependent progression of the damage is directly related to the autonomous healing process as indicated in Figure 1.15. Figure 1.15(a) indicates that the material which has capability for one-off fully recovery action in case of damage. The any further damage formation in the structure results in final rupture. The material as indicated in Figure 1.15(b) shows more than one healing actions that involves partially recovery of damage. In this type of material, final rupture occurs after a few healing cycles. The shown material in Figure 1.15(c) indicates ideal self-healing action which has limitless lifetime based on subjected load conditions. As depicted in Figure 1.15 self-heling performance of materials is influenced by both the cycle of damage development and the healing rate of damage (Ramesh et al., 2020).

Until present, several studies conducted in implementing self-healing ability to the materials. Based on these studies self-healing materials are broadly classified in three groups: capsule based, vascular and intrinsic (Blaiszik et al., 2010).

1.2.1. Self-Healing Mechanisms

Basically, self-healing materials can be categorized into two groups: autonomous and non-autonomous (Hager et al., 2010). If these materials need an external factor to repair the damage or

rupture in their structure, they are called non-autonomous self-healing materials, on the other hand if they do not demand any stimuli they are called as autonomous self-healing materials.

1.2.2. Non-autonomous Self-Healing

Non- autonomous self-healing materials require an external factor or energy which can be provided by light, heat or pH (Mobaraki et al., 2020a). Light has a vital role in triggering the self-healing properties, as rapid switching, remote activation and accurate targeting (Habault et al., 2013). Switching off and on the self-healing property of a material was studied by Yang et al. (2017) on acrylamide hydrogel having a self-healing ability when it was exposed to a visible light, but under the UV light, self-healing property disappeared. In another study, Hu et al. (2018) developed an innovative design for composites. The light energy turned into heat energy due to the Cu_2S-Ag nanoparticles on the crack interface which provided a self-repairing action by reducing the viscosity of resin and help it to diffuse in the ruptured area. Also, Kim et al. (2013) has studied on non-autonomous healing with carbon-based nanoparticles. Self-healing of the composite material with polyurethane matrix and graphene inclusive is occurred via induction where the wavelength is near the IR. The result is enhanced glass transition temperature and modulus that increases elongation at break.

The other external factor is heating energy for non- autonomic self-healing action. Sun et al. (2018) investigated the effect of temperature on the self-healing ability of asphalt binders by the help of computer simulation. Additionally, the influence of density, concentration percentages and mean square displacement were evaluated to define the self-repairing character of asphalt via heat. As the result of this investigation, they determined the optimum healing temperature range is between 40.3 °C - 48.7 °C. It is crucial to note that subjecting the process to higher temperatures may lead to irreversible deformations. González et al. (2018) explored the potential of microwave heating in augmenting the self-healing properties of metal fiber-reinforced asphalt mixtures. At the end, they observed healing in asphalts. Also, in another study, Vaiyapuri et al. (2013) worked on polymer nanocomposite that containing gold nanoparticles. They observed that the network structure of the composite can be disrupted under heat (about 60 °C) and completely reformed to its original shape upon cooled down to ambient temperature (Figure 1.16).

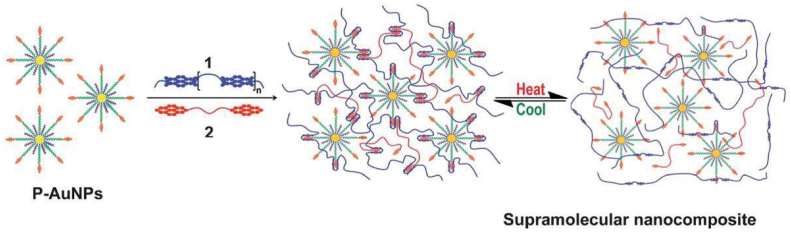


Figure 1.16. Schematic explanation of disruption and reformation of polymer nanocomposite with gold nanoparticle inclusive (Vaiyapuri et al., 2013)

1.2.3. Autonomous Self-Healing

The composite material which has autonomic self-healing ability, does not require any external stimuli because, repairing action occurs by itself as damage appeared (Hager et al., 2010). Recently, several autonomous self-healing techniques was developed and implemented in particular areas. Autonomous self-healing mechanisms differ from each other by their triggering the healing actions against a damage. The healing volume, the healing repeatability and the recovery rate designates the functionality type of mechanism. Autonomous self-healing materials are classified in two categories as extrinsic and intrinsic. And extrinsic materials divided into two groups: microcapsule based and microvascular based. The autonomous self-healing methods are demonstrated schematically in Figure 1.17.

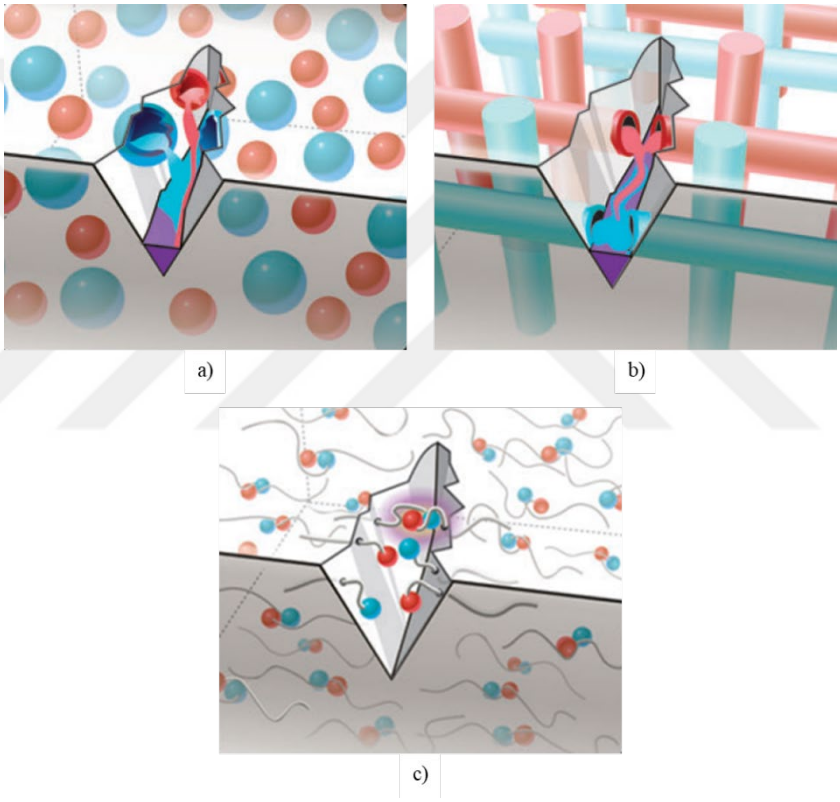


Figure 1.17. Autonomous self-healing methods: a) capsule based, b) microvascular based, c) intrinsic approach (Blaiszik et al., 2010)

Capsule Based Self-Healing Mechanism

Capsule-incorporated self-repairing materials function as remedial agents enclosed within discrete capsules. In this approach, the healing substance is conserved within microcapsules till they are damaged or dissolved. In an instance of damage, capsules are ruptured, thereby the healing substance is released along the location of damage. After release, the polymeric reaction of substance takes place by combining with catalyst and this triggers self-healing of broken bonds.

This mechanism has some advantages such as: (i) the technology of encapsulation techniques has matured, (ii) the incorporation of microcapsules which contain self-healing agent into the polymer by applying available blending techniques is simple, (iii) utilizing this method does not necessitate any changes in the molecular structure of polymer composite (Zhu et al., 2015). Nonetheless, one of the most crucial disadvantages of this mechanism is, the low number of healing repeatability. According to the type of microcapsule, the healing action occurs only one time or a few times after the capsules are ruptured (Zhu et al., 2013).

There are numerous techniques for encapsulation of the healing agents to protect against external factors before, during and after mixing with polymer matrix so that remain inactive until a triggering action occurred.

White et al. (2001) developed a self-healing material that uses capsules containing dicyclopentadiene and Grubbs' impetus (Figure 1.18). During the material formation, the capsules are integrated into the polymeric matrix. When damage occurs and a crack forms, the capsules release a healing substance into the crack. This substance then enters the crack and undergoes clumping via the ring-opening metathesis polymerization process, which is facilitated by Grubbs' impetus. In this process, the cyclic olefin undergoes a transformation into a polymeric substance through the opening of strained rings within the monomers and subsequent recombination, resulting in the formation of extended connections.

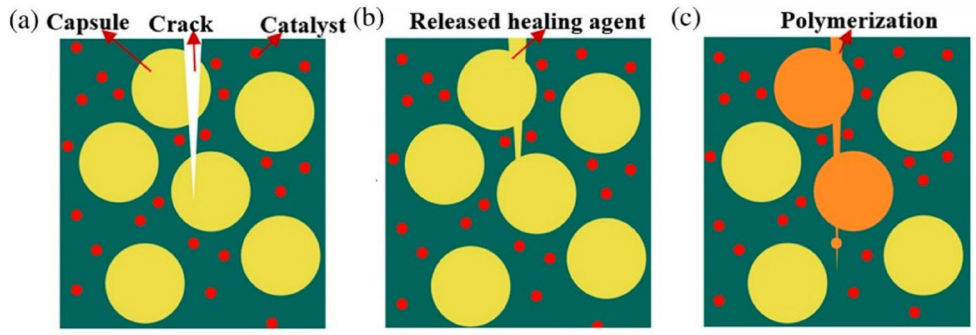


Figure 1.18. Schematic illustration of self-healing via capsules (Xue et al., 2019)

Vascular Based Self-Healing Mechanism

Vascular self-healing systems are an alternative approach to create self-healing properties in polymeric composites. This concept, first proposed by (Dry and Sottos, 1993) involve embedding a healing substance in a network of capillaries or hollow channels, similar to blood vessels in biology. These capillaries are connected until damage triggers the self-healing process and the cracks in the polymer matrix resulting from this damage are repaired.

The vascular system's operation (Figure 1.19) can be compared to a healing system based on capsules. Both systems require careful consideration of mechanical description, activation mechanism, and healing process. The main difference lies in the manufacturing and composition of

the matrix material. The advancement of self-healing techniques is significantly impacted by various factors including the production method, the similarities between systems, the healing agent, and the materials utilized (Blaiszik et al., 2010).

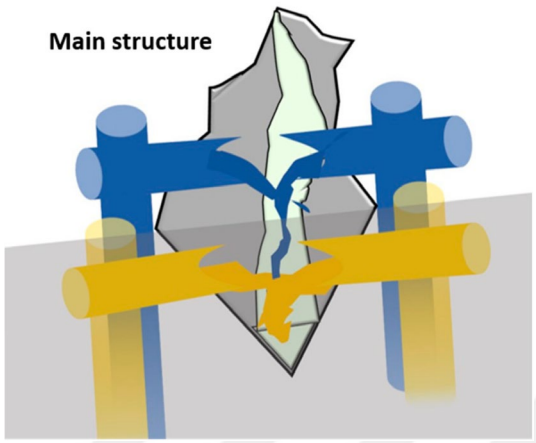


Figure 1.19. Schematic illustration of vascular self-healing mechanism (Kahar et al., 2021)

If self-healing composites based on capsules imitate the inherent healing mechanism at a cellular level, then self-repairing materials equipped with a vascular system imitate, at a larger scale, the healing process facilitated by the vascular and circulatory systems in living organisms. By incorporating a circulation mechanism, these materials can be replenished with healing agents, allowing for continuous delivery of the healing substance and control over its flow (Y. Wang et al., 2015).

Vascular network-based self-healing polymeric systems offer several advantages such as;

- In contrast to microcapsule systems, vascular-based self-healing polymeric systems allow for the use of a greater amount of healing agent.
- Unlike microcapsule systems, the fibers can be interconnected to create a network, enabling the healing of a larger area.
- These systems have the capability to continuously supply and reload the healing agent.
- This approach allows for the use of different healing agents at different times, making it possible to treat various types of damage (Herbst et al., 2013; Mobaraki et al., 2020b).

The mechanical characteristics of matrix are directly influenced by factors including volume fraction and distribution of channels, bonding and stiffness of hollow fibers. Properties such as chemical reactivity, viscosity, and surface wettability are considered when choosing a healing substance for a vascular system. The significance of viscosity and wettability becomes apparent in situations where damage has been occurred (Colquhoun and Klumperman, 2013). Hollow glass

fibers are commonly used to make self-healing materials. Different methods like 3D printing, melt spinning, electrospinning, and replication are used to design the polymeric matrix (Das et al., 2016; Dry, 1994; Lanzara et al., 2009; Norris et al., 2011; Pang and Bond, 2005b; Therriault et al., 2003; Wang et al., 2015; Williams et al., 2007). Also, Gergely et al. (2018) utilized a hybrid microcapsule-microvascular system to restore impact damage and enhance healing efficiency. Two different healing substances were selected, with microcapsules healing microcracks and the microvascular network restoring lost damage volume.

Intrinsic Self-Healing Approach

The intrinsic mechanism is more advantageous than the extrinsic approach. This healing process can happen through reversible chemical bonding, either within the polymer itself or when exposed to specific environments. If the healing reaction occurs without external exposure, it is referred to as autonomic (Scheiner et al., 2016). A matrix possessing intrinsic self-healing mechanism offers many benefits, such as improved mechanical, optical, and chemical properties. Moreover, it is easier to fabricate and process composites with intrinsic self-healing mechanism. Typically, three distinct categories of intrinsic mechanisms are employed: chain diffusion, reversible covalent bonds, and supramolecular force (Ponnamma et al., 2017).

Incorporating thermally reversible reactions, hydrogen bonding, ionomeric coupling and a dispersed meltable thermoplastic phase, researchers have successfully engineered intrinsic self-heating materials (Zechel et al., 2017). The working principle of these materials is simpler compared to capsule-based and vascular-based self-healing materials. In this system, the matrix itself has the ability to heal, eliminating the need for additional healing agents. This avoids many of the problems associated with the compatibility and combination of healing agents in capsule-based and vascular-based self-healing materials.

1.2.4. Healing Performance Assessment

Healing performance in polymer composites is evaluated by healing efficiency. The healing efficiency of a polymer composite refers to its capacity to autonomously repair and restore its mechanical characteristics, such as fracture toughness, tensile strength and surface finish (Saini and Jain, 2017; Van Tittelboom et al., 2011). Wool and O'Connor (1981) proposed a method to quantify the extent of self-healing in polymer composites in order to attain the desired range of properties. This approach has been widely adopted to compare the effectiveness of self-healing in different polymer composites. Various tests exist to simulate the self-healing effect, which are specific to the type of damage incurred by the material. These tests involve subjecting the healed composite to various mechanical tests, such as tensile, flexural, or impact tests. Healing rate and repeated healing capability are also evaluated (Hansen et al., 2009; Keller and Crall, 2018). In general, healing

efficiency is calculated as the ratio of the fracture toughness of the healed sample to the fracture toughness of the virgin sample (Brown et al., 2002; Wool and O'Connor, 1981).

1.2.5. Self-Healing Applications in Polymer Composites

Fiber-reinforced epoxy composites find extensive application in aerospace, comprising up to 50% of the overall weight in aircrafts like Airbus A350 XWB and Boeing 787 Dreamliner. These composites are effective in detecting and repairing impact damage, making them suitable for safe aircraft design. Identifying and measuring impact injuries on polymer composites is challenging, so extensive care is required. One effective method to address this issue is through the utilization of self-healing polymer composites, which can repair weaknesses caused by impact loading and create lightweight yet strong fuselages (Kumar et al., 2019).

Tan et al. (2008) conducted a study that concentrated on polymer composites for aerospace purposes. The researchers investigated a polymer composite created through a moulding method. In order to assess its effectiveness, the specimens were subjected to three-point bending tests while being exposed to impact loads. The findings from these tests revealed that the self-healed composite exhibited an impressive restoration of material strength, reaching a maximum of 47%. As a result, incorporating self-healing properties into polymer composites has the potential to significantly improve their capacity to endure impact damage in aircraft structures.



Figure 1.20. Self-healing applications in aircrafts (LeCompte)

Researchers in the aerospace industry have dedicated their efforts to investigating the mechanical characteristics of self-healed epoxy composites (Bond et al., 2008; Williams et al., 2007). Bond et al. (2008) produced polymer composites by employing a self-repairing method to analyse the effects on impact strength. Additionally, this research examined the effectiveness of composites in terms of their ability to self-heal in relation to both flexural and compressive strength. The study

reported the bending strength of a hollow glass fibers embedded aerospace-grade polymer composite, demonstrating a significant strength recovery of 97% under quasistatic loads. Furthermore, the self-healed composite demonstrated a recovery rate of approximately 92% in strength as result of compression after impact test. These findings indicate self-healing in polymer composites have great potential for use in aerospace fuselages.

Furthermore, fiber-reinforced polymer composites having self-healing features are utilized in aircraft structures because of their superior properties. They have superior fatigue and crack resistance, enabling them to repair any damage prior to its potential failure. Studies (Guadagno et al., 2010; Teoh et al., 2012) have shown strong recovery of mechanical properties and the potential to replace conventional laminates in aerospace structures. Moreover, they facilitate reduced maintenance and weight reduction by means of self-repair. These composite materials possess the potential to enhance the damage resistance, service life and overall safety of aircraft. Other studies have shown better flexural strength and aerospace-grade glass fiber polymer composite applications (Norris et al., 2011; Coope et al., 2014).

Coatings and paints play a vital role in the aerospace industry for protecting the fuselage and aero structures from environmental damage and corrosion. These coatings have the advantage of self-repairing when cracks occur and can also shield aerospace components from corrosion using self-healing polymer composites. Although the aerospace structure components hold greater significance than coatings in polymer composites, any damage to these coatings does not have a significant impact on the overall strength of the structure. Zhao et al. (2011) developed a corrosion protective coating for steel alloy material by combining epoxy resin with microcapsules containing urea-formaldehyde. Notably, the incorporation of microcapsules significantly contributed to preserve the corrosion-free state of the coated steel alloy specimens, even in situations where the coating was damaged.

Self-healing epoxy composites have gained attention since the 2000s. They have various applications in the aerospace field and can address issues like fatigue, impact resistance, and surface corrosion. The process of self-healing is accomplished by utilizing healing agents that consist of microcapsules and vascular networks. Kumar et al. (2019) demonstrated the versatile applications of these composites, which can be used in aerospace fuselages, anticorrosion coating, engine blades, and combustion chambers.

2. PREVIOUS STUDIES

2.1. Self-Healing via Vascular Systems

The self-healing properties of fiber-reinforced polymer composites via microvascular channels or networks are investigated by various studies. There are various methods developed to generate microvascular channels into the composite structure.

2.1.1. Sacrificial Fibers and Scaffolds Methods

Lewis and Gratson (2004) and Therriault et al. (2003) developed a method using fugitive ink to create microvascular networks in 3D as shown in Figure 2.1(a). They used a robotic deposition apparatus to print paraffin-based organic ink layer by layer. The ink was then melted and removed under vacuum, leaving behind a hollow microvascular network. Scaffolds with diameters ranging from 10 to 300 μm can be produced in this method. Alternative fugitive inks, including a mixture of microcrystalline wax and petroleum jelly, were also considered. However, removing the liquefied sacrificial substances from small vessels and trapped liquids proved challenging, resulting in the residue (Y. Wang et al., 2015).

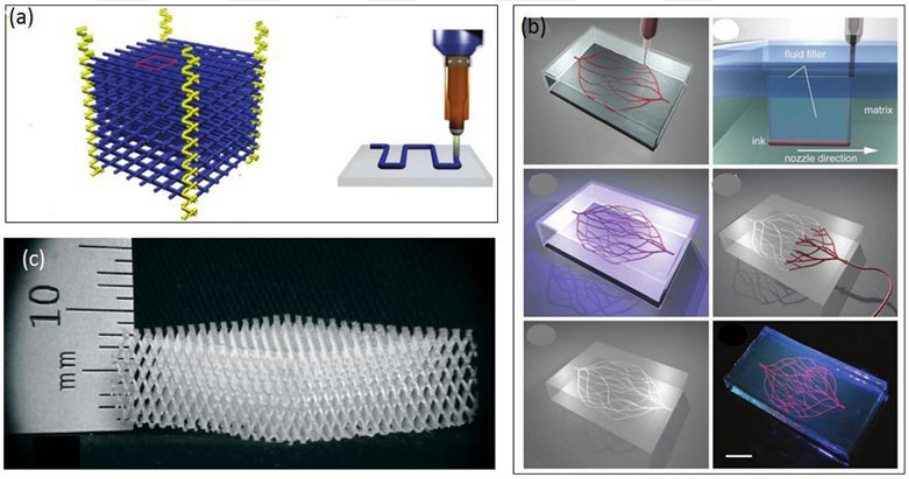


Figure 2.1. Fabrication of scaffolds. (a) With 3D printer (Therriault et al., 2003); (b) biomimicking pattern with 3D printer (W. Wu et al., 2011); (c) self-propagated photopolymer (Jacobsen et al., 2007)

Furthermore, recent studies have enhanced the printed design by transitioning from a basic uniform pattern to a biomimetic pattern resembling the veins of a leaf (W. Wu et al., 2011), as depicted in Figure 2.1(b). By adjusting the pressure within the printing nozzle, it was achieved a varying size of the network. In order to enhance the efficiency of printing process, Hansen et al. (2013) evolved a multi-nozzle array capable of printing multiple lines at the same time. To enhance the mechanical characteristics, halloysite nanotubes were incorporated with sacrificial fibers. After

the fibers dissolved, these nanotubes effectively enveloped the internal surface of the microvascular system, thereby providing structural reinforcement (Olugebefola et al., 2013).

Additionally, the process of solidification through light activation using photopolymers can be utilized to create sacrificial elements through 3D printing. In previous studies conducted by Jacobsen et al. (2007), they successfully manufactured interconnected photopolymer waveguides by employing self-propagation, resulting in the creation of open-cellular micro-truss structures (Figure 2.1(c)). Schaedler et al. (2011) further enhanced this method to fabricate metallic vascular networks, while Roper et al. (2015) extended it to fabricate bicontinuous fluid networks.

The sacrificial material-removing procedure can be improved by treating the spun fibers chemically or physically. Suitable catalysts can speed up the thermal depolymerization of impregnated poly-lactic acid (PLA), as shown in a study by Dong et al. (2012). PLA fibers were combined with tin (II) oxalate catalyst to reduce the depolymerization temperature (Figure 2.2). To create a microvascular network in a fiber-reinforced composite, one can surround PLA sacrificial fibers with reinforcement fabrics and then subjected to heat treatment (Patrick et al., 2014; Coppola et al., 2014).

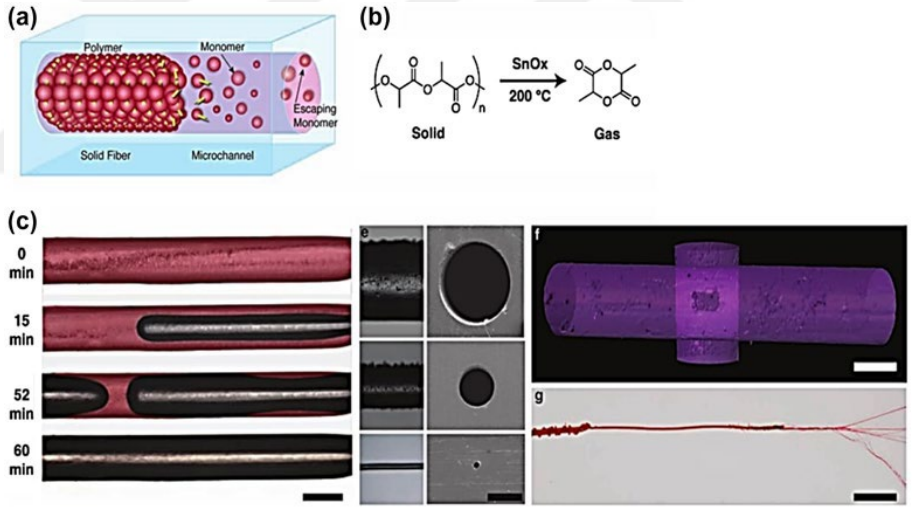


Figure 2.2. Degradation of PLA fiber (Esser-Kahn et al., 2011)

Patrick et al. (2014) fabricated the composite textile reinforcement made by stitching a special type of PLA filament infused with a catalyst into layers of woven fabric. Then, by using vacuum-assisted resin transfer moulding (VARTM), this preform is transformed into a laminate. They used a sacrificial material-removing process to create a three-dimensional microvasculature throughout the composite. For healing purposes, a two-part chemistry consisting of resin and hardener was employed and stored in separate channels within the epoxy matrix. Also, they studied two different types of 3D vascular design parallel and herringbone (Figure 2.9), and they investigated the self-healing action against delamination by conducting a double cantilever beam (DCB) tensile

opening (mode-I) test. As a result, they observed an achievement in the healing process with a 3D vascular system.

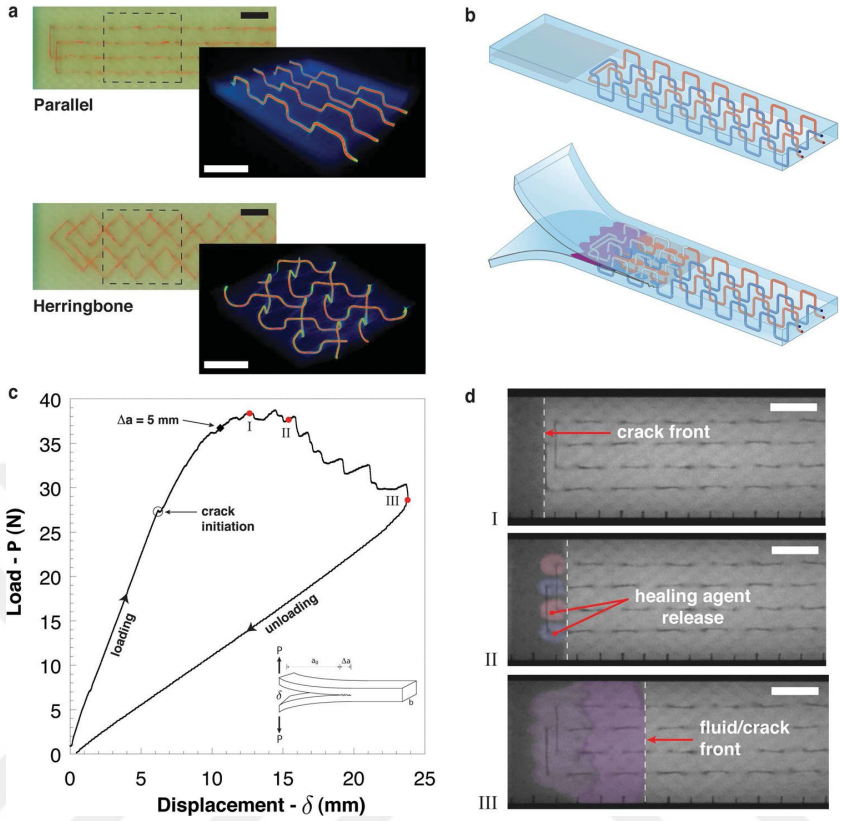


Figure 2.3. Self-healing process of a composite including 3D fabricated vascular system (Patrick et al., 2014)

Norris et al. (2011) studied developing self-healing composites that are inspired by the damage tolerance and self-healing abilities of bones. They incorporated healing agents into hollow vessels with a one-dimensional structure, which were then embedded within a fiber-reinforced polymer (FRP). By incorporating a simple vasculature design into a fiber-reinforced polymer composite using a "lost wax" process, a self-healing function was achieved in this literature study. This resulted in a remarkable recovery (≥96%) in compression strength after impact as shown in Figure 2.3.

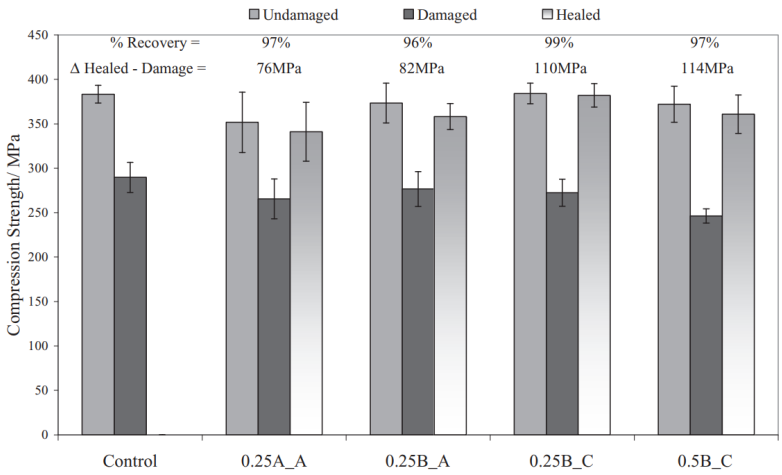


Figure 2.4. Compression strength recovery (Norris, Meadway, et al., 2011)

Electrospinning and melt-spinning are two processes that create fibers from liquids. The manufacturing procedures bear resemblance to the production method of cotton candy. The cotton candy machine was, in fact, the initial apparatus employed for melt-spinning sacrificial fibers. After the production of the sugar fiber, it was subsequently positioned within a Teflon mold. Subsequently, a mixture of degassed uncured resin and hardener was poured over the sugar. After the mixture was cured, devices were submerged in a water and ethanol solution. This dissolved the sugar, resulting in the creation of a micro-channel network within the polydimethylsiloxane (PDMS) matrix as shown in Figure 2.4 (Bellan et al., 2009).

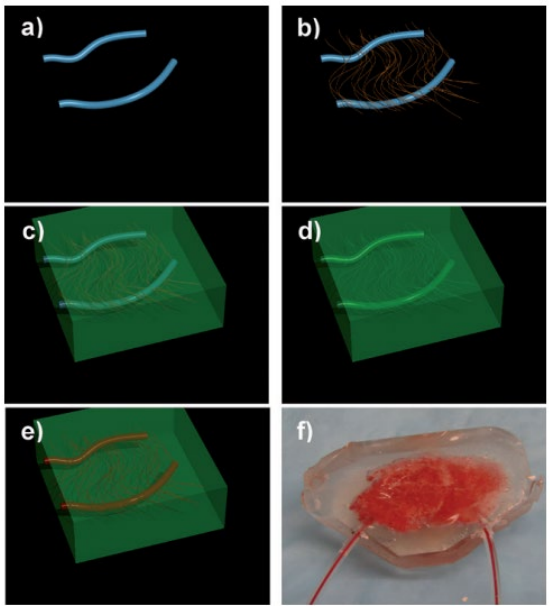


Figure 2.5. An illustration of the steps in the PDMS construct fabrication process (Bellan et al., 2009)

Wu et al. (2013) and Gualandi et al. (2013) used electrospinning which offers the possibility of constructing core-shell vascular network without the need for degradation of sacrificial fiber and

injection of healing agents. During the electrospinning process, the dicyclopentadiene (DCPD) healing substance was directly encapsulated within polyacrylonitrile shells. When a fracture transpired, the rupture of these shells allowed the release of DCPD healing substance, facilitating the restoration of the damage.

Melt-spinning and electrospinning techniques offer a quick and easy means of fabricating fine fibers with small diameters. Nevertheless, this approach is limited to producing individual sacrificial fibers and arranging them in a specific pattern must be done by hand. The development of more sophisticated positioning techniques is still pending. Core-shell fibers exhibit excellent properties for self-healing materials, but they lack the ability to form interconnected networks or allow for the refilling of the healing agent. Consequently, their functionality resembles that of an enhanced capsule-based self-healing material rather than a vascular one.

Soft lithography is a useful technique for creating microfluidic networks, which can be employed in the production of microvascular networks for self-healing materials. Golden and Tien (2007) developed technique that involved the utilization of gelatine as a sacrificial material, enabling the formation of a hexagonal beehive structure (Figure 2.5). This technique involved creating a vascular network pattern and replicating it on a glass or pre-oxidized PDMS substrate. The gelatine was then poured into the substrate and solidified. After removing the solid gelatine, it was integrated into a hydrogel and subjected to heat treatment. This process left behind a microvascular network within the hydrogel, with channel diameters as small as 6 μm. PDMS can also be used to directly replicate suitable structures found in nature. He et al. (2013) used a comparable approach to reproduce leaf venation and create interconnected vascular networks (Figure 2.6).

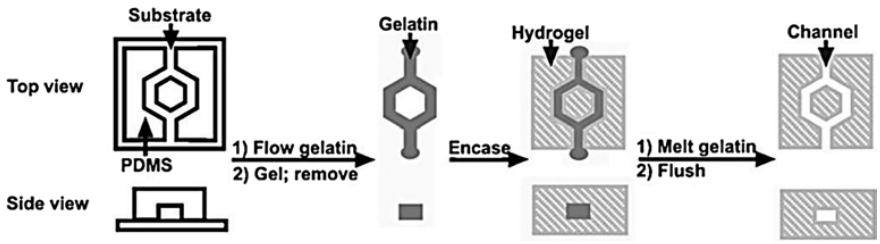


Figure 2.6. Building micro-fluidics inside hydrogel with soft lithography (Golden and Tien, 2007)

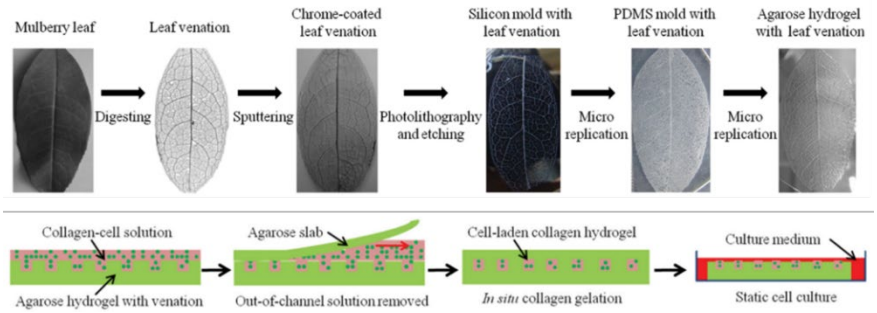


Figure 2.7. Schematic illustration of the microreplication process from natural leaf to synthetic materials (He et al., 2013)

The combination of alternative manufacturing techniques can be employed to duplicate designs. Bellan et al. (2012) used melt-spinning to create small-diameter fibers and soft lithography to make primary vessels. Replicating established patterns is great in terms of mass production, but not efficient for making a single item (Wang et al., 2015).

2.1.2. Electrostatic Discharge Method

Electrostatic discharge is a fast way to create microvascular networks based on natural designs. Huang et al. (2009) used an electron beam to irradiate polymethyl methacrylate (PMMA), causing electrical charges to build up. Connecting the specimen to the ground resulted in a lightning-like discharge, forming a tree-like network within the block as shown in Figure 2.7.

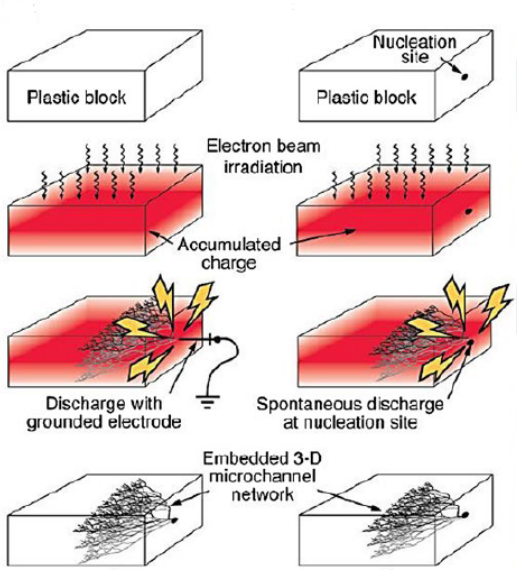


Figure 2.8. Electrostatic discharge to fabricate vascular patterns (Huang et al., 2009)

This technique allows for rapid and efficient construction of vascular networks, but the resulting pattern is uncontrollable, leading to uncertain network quality. Further investigation is needed to understand the discharge process's performance and properties (Y. Wang et al., 2015).

2.1.3. Laser Direct-write Method

In the realm of micro-fluidics devices, laser direct-write techniques are employed to create channels. These channels can serve as conduits within vascular systems. In order to produce micro-channels successfully on a PDMS block, Lim et al. (2003) used a high-brightness diode-pumped slab laser.

Lasers have the capability to directly create intricate two-dimensional (2D) designs onto polymeric materials. Nevertheless, the production of three-dimensional (3D) structures using lasers is challenging and inefficient (Wang et al., 2015).

2.1.4. Hollow Fiber Method

One way to create self-healing fiber-reinforced composites is by installing tubes filled with the healing agent inside (Pang and Bond, 2005a; Trask and Bond, 2006). This method involves using hollow fibers to separate the restorative substance and the matrix as shown in Figure 2.8. When damage occurs, some of the fibers break and release the healing substance. The procedure of incorporating the empty fibers into the main matrix is similar to that of regular fiber-reinforced materials. However, the minimum impact on the composite is observed when the hollow fibers are arranged in parallel with the reinforcement fibers (Kousourakis and Mouritz, 2010). Employing hollow fibers exhibits a drawback in that they are unable to create interconnected networks, as well as refilling them is challenging.

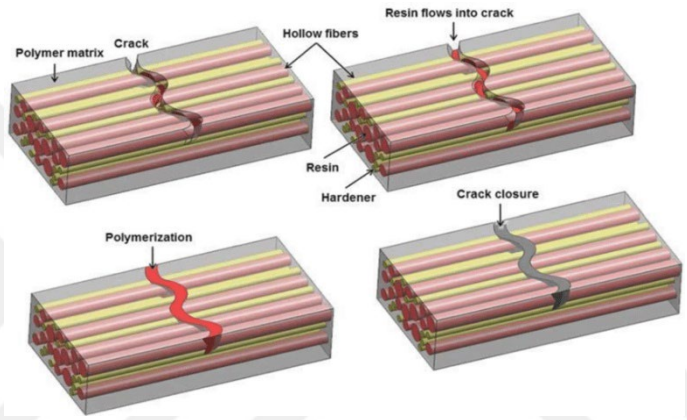


Figure 2.9. Schematic demonstration of the self-healing concept using hollow fibers (Ramesh et al., 2020)

2.1.5. Other Studies

Saeed et al. (2016) proposed a method consisting of two stages of composite molding as shown in Figure 2.10. In the initial stage, during the moulding process, cavities were created by placing PTFE or extruding soft wax onto the surface of a composite laminate. During the second stage, this laminate with cavities was bonded with another composite laminate during the molding process and microchannels were created between these laminates. They evaluated the effectiveness of joining the composite laminates through interlaminar shear and flexural testing.

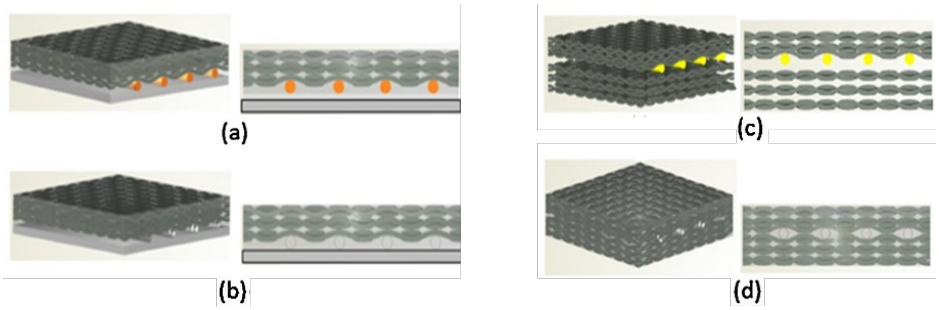


Figure 2.10. Schematic demonstration of step-molding technique (Saeed et al. 2016)

Bekas et al. (2017) conducted research on incorporating nano-reinforcement into an epoxy healing agent to enhance the self-healing capabilities of fiber-reinforced composites, shown as a graphical abstract in Figure 2.11. They employed multi-walled carbon nanotubes (MWCNTs) as the nanoscale reinforcing phase in three different weight contents. Dynamic viscosity measurements were employed to assess the rheological characteristics of the nanomodified epoxies. The impact of multi-walled carbon nanotubes (MWCNTs) on the healing efficiency of fractured glass fiber reinforced composites (GFRPs) was assessed through the infusion of the resultant nanocomposites. They observed that nano-enhanced healing agent increased the healing efficiency by approximately 190% through additional energy consumption mechanisms (Figure 2.12), as confirmed by the Scanning Electron Microscopy (SEM) study.

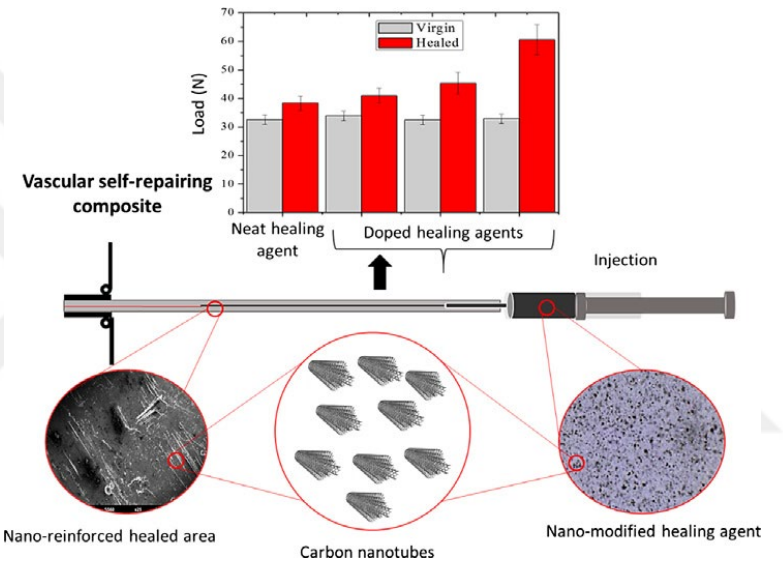


Figure 2.11. Graphical abstract of nano-reinforced polymeric healing agents for vascular self-healing composites (Bekas et al., 2017)

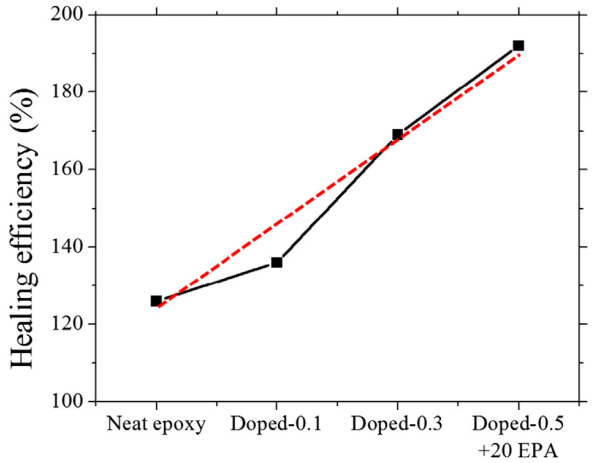


Figure 2.12. Healing efficiency vs healing agent system (Bekas et al., 2017)

Wu et al. (2012) offered a braiding method to create microvascular channels. They used a four-step braider machine to make fabric preforms including two axial place holders, made of trilene, at each braid as shown in Figure 2.13. They also coated the braided preforms with carbon nanotube to be able to sense the crack filling during healing. VARTM process was employed for curing the braided fabric preform. After the curing, they remove the axial place holders, and two separate microvascular channels were formed in a braid. When the crack occurred, healing agents were mixed in the zone between channels. They investigated the mechanical effects of channels and sensing process of damage.

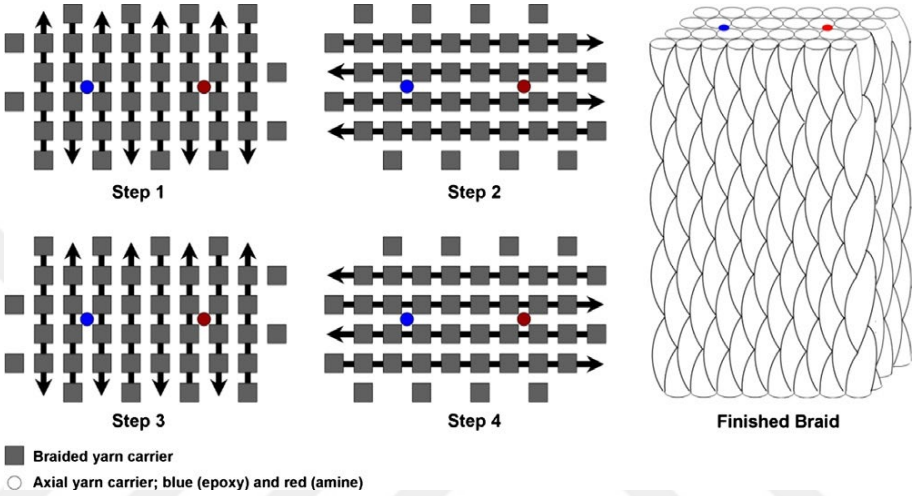


Figure 2.13. Channel forming method with four step braiding.

2.2. Aim of The Study

Composite structures are widely used in many industries with their unique and superior properties. Also, it is crucial to use composites in critical structures in aerospace and defence industries. However, their low crack resistance and poor off-axis strength makes their usage limited. Also, interest in smart materials and composites is increasing to overcome these types of problems. Self-healing composites are crucial in the field of smart materials. In furtherance, investments to global self-healing market are raising day by day.

This thesis aimed to improve the self-healing properties of composite structures via an innovative microvascular channel creating method without adversely affecting the mechanical properties. And secondly, it is aimed healing in a short time and in wide temperature range.

3. MATERIAL AND METHOD

3.1. Materials

Carbon fabric with epoxy polymer matrix was used in this thesis work for manufacturing the carbon fiber reinforced polymer composite (CFRP) laminate. Also, to achieve to build a microvascular network in CFRP laminate, polyamide monofilaments have been used. Besides all these, Grubbs' catalyst integrated in the matrix and 5-Ethylidene-2-Norbornene (5E2N) monomer later injected into microchannels, were used to achieve self-healing during microcracking of CFRP composite structure.

3.1.1. Carbon Fabric

In this study, high-strength aerospace-grade carbon fabric is used as reinforcement material to manufacture CFRP composite structures. These fabrics were supplied by Hexcel Corporation. Table 3.1 indicates the physical and mechanical properties of the fabric employed in this study.

Table 3.1. Physical and mechanical properties of carbon fabric (*Toho Tenax Impregnated Strand Test Method. Based on JIS R7601 or DIN 29965)

Property	Value
Product brand description	HexForce® G0904 D 1070 TCT HS
Type of yarns	TENAX E HTA 40 E13 3K
Fabric image description	Plain Weave, continuous fibers
Areal weight	193 g/m^2
Thickness	0.20 mm
Density	1760 kg/m^3
Tensile strength	4205 MPa
Tensile modulus*	237 GPa
Elongation*	1.78%

3.1.2. Polymer Matrix

For the matrix material in this project, low-viscosity epoxy polymer resin and its hardener with superior mechanical and dynamic properties were used. The Araldite® LY 5052 epoxy and Aradur® 5052 hardener were supplied by Huntsman Corporation. Table 3.2 presents the chemical and physical characteristics of epoxy resin and its hardener. Additionally, the matrix properties as mixture of epoxy resin and hardener are provided in Table 3.3. The curing temperature of this matrix material is defined as 120 °C in a curing oven.

Table 3.2. Chemical and physical properties of epoxy resin and its hardener

Property	Epoxy Resin	Hardener
Product brand description	Araldite® LY 5052	Aradur® 5052
Aspect (visual)	clear liquid	clear liquid
Viscosity at 25 °C (ISO 12058-1)	1000 – 1500 mPa.s	
Density at 25 °C (ISO 1675)	1170 kg/m^3	940 kg/m^3

Table 3.3. Physical and mechanical properties of the matrix

Property	Matrix
Mixed products	Araldite® LY 5052 / Aradur® 5052
Mixing ratio by weight	100:38
Initial mix viscosity	500 - 700 mPa.s @ 25 °C
Build-up viscosity	1500-3000 mPa.s @ 25 °C
Flexural strength	116-122 Mpa @ 8h & 80 °C
Flexural modulus	2.7-3 GPa @ 8h & 80 °C
Tensile strength	84-86 Mpa @ 8h & 80 °C
Tensile modulus	3-3.2 GPa @ 8h & 80 °C

3.1.3. Self-Healing Catalyst

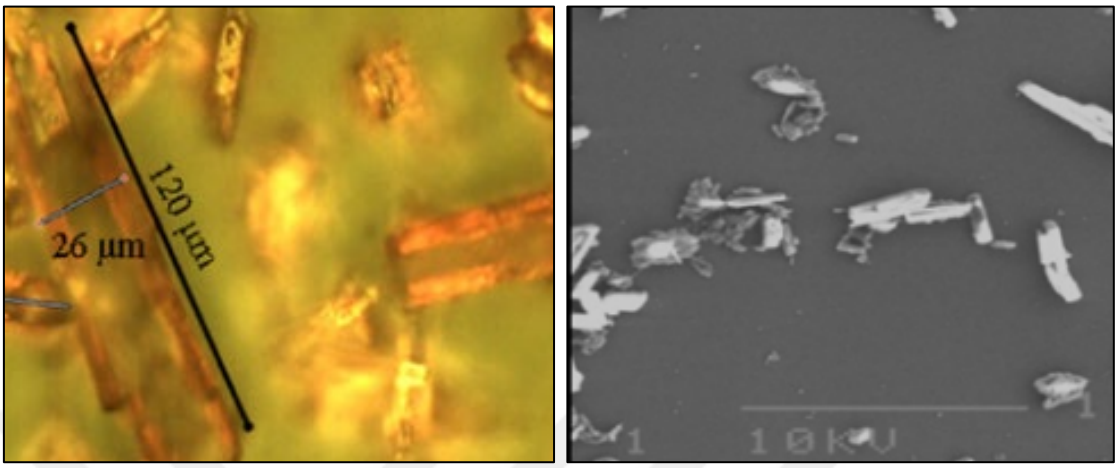
In this study, 1st Generation Grubbs' Catalyst® M102 is used as a catalyst to trigger the ring-opening polymerization reaction of the self-healing agent leaking into the crack zone. The Grubbs' catalyst was procured from Sigma Aldrich. The chemical properties of Grubbs' catalyst utilized in this study is presented in Table 3.4.

The Grubbs' catalyst stands out due to its easy handling and fast initiating properties. On the other hand, it has good functional group tolerance to aldehydes, and it is stable in air and moisture (Elias, 2008).

Table 3.4. The chemical properties of the catalyst (Grubbs' Catalyst® M102)

Property	Value
Product brand description	Sigma Aldrich Grubbs Catalyst® M102
Empirical formula	C43H72Cl2P2Ru
CAS number	172222-30-9
Molecular weight	822.96
Reaction suitability	Core: ruthenium Reagent type: catalyst Reaction type: Ring-Opening Polymerization
Melting Point	153 °C

The optical and SEM micrographs were utilized to carry out the dimensional measurements of 1st Generation Grubbs' catalyst by Aïssa et al. (2012). The catalyst was defined as rods up to ~30 µm in width and ~120 µm in length as shown in Figure 3.1.



(a) (b)

Figure 3.1. Dimensional measurements with (a) Optical and (b) SEM micrographs of 1st Generation Grubbs' catalyst

3.1.4. Self-Healing Agent

As a self-healing agent, the 5-Ethylidene-2-Norbornene (5E2N) monomer was used in this study. Table 3.5. gives the chemical properties of the 5E2N monomer.

Table 3.5. The chemical properties of the healing agent (5-Ethylidene-2-Norbornene)

Property	Value
Product brand description	Sigma Aldrich 5-Ethylidene-2-norbornene
Empirical formula	C_9H_{12}
CAS number	16219-75-3
Molecular weight	120.19
Form	Liquid
Density	0.893 g/mL at 25 °C
Boiling Point	146 °C
Vapor pressure	4.6 mmHg (20 °C)

In addition, the reaction times of the 5E2N monomer are much shorter with the Grubbs' catalyst as can be seen in Figure 3.2 (Aïssa et al., 2012). Also, as indicated in Figure 3.3, the 5-Ethylidene 2-Norbornene agent is in liquid form between -80°C and 148°C, costly cheap and less harmful to the environment than other agents (Aïssa et al., 2012).

The operating temperatures of the 5E2N agent, correspond to the temperature range that aircraft are exposed to during service and since it reacts more quickly, critical cracks can be healed

in a short time. As a result of these multiple considerations, 5E2N was chosen as the self-healing substance.

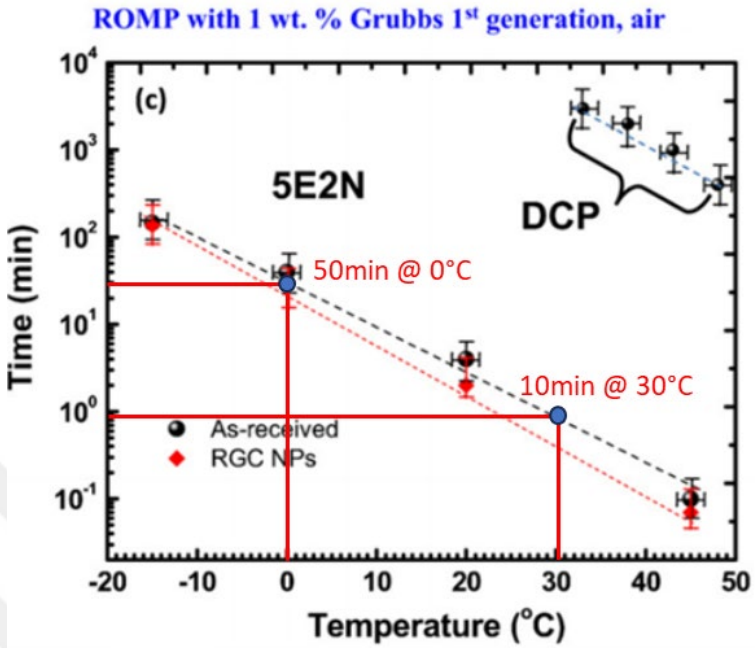


Figure 3.2. The reaction times of the 5E2N and DCP monomers with Grubbs' catalyst

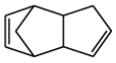
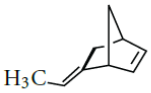
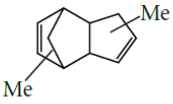
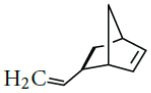
Compound	Toxicity	T_{melt} (°C)	T_{boil} (°C)	USD$/L
Dicyclopentadiene (DCPD)	Flammable, harmful 	32.5	170	~70
5-Ethylidene-2-norbornene (5E2N)	Harmful 	−80	148	~150
1,5-Cyclooctadiene (COD)	Harmful 	−69	150	~350
Methylcyclopentadiene dimer (MCPD)	Poisonous 	−51	70–80	~400
5-Vinyl-2-norbornene (5V2N)	Harmful 	−80	141	~200

Figure 3.3. The comparison of properties of different monomers (Aïssa et al., 2012)

3.1.5. Consumables

The consumables given in the Table 3.6 are used in this project with their properties and for the purposes remarked as below.

Table 3.6. The properties of consumables

Name of Consumable	Property	Supplier	Purpose of Using
Perforated release film FLD150-30/P3	Stands up to 150 °C Thickness: 30 µm	Dost Kimya	Allows controlled removal of excess resin
Breather Fabric 150	Stands up to 185 °C Weight: 150 g/m^2	Dost Kimya	To absorb excess resin
Vacuum Nylon TBL170-50	Stands up to 175 °C Thickness: 50 µm	Dost Kimya	To create a controlled environment
Vacuum sealing tape	Stands up to 130 °C	Dost Kimya	Sealant for vacuumed atmosphere
PTFE vacuum hoses	Stands up to 280 °C	Dost Kimya	Help to maintain proper pressure inside the vacuum bag
Nylon (PA6) monofilament	Stands up to 180 °C Diameter: 450 µm	Market	Microvascular channel building monofilament
Polivaks Max-9	Stands up to 200 °C	Yontar Polyester	To ease of removal of composite from the mold and to coat the monofilament

3.2. Method

This section provides the methods adopted in this study for the production of composite structures with microvascular channels, self-healing applications, preparation of test specimens, morphological inspections and performing the characterization tests for the modified microstructures. For the formation of microvascular channels inside the composite structure, different methods were followed in the scope of this study, by trying different configurations and materials. The systematic flow chart followed in this thesis to build a novel self-healing mechanism is provided in Figure 3.4. According to the ASTM D790 and ASTM D5045 standards, tests were performed and specimens in different configurations were manufactured based on these standards.

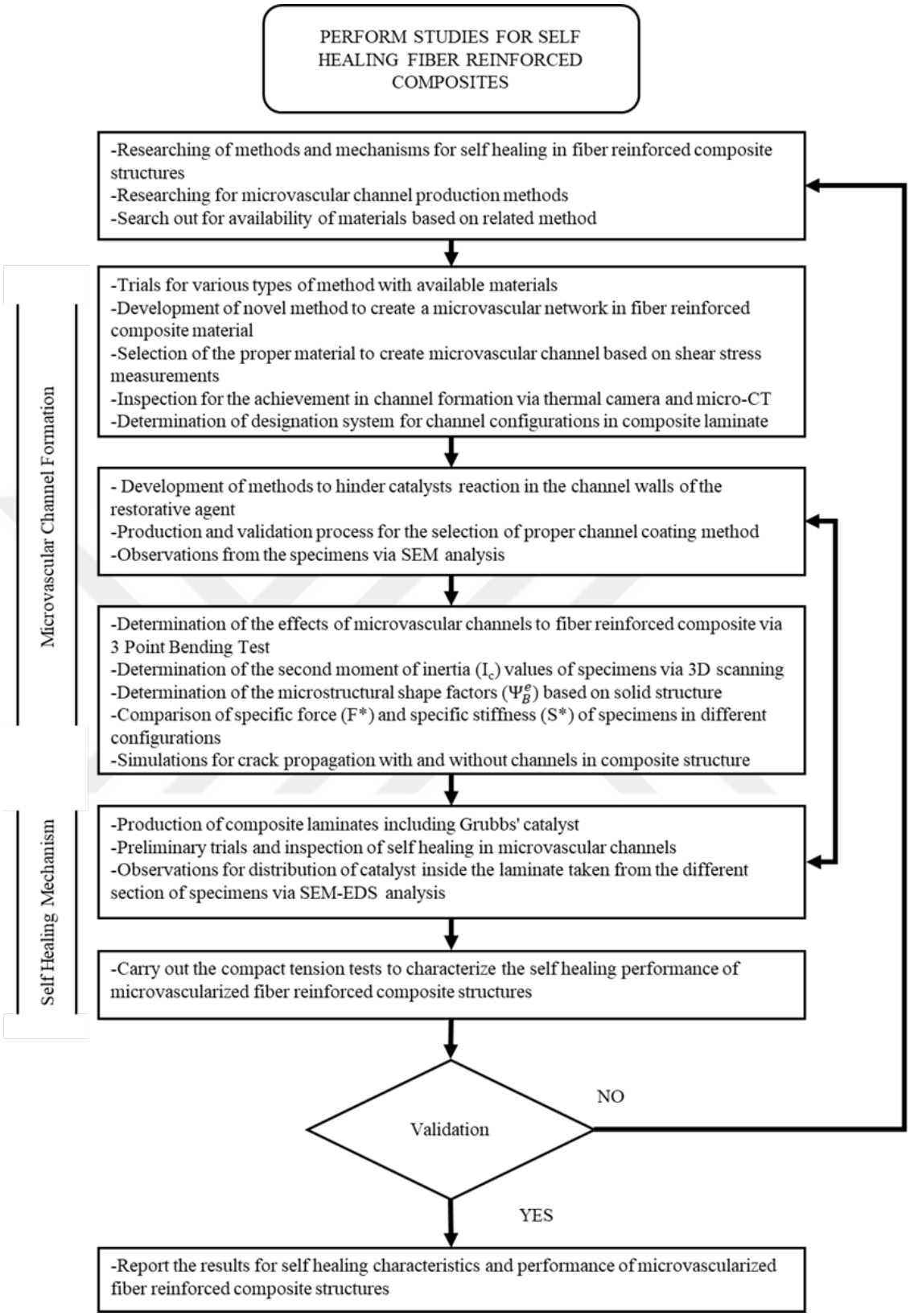


Figure 3.4. Flowchart demonstrating a systematic approach for building of novel self-healing mechanism for CFRP composite laminates

3.2.1. Manufacturing of Composite Structures

Hand lay-up and vacuum bagging method as outlined in Figure 3.5 is used for the production of CFRP composite laminates. Grubbs' catalyst is mixed with matrix polymer with the help of a 3-Roll Mill machine. The production steps are explained in this section. First of all, the size of the workpiece is specified according to the specimen dimensions and quantities.

According to the dimensions, 400x400 mm^2 MDF moulds for the hand lay-up and oven curing operations were manufactured as shown in Figure 3.6. The carbon fabrics and vacuum bagging consumables were cut in proper sizes. For the first experiment, the laminates are composed of four layers and for the others, all have eight layers of carbon fabrics.

In this study, the mass of the matrix material should be equal to the 1.25 times mass of the carbon fabric. For the 146 grams of fabric, 182 grams of epoxy-hardener mixture is prepared. Since the mixing ratio is 100:38 in weight, the weight of epoxy resin and its hardener should be 132 grams and 50 grams, respectively.

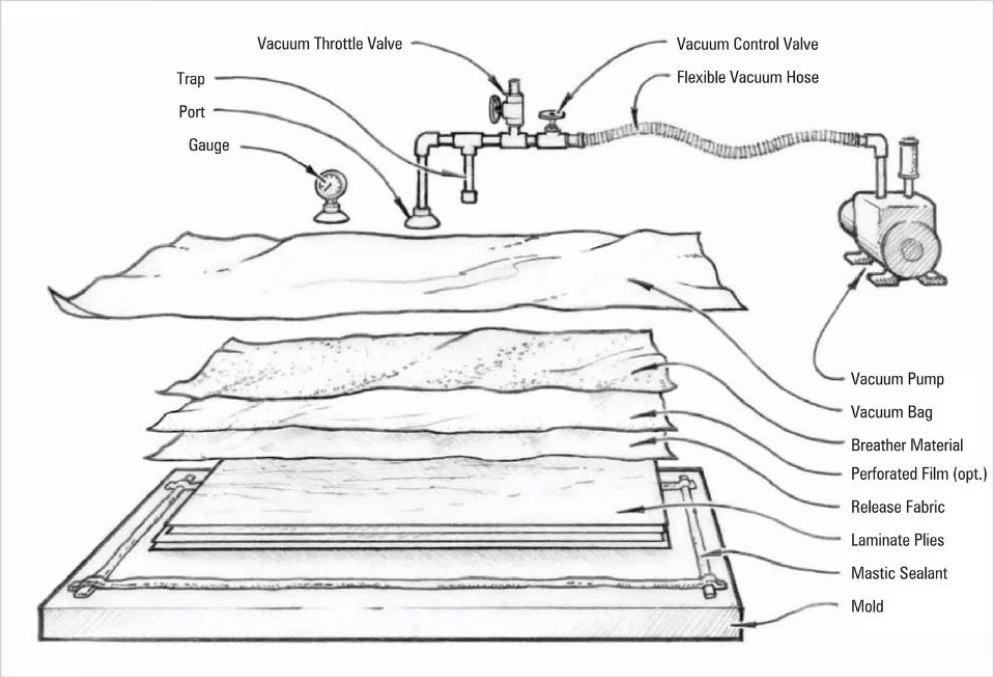


Figure 3.5. Outline of composite laminate production with vacuum bagging method (Vacuum Systems for Composite Manufacturing)



Figure 3.6. MDF molds manufactured for the hand lay-up and oven-curing operations

The weight of the Grubbs' catalyst in the CFRP composite laminate is determined as 2% of the total weight of the polymer matrix. So, if the structure involves Grubbs' catalyst, the weight of the catalyst based on the 182 grams of epoxy-hardener mixture should be 3.714 grams. The total weight of the matrix should be uploaded to 185.7 grams.

Mechanical mixers are not sufficient to mix Grubbs' catalyst into the epoxy resin homogeneously without clumping. Therefore, the epoxy resin was blended with Grubbs' catalyst by using the Fersah Makine 3 Roll Mill machine. After getting a homogeneous mixture, hardener was added to the mixture and finally, matrix material was obtained.

Figure 3.7 shows the general configuration of the 3 Roll Mill machines. The distance between the drums can be adjusted in micron resolution in the device. In the scope of this study, the distance between the feeding roll and the center roll is set to 180 µm and the distance between the apron roll and the center roll is set to 150 µm. The speed of the feeding roll is adjusted to 100 rpm. In order to obtain a homogeneous mixture, the collection and mixing processes were repeated 10 times. Figure 3.8. represents the mixing process of Grubbs' catalyst with 3 Roll Mills.

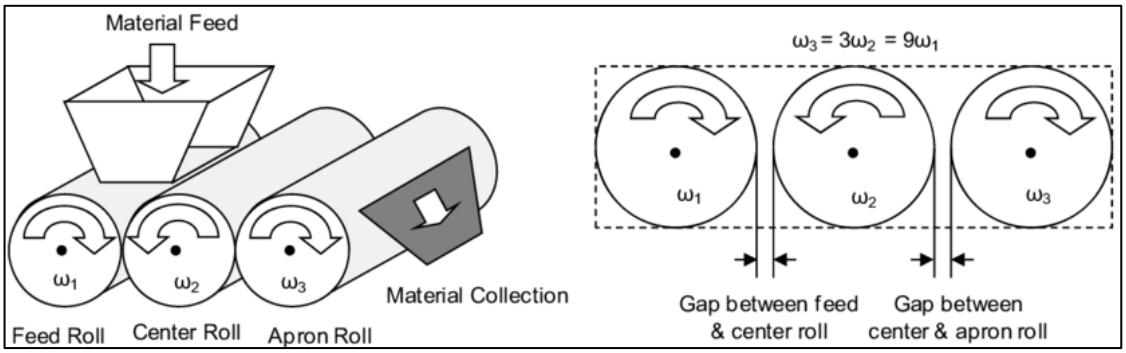


Figure 3.7. The general configuration of 3-Roll Mill Machine

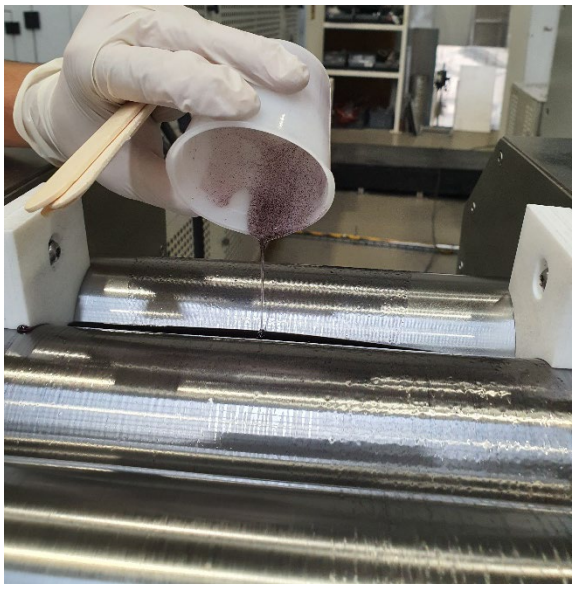


Figure 3.8. The mixing process of Grubbs' catalyst with 3-Roll Mills

Molds are coated with mold release agent and all required materials were put in an order as shown in Figure 3.9 and hand lay-up process is started as shown in Figure 3.10 by applying the epoxy resin to each layer of fabrics with a paint brush.

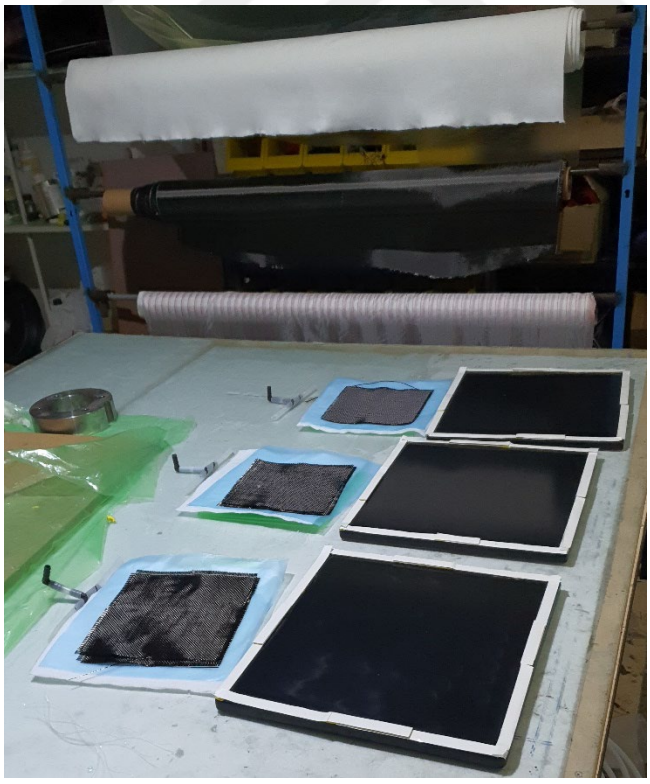


Figure 3.9. Preparation for the hand lay-up and vacuum bagging operations

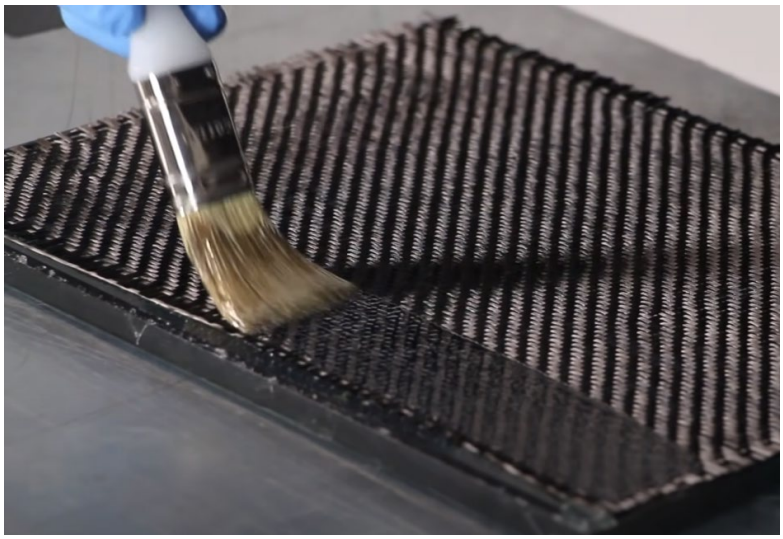


Figure 3.10. Hand lay-up operation of CFRP composite laminate

After the hand lay-up process is finished, the vacuum bagging is applied. The perforated release film is used between the breather and laminates to prevent them from adhesion. Then, a vacuum breather is placed on the top of the release film and all package is covered with vacuum nylon by attaching it to the sealant tape as shown in Figure 3.11.

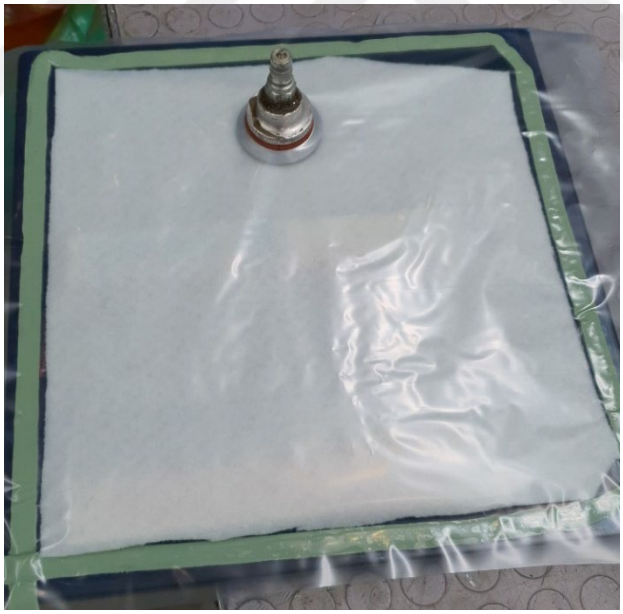


Figure 3.11. Vacuum bagging operation

The package is vacuumed via a vacuum pump, as the last step of the vacuum bagging method. Vacuum is applied at room temperature (25°C) for 30 minutes and then the molds are put into the hand-made curing oven at 120 °C under the vacuum atmosphere for 4 hours as shown in Figure 3.12. During this process, entrapped air bubbles inside the structure and excess resin in the laminate are evacuated.

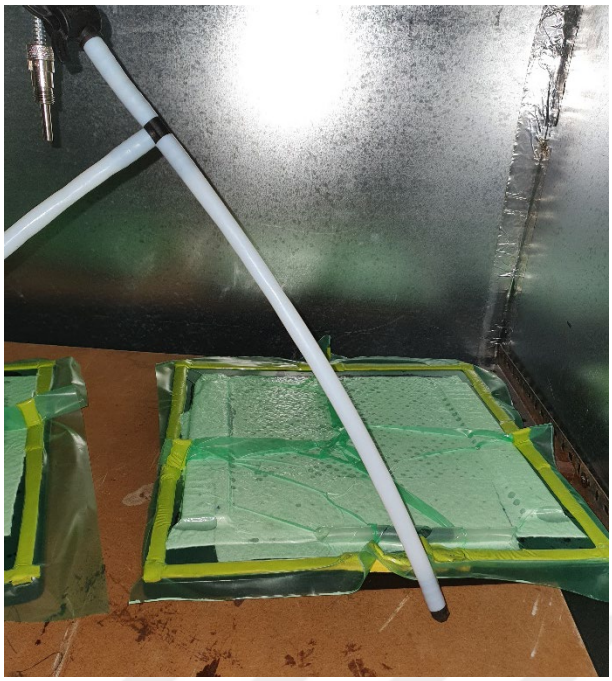


Figure 3.12. Molds in the curing oven under the vacuum atmosphere

After this process, the laminates were kept for nearly one week at room temperature for curing. Then, the laminates were cut based on the dimensions in standards that were previously defined for the related tests, with the help of the Diacam CNC Router, as depicted in Figure 3.13. In order to avoid from delamination and burrs during cutting operation, compression cutter is used instead of traditional end mills. If there are still burrs, they are grounded with sandpaper.



Figure 3.13. The specimen cutting with a CNC router

3.2.2. Manufacturing of Microvascular Channels

There are many methods for creating microvascular channels inside the composite structure for self-healing purposes. In the scope of the project, some available methods were investigated for material availability. Finally, a novel method was invented to create a microvascular channel into the CFRP composite structure.

Trials of Various Methods for Microvascular Channel Production

At the beginning of this study, it is focused on building the microvascular channels in the CFRP composite via the sacrificial fibers method. In this context, a material was investigated with a decomposition temperature between 180 °C, which is the maximum autoclave temperature, and 240°C, the temperature at which the delamination of the composite structure begins (Esser-Kahn et al., 2011). In this research, CES software in the CU Mechanical Engineering infrastructure was used. Thanks to this program, research and trials related to the supply and applications of the determined materials were carried out.

Based on the research, Bi58Sn42 Alloy wire, having 138 °C melting temperature, can be procured from the market as solder wire in 2 mm diameter. The diameter was reduced to 0.8 mm with a wire drawing machine in the jewellery workshop. Then, the wires were placed into the composite structure during manufacturing. After that, the specimens are subjected to 140 °C temperatures in the curing oven, and the behaviour of melted alloy wire has been observed.

Monofilament Removal Method for Microvascular Channel Production

Since a material that can operate in the specified temperature range (which is between 180°C - 240 °C) cannot be supplied, a novel method of pulling out monofilament materials placed in the composite was experienced as an alternative method for channel production. Within this scope, various materials (aluminium wire, galvanized steel wire, polyamide monofilament, etc.) were placed inside the carbon fiber composite structure during the hand lay-up process. After the curing, the process of pulling out the materials was tried for all the selected monofilament materials.

The wires and monofilaments which consist of different kinds of materials are placed in the composite laminates as demonstrated in Figure 3.14 in various configurations and it was tried to be removed by pulling them out of the structure. While selecting the most suitable material for the channel formation process, the pulling forces required to remove the test materials from the composite structure were measured with an Algol 50 kg-f Analog Push-Pull Force Gauge having 0.05 precision, as can be seen in Figure 3.15. Wires and monofilament were fixed to the gauge with intermediate apparatus and slowly pulled. The readings are recorded and the average shear stress values between the laminate and wire interface are evaluated based on 0.8 mm in wire diameter and 200 mm in wire length by using Equation 3.1. Also, the shear fracture forces of polyamide

monofilaments of different diameters are calculated by using the equation 3.1 for the allowable shear stress of 35 MPa (ANSYS Inc.).

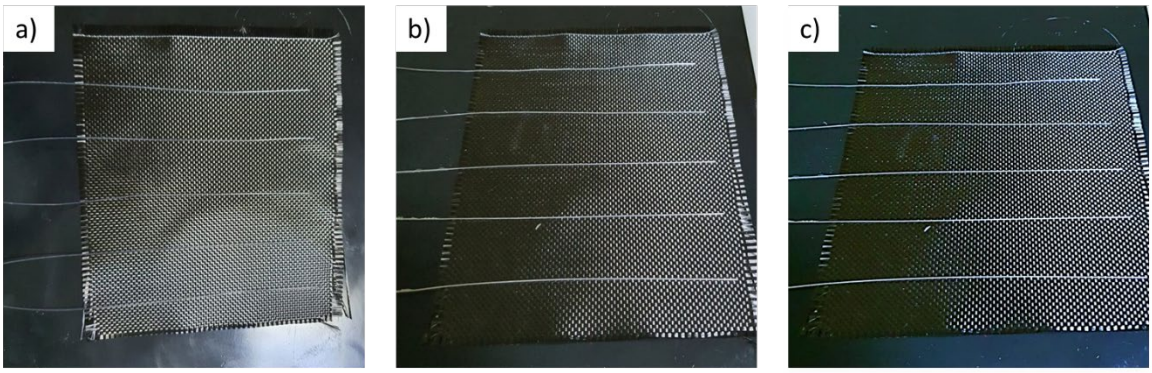


Figure 3.14. a) Polyamide monofilament, b) aluminium wire and c) galvanized steel wire placed in the composite structure for pulling force measurements

$$\tau = \frac{F}{\pi D_c L_c} \qquad 3.1$$

where,

F : Pulling force measured by analogue gauge, N

D_c : Diameter of monofilament or wire, mm

L_c : Length of monofilament or wire, mm

τ : Shear stress during pulling of monofilaments, MPa

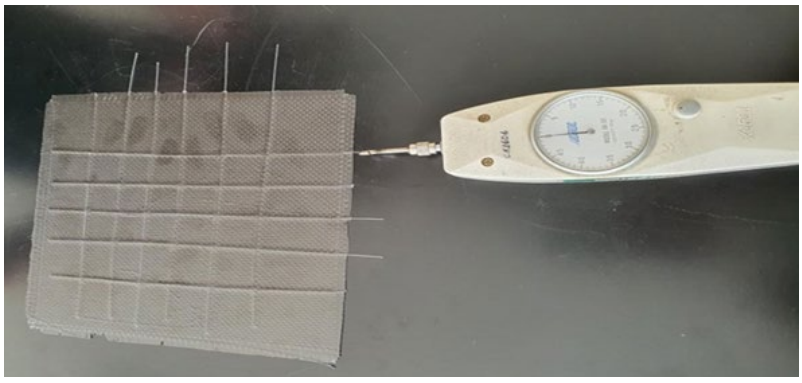


Figure 3.15. Measurements of shear forces of different monofilaments tried in pull-out method

It is necessary to observe channel continuity and production of microvascular channels properly. Since there are two methods followed in the scope of this study. First, hot water was injected into the microvascular channels, with an injector, and the flow and heat distribution in the channels were observed with the FLIR C5 thermal camera. In the samples manufactured for thermal camera monitoring, the channels were produced to be interconnected, as in Figure 3.16. So, the

application of this novel microvascular channel-building technique in complex orientations and transfer achievement between channels can be easily seen via thermal distribution during the injection of hot water.

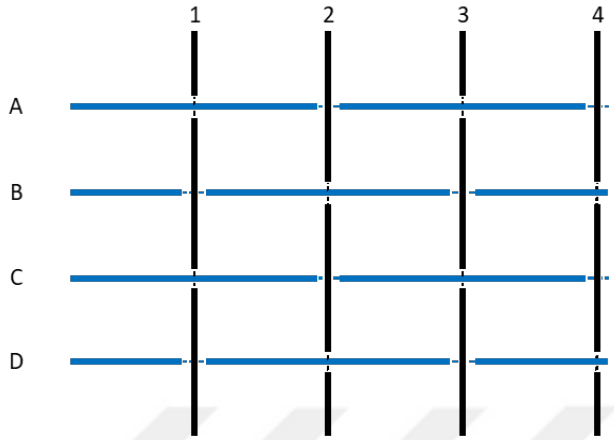


Figure 3.16. The interconnected channel configuration for thermal camera monitoring

The second method to see the channel formation into the CFRP laminate is micro-computed tomography (μCT). It is an imaging technique that allows the different density components of solid samples to be examined in high resolution, non-destructively in 3D.

In this study, the micro-CT scanning was performed by North Star Imaging Inc. X5000 Industrial CT X-Ray Inspection device. Scans were conducted at 68 kV voltage, 750 μA current and with 51 microns focal spot size in micro-focus focal spot mode, in this study.

A special frame containing monofilament parallel wires for channel configuration, shown in Figure 3.17, are produced to adjust and keep the distances between channels at constant gap for different configurations.

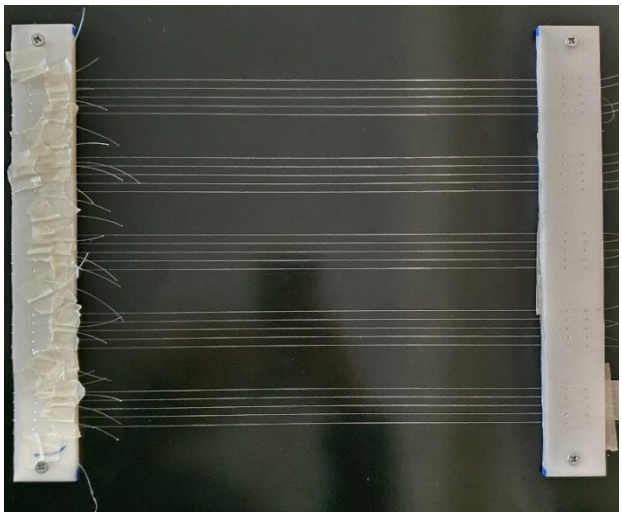


Figure 3.17. A special frame containing parallel monofilament wires for the channel configuration to keep the distances between channels at a constant gap

Designations of Microvascular Channels in Composite Laminate

Table 3.7 gives the code system used to determine the configuration of the channels placed in the composite structure. Experimental studies were carried out depending on these configurations. In order to better understand the code systematics used, as an example, 1710D states that there are empty channels between the first layer and the seven consequent layers (17), with a distance of 10 mm between channels (10) and the 3-Point Bending (3PB) Test was applied to the composite structure as the surface close to the channel is downward (D) whereas U represents upward position of faces which are close to microvascular channels during 3PB Test. Additionally, "26" in the 2610D configuration, represents that, there are empty channels between the second layer and the six consequent layers of composite laminate and E00 represents the solid composite laminate which does not contain microvascular channels. On the other hand, E1710D means that the channels are filled with epoxy (E) after the production of the 1710D configuration. The main reason for this configuration is to observe the results of solid composite laminate with a similar cross-sectional shape. Since the fluctuation of the laminate surface affects the shape factor, the channels were filled with epoxy in a specified configuration in order to make an accurate comparison between geometries, containing the channel hole and without the hole.

Table 3.7. The configurations of positions of channels in the CFRP composite laminates

Code	Fabric/Channel* Layers	Distance Between Channels	Position of Faces Close to Channels in 3PB Test	Channel Situation
1710D	1+C*+7	10 mm	Downward	Empty
1710U	1+C*+7	10 mm	Upward	Empty
1705D	1+C*+7	5 mm	Downward	Empty
2610D	2+C*+6	10 mm	Downward	Empty
E1710D	1+C*+7	10 mm	Downward	Filled w/ epoxy
E00	8	-	-	N/A
C*: There is channel-building monofilament between specified layers N/A: Not available				

Methods to Hinder The Restorative Agent Reaction with The Catalysts on The Microvascular Channel Walls

In the literature, for the mechanisms containing micro-channels, the self-healing process is usually carried out by filling the self-healing agent and the catalyst, in liquid form, through separate channels and the propagation of crack grows along these two channels. This healing is achieved by the ring- opening polymerization that occurs when the catalyst and agent came into contact.

In this thesis work, a self-healing mechanism is created by dispersed Grubbs' catalyst in the matrix of the composite laminate and the restorative agent is present in the channel. Since the ring-opening polymerization reaction occurs when the 5E2N agent comes into contact with Grubbs'

catalyst as soon as it is injected into the channel, a method was developed in this work. The developed method relies on coating the inner walls of the channels using various special coating chemicals as a solution to hinder earlier chemical reactions.

In order to coat the walls of the channels, two methods are conducted with wax-coating and epoxy-coating. And, to observe the difference between the neat and coated channels, CFRP composite laminate test specimens having uncoated, wax-coated and epoxy-coated channels, were produced.

In order to form the coated surfaces on the walls of the channels, first of all, the polyamide monofilaments were coated with neat epoxy (which is epoxy does not include Grubbs' catalyst) and mould-release agent (wax). Afterwards, these monofilaments were placed in the composite structure and CFRP composite laminate specimens were produced by vacuum bagging method. When the monofilament yarns are pulled out from the composite laminate after the curing cycle is completed, the coatings around the polyamide monofilament stick to the channel wall. Figure 3.18 illustrates how the coating method is applied to the wall of the microvascular channels.

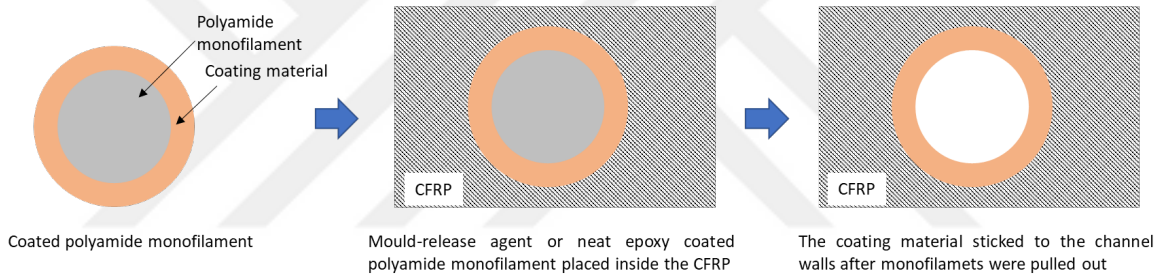


Figure 3.18. The representation of the channel coating method

The 5E2N healing agent was injected into the neat and coated channels as presented in Grubbs' catalyst dispersed composite laminate as shown in Figure 3.19(a). After the channels were completely filled with the restorative agent as observed in Figure 3.19(b), both ends were closed with sealing tape immediately as in Figure 3.20 and were left to stand in the composite structure for a week.

After one week, channel states for different types of coating applications are observed, after injection of the healing agent into the laminate.

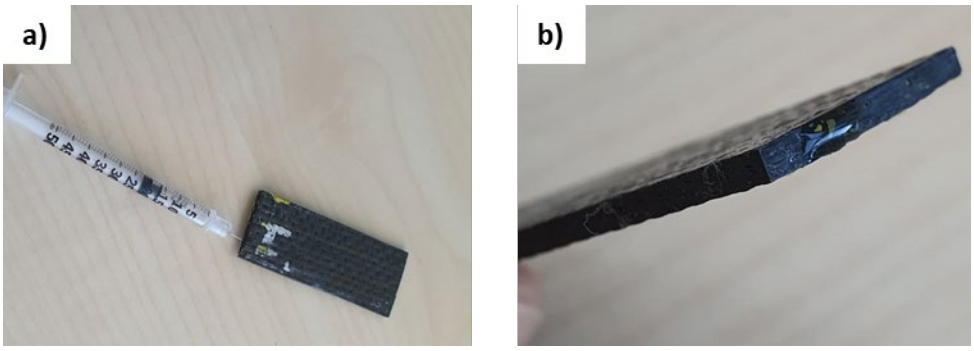


Figure 3.19. a) Injection of 5E2N monomer into channels and b) CFRP laminate after injection

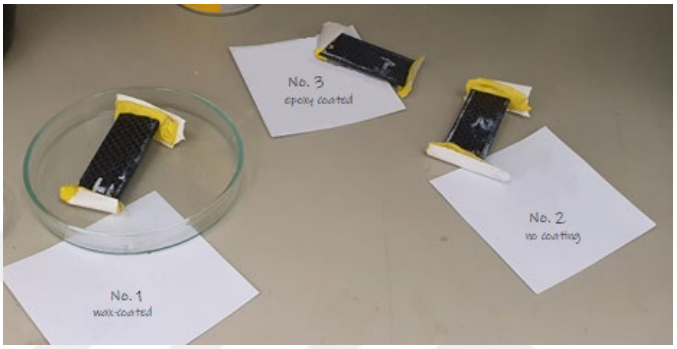


Figure 3.20. Different types of specimens of 5E2N were injected into the microvascular channels

3.2.3. Determining The Effect of Channels on The Strength of Composite Structure

In order to obtain the effect of the channels on the strength of the composite structure, the 3-Point Bending Tests were carried out according to the ASTM D790 standard on Instron 8801 (100 kN ±2N) universal test machine as in Figure 3.21.

In highly anisotropic materials, deflections in the shear direction at a low length/depth (L/d) ratio significantly reduce the modulus of elasticity. Therefore, the L/d ratio is set as 60:1 for a more accurate result. Since, the thickness of the specimens is approximately 2 mm, the span length is specified as 120 mm and width is 40 mm. Tests were applied to the samples at a speed of 4 mm/s.

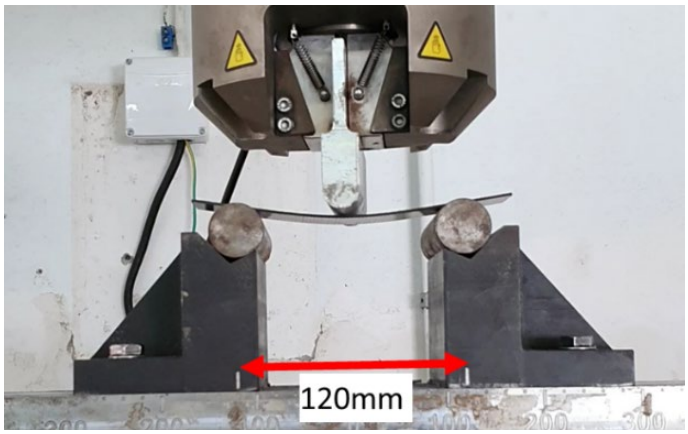


Figure 3.21. Performing the ASTM D790 Three-Point Bending Test for different microvascular channel configurations

The cross-sectional areas of the produced samples were scanned with the help of a Hexagon RS6 3D scanner and dimensional controls were conducted to evaluate the results of tests, accurately. Figure 3.22 shows the cross-sections of laminates in different configurations.

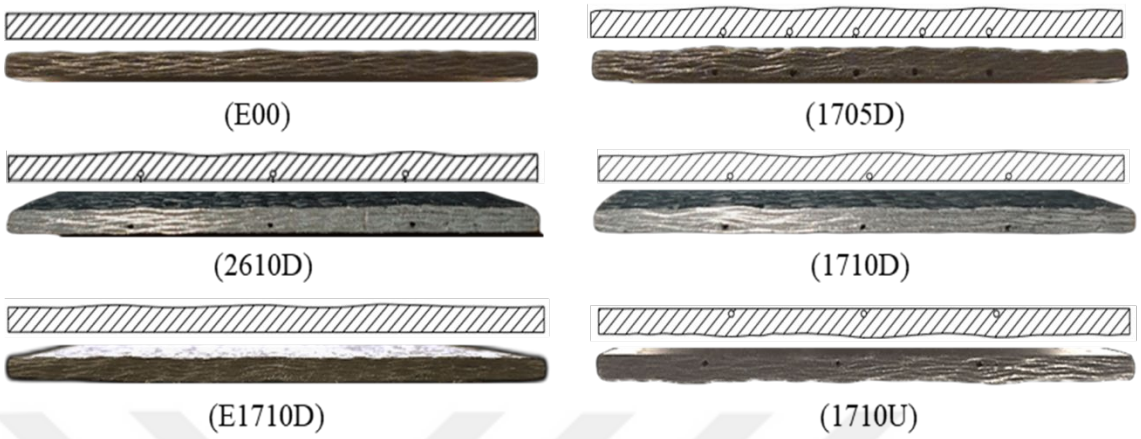


Figure 3.22. The cross-sectional images of different configurations

In the scans, it was observed that the composite structures with different channel configurations do not have the same cross-sectional area and geometry. This is because the laminates which have microvascular channels have corrugated top surfaces. Different configurations have different cross-sectional areas and second moment of area (I) values changing with channel position and quantity in the laminate. Also, it is hard to produce composite laminates with tight tolerances in thickness by vacuum bagging method.

The corrugated surface on the composite laminates creates a shape factor effect which changes the structure's stiffness and strength by changing the inertia and modulus values. Since the change in geometry is on small scale, the shape factor is considered a microscopic shape factor (Ψ). In order to compare the test results for the specimens in different microvascular channel configurations properly with each other's, the influence of the microscopic shape factors of the samples on the test results are eliminated. This elimination is obtained by dividing the results acquired from 3-point bending tests by the evaluated shape factors and as a result, the strength values regardless of the shape factor are evaluated as referred in detail in the next section.

Determining The Shape Factor of Laminates

While evaluating the shape factors, the E00 configuration was taken as the original solid shape without microchannels. The force and stiffness values obtained as results of the tests were divided by the shape factors. Then, the specific force and specific stiffness values were calculated according to the original structure. The new specific force and specific stiffness values are comparable values, regardless of the influence of the shape factor.

The solid which has a micro-structured shape, can be regarded as a new material with its modulus, strength density and so forth (Ashby, 2011b). So, the microscopic shape factor values can be evaluated by comparing the flexural modulus and moment of inertia values. Equation 3.2 shows the evaluation of the shape factor.

$$\Psi_B^e = \frac{S}{S_s} = \frac{EI}{E_s I_s} \tag{3.2}$$

On the other hand, the flexural modulus can be calculated as given in Equation 3.3 according to the ASTM D790 standard. If we evaluate the equation including the second moment of area (*I*), where its value is calculated as in Equation 3.4, the new equation for the flexural modulus will be as in Equation 3.5.

$$E = \frac{mL^3}{4bd^3} \tag{3.3}$$

where,

E : Modulus of elasticity in bending, MPa

L : Support span, mm

b : Width of beam tested, mm

d : Depth of beam tested, mm

m : Slope of the tangent to the initial straight-line portion of the load-deflection curve, N/mm

$$I = \frac{1}{12} bd^3 \tag{3.4}$$

$$E = \frac{mL^3}{48I} \tag{3.5}$$

After the modifications in the above equations, the second moment of area (*I*) values obtained from the 3D scanning for related configurations are directly used in Equation 3.5. The main reason to directly use the second moment of area (*I*) values is, that the top surfaces of the laminates do not have a flat geometry.

While the slope for the modulus measurements is calculated, the range between the 10% - 40% of maximum force values is taken into consideration to represent the values on the initial straight-line portion of the load-deflection curve, as shown in Figure 3.23.

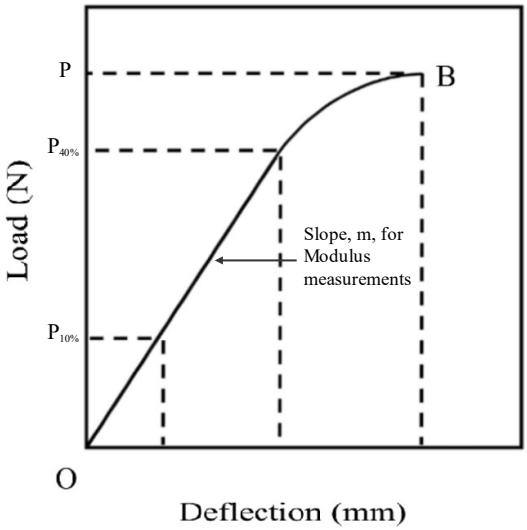


Figure 3.23. The representation of the 10% - 40% portion of the load-deflection curve for the slope calculations

After all modifications and calculations, the microstructural shape factors are evaluated for all related configurations by using Equation 3.2.

Comparison of the Results Irrespective of The Shape Factor

After the evaluation of microscopic shape factors for each configuration, the specific stiffness and specific force values are compared. The specific stiffness values are obtained by dividing the stiffness calculated from experimental test results (as shown in Equation 3.6) by microscopic shape factors of related configuration as shown in Equation 3.7.

$$S_{xx} = \frac{F_{max}}{\delta_{max}} \tag{3.6}$$

where,

S_{xx} : Stiffness of related configuration, N/mm

F_{max} : Maximum force obtained from test results, N

δ_{max} : Maximum displacement obtained from test results, mm

$$S^*_{xx} = S_{xx}/\Psi^e_{B\,xx} \tag{3.7}$$

where,

S^*_{xx} : Specific stiffness of related configuration, N/mm

$\Psi^e_{B\,xx}$: Microscopic shape factor values of related configuration

On the other hand, force values are modified irrespective of the shape factor to make a proper comparison on strength of laminates. The specific force values are obtained by dividing the force taken from experimental test results to microscopic shape factors of related configuration as shown in Equation 3.8.

$$F_{xx}^{*} = F_{xx}/\Psi_{B}^{e}{}_{xx} \tag{3.8}$$

where,

F_{xx}^{*} : Specific force of related configuration, N

F_{xx} : Force value of related configuration, N

The comparison is made between the specific stiffness values of all configurations according to the stiffness value of the solid structure and between the specific force values of all configurations according to the force value of the solid structure. These comparisons will give some knowledge about how the microvascular channels affect the mechanical properties of composite structures.

3.2.4. Morphological Characterization Methods

After completing the 3-Point Bending Tests, analyses were conducted utilizing a Scanning Electron Microscope (SEM) in order to observe the behaviour of the channels in the fracture zone. At the same time, SEM was used to see the cross-sections of channels after coating the channel walls and to validate the state of ring-opening polymerization reaction after injection of the healing agent into the channels.

SEM analyses were performed using the FEI Quanta 200 FEG E-SEM instrument. The samples were coated with Au/Pd thin film before analysing the microstructure. Images were taken at 10 kV acceleration voltage, in high resolution.

The distribution of Grubbs' catalyst in the composite laminate was analysed with the SEM-EDS analysis. The same E-SEM instrument is used for EDS analyses. The section, which is randomly taken from the composite laminate, having 1800 µm x 1400 µm surface area, was analysed. In these analyses, Phosphorus atoms (P) in the Grubbs' catalyst ($C_{43}H_{72}Cl_2P_2Ru$) in the relevant cross-sectional area were monitored by the mapping method.

3.2.5. Preliminary Inspection of Self-Healing in Microvascular Channels

The first inspection of a chemical reaction is carried out based on visual inspection. First of all, the 5E2N healing agent is dripped on a fair amount of Grubbs' catalyst and the reactions are observed visually by noticing the time. After that, the 5E2N healing agent is injected into the microvascular channels in the composite structures, one of them neat and the other containing

Grubbs' catalyst. The channels in the laminate containing Grubbs' catalyst, don't have any coating on its walls. After waiting a significant time, the polymerization inside the channels is observed by taking sections from the composite laminate. These observations were performed using SEM for the cross-sections in the related locations.

3.2.6. Self-Healing Characterization with Compact Tension Test

The compact tension test based on ASTM D5045 standards is performed to observe the operation of the self-healing process during crack propagation. In Figure 3.24, the technical drawing and a picture of the CFRP composite specimen manufactured to use in this experiment are presented. The specimen is mounted from the holes to the machine using special fixtures. Then, loading at a specific rate is applied to the material as shown in Figure 3.25, to initiate the crack propagation from a tip of the pre-cracked zone. In the next step, the load is released, and the self-healing action is observed when crack propagation coincides with the channel. After a while, the load is once again applied to the specimen, and the behaviour of the strength and self-healing mechanism in the crack zone is observed.

Two different approaches are followed during tests: Approach 1 is, that microvascular channels are filled with the healing agent, and subsequently the load is applied till the Crack Tip Opening Displacement (CTOD) value reaches a specified point where, just before the force reaches to the maximum value and crack initiated to propagate. At this point micro-cracks occur in the crack zone. After this, the load is released and specimens are held for different durations at room temperature so that the healing agent penetrates the micro-cracks, and healing action is completed during these durations. Approach 2 is, that microvascular channels are filled with the healing agent, and subsequently the load is applied to the specimens till the fracture is detected at a point where the force reaches the maximum value and then begins to decrease. At this point macro-cracks occur in the crack zone. Then, the load is released, and specimens are held for different durations at room temperature so that the healing agent penetrates the macro-cracks, and healing action is completed. For both approaches, to observe the effect of time on the self-healing mechanism, different durations are conducted, and these durations are called as healing time.

The compact tension tests are performed with the Shimadzu Autograph AG-IS 100 kN Universal Tensile Test Machine. Tests were applied to the samples at a speed of 2 mm/s and were conducted at a temperature of approximately 18 °C.

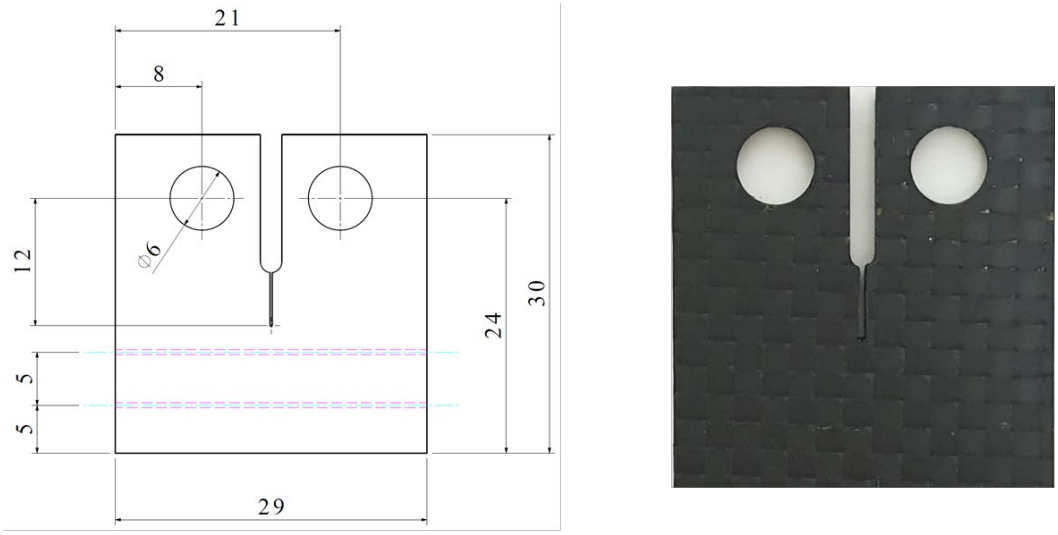


Figure 3.24. a) The technical drawing and b) a picture of the CFRP composite specimen manufactured based on ASTM D5045 to use in compact tension tests

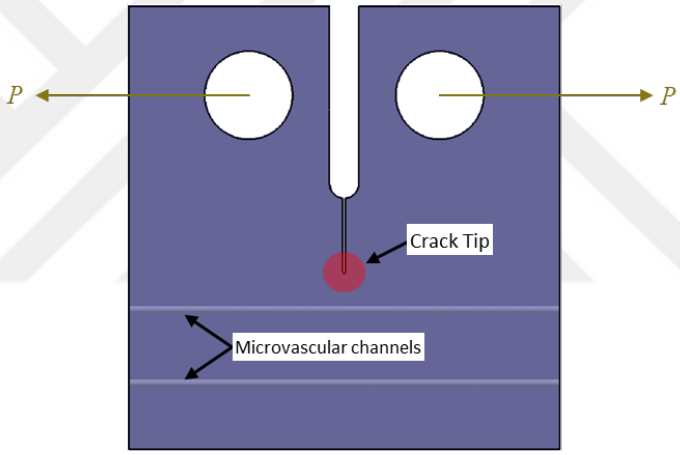


Figure 3.25. The demonstration of loads applied to the specimen to initiate crack propagation

The tests are conducted in different scenarios and for different healing times to determine the optimum healing conditions and to observe healing action while the crack is propagating. The test specimens are designated based on these scenarios as shown in Table 3.8. As an example, the coding of CTFB30 states that compact tension is applied to the specimen as shown in Figure 3.24(a), the channels are filled with a restorative agent (F), the test is stopped at a specific point before the force reaches to the maximum value and when the micro-cracks occurred (B) and then, the load is released and specimen is left to heal for 30 minutes (30). Also, code “A” in the CTFA30 states that the test is stopped after the fracture is detected at the point where, the force reaches the maximum value and then begins to decrease. At this point macro-cracks occur. At the same time, the CTS code represents the solid laminate without microvascular channels and CTE represents the virgin specimens with empty channels.

Table 3.8. The designations for specimens used in compact tension tests

Code	Channel Situation	Load release	Healing Time
CTS	Not Available	-	-
CTE	No agent	-	-
CTFB30	Filled with agent	When microcracks occurred	30 min.
CTFB60	Filled with agent	When microcracks occurred	60 min.
CTFB120	Filled with agent	When microcracks occurred	120 min.
CTFB150	Filled with agent	When microcracks occurred	150 min.
CTFA30	Filled with agent	When macrocracks occurred	30 min.
CTFA60	Filled with agent	When macrocracks occurred	60 min.
CTFA120	Filled with agent	When macrocracks occurred	120 min.
CTFA150	Filled with agent	When macrocracks occurred	150 min.

Additionally, the images of the crack zone are observed with a Nikon SMZ-745T stereo microscope after completing compact tension tests. The images give an idea about the situation of the crack zone and behaviour of the healing agent in this region.

The healing efficiency is evaluated based on calculations of Mode-I strain release rate (G_I) which is a measure of resistance to crack propagation where the crack faces move apart normal to the crack plane. The healing efficiency of a crack is expressed in literature as the ability of a healed sample to recover critical strain energy release rate (G_{Ic}) over the entire crack length (Wool and O'Connor, 1981; Brown et al., 2002),

$$\eta = \frac{G_{Ic_{healed}}}{G_{Ic_{virgin}}} \tag{3.9}$$

where, $G_{Ic_{healed}}$ is the critical strain energy release rate of the virgin specimen and $G_{Ic_{healed}}$ is the critical strain energy release rate of the healed specimen.

The measurement of strain energy release rate involves quantifying the amount of energy per unit area that is necessary for the propagation of a crack. The area method was employed in calculating the change in strain energy, which corresponds to the area under the load-displacement curve. Equation 3.10 illustrates the formula for the strain energy release rate at a specific incremental crack length (Δa).

$$G_I = \frac{\Delta U}{\mathrm{B}\Delta a} \tag{3.10}$$

where, ΔU is the change in strain energy, B is the width of crack and Δa is the crack length (Hashemi et al., 1990). For the same crack length and specimen width, the definition of healing efficiency can be simplified as the ratio of area under the load-displacement curve of healed specimen (ΔU_{healed}) to area under the load-displacement curve of virgin specimen (ΔU_{virgin}), as indicated in equation 3.11.

$$\eta = \frac{\Delta U_{healed}}{\Delta U_{virgin}} \qquad 3.11$$

4. RESULTS AND DISCUSSION

In the scope of this study, carbon fiber reinforced epoxy polymer composite laminates containing microvascular channels for the purpose of self-healing mechanism within the composite, in different configurations, were manufactured and the self-healing ability of the composite structures was observed.

Initially, the sacrificial fibers method was attempted to create microvascular channels in the composite structure. Degradation temperatures for some materials such as polyamide, polypropylene filaments and Bi58Sn42 bismuth tin alloy have been researched. However, these materials could not fulfil the thermal requirements of the sacrificial fiber method. Also, time-consuming pre- and post-processes are required in the sacrificial fiber method that Esser-Kahn et al. (2011) followed.

A novel method for the microvascular channel building into composite laminate was developed in this study. The effect of microvascular channels on the mechanical properties of the composite laminate was investigated by subjecting specimens to a 3-point bending test. Since the corrugated top surfaces appeared after building microvascular channels on the composite structure, the test results were modified as discussed in the previous section based on the microscopic shape factors. In this way, the effect of microscopic shape factor was eliminated, providing a more appropriate evaluation on the mechanical effects of microvascular channels.

The healing ability and properties of the composite structure having self-healing mechanism have been observed by the compact tension test, and the results were discussed in this section.

4.1. Discovery of Novel Microvascular Channel Production

Based on the sacrificial fiber method, the fiber material should stand up to maximum autoclave temperature, and it should decompose before reaching the minimum delamination temperature (Esser-Kahn et al., 2011) which are 180 °C and 240 °C for the epoxy that is used in this study, respectively. Candidate materials were determined using the CES software according to their melting and degradation temperatures. The decomposition temperatures of the candidate materials are determined and listed in Table 4.1. These materials are then investigated using the CES software whether they are suitable for the sacrificial fiber method. All of the selected materials are found to be outside of the required temperature range except for the PLA fiber treated with Tin Octoate (SnOx). Even though, PLA fiber treated with Tin Octoate (SnOx) appeared to be suitable material for the sacrificial fiber method in the first instance, the procurement of PLA fibers at the required diameters was found to be difficult in Turkey and most importantly, the pre-and post-processing requirements are quite time-consuming.

Bismuth wire was also placed in the composite structure and the sacrificial fibers method was applied. However, after the wire was melted, it could not be removed from the structure by vacuum suction.

As a result of all these studies, existing techniques to create microvascular channels into the composite structure were found to be not convenient within the bounds of possibility. A new, practical and easy method which is industrially applicable was essential to create microvascular channels in the composite structure.

Table 4.1. Properties of commercial candidate materials for the sacrificial fiber method determined with CES software

Material	Melting Temperature (°C)	Degradation Temperature (°C)
PLA (Polylacticacid)	190-200	290
PLA+SnOx (Polylacticacid + Tin Octoate)	N/A	200
PA11 (Polyamide/nylon 11)	180-190	440
PA6 (Polyamide/nylon 6)	210-220	398
PPE+PA (Polyphenylene ether + polyamide blend)	177-222	N/A
TPO (Thermoplastic polyolefin elastomer)	164-183	400
PP (Polypropylene)	160	447
PA612 (Polyamide/nylon 612)	195-219	473
Bi58Sn42 Bismuth Tin alloy	138	N/A

The monofilament removal method which is novel considering the existing methods in the literature was developed and applied successfully as a new method to create microvascular channels into the composite laminates. As an output of this study, a new technique and procedure was invented, and it is immediately protected by a patent application. It is going to be introduced to the literature after the international patent pending is completed.

4.1.1. Material Selection for Channel Formation

Even though, polyamide monofilaments were to be suitable materials for the patent-protected technique to create microvascular channels within the composite laminate, the possibility of using aluminium and galvanized steel wires were also investigated together with polyamide monofilaments. Sample plain-woven composite laminate specimens were produced containing polyamide, aluminium, and galvanized steel wires at the inner layers. The wires or monofilaments embedded into the composite laminate are then pulled out of the structure by applying a pulling force to build microvascular channels. During the removal process, because of the different coefficients of friction of the different materials, the pulling forces were measured and found to be different. So, while selecting the most suitable material for the channel formation process, the measurements for the pulling forces for wires and monofilaments which consist of different kinds of materials were tested.

According to the measurements, the average tensile forces for polyamide monofilament, aluminium wire and galvanized wire were determined as 5.6 kg-f, 19.9 kg-f and 30.2 kg-f, respectively for the specimen length of 200 mm and wire diameter of 0.8 mm. The average shear stress values are also obtained using equation 3.1 as shown in Table 4.2.

The main reason why polyamide monofilament is easily removed from the composite laminate is the polyamide does not form any bond and interaction with epoxy polymer. On the other side, since the thermal expansion coefficient of Polyamide ($85x10^{-6} K^{-1}$) (ANSYS Inc.) is higher than that of the plain-woven composite laminate through-the-thickness direction ($56.5x10^{-6} K^{-1}$) (Joven et al., 2012), the monofilaments expand during the curing process (at 120 °C) and shrink more than laminate during cooling. Hereby, it becomes easier to remove the polyamide material than the remaining candidates.

Table 4.2. Pull-out resistance force measurements for 200 mm specimen length and average shear stress values during pulling out of different materials

Type of Material	Pull-out Resistance Force (N)	Shear Stress during Pulling out (MPa)
Nylon based monofilament	54.77	0.11
Aluminium wire	195.38	0.39
Galvanized steel wire	295.94	0.59

Based on these results, polyamide monofilament was selected as the best material for the channel formation process, and this novel method with this material is used to create microvascular channels inside the composite specimens in the remaining section of the study. Also, the pulling-out and fracture forces of polyamide monofilaments of different diameters in 1-meter lengths are given in Table 4.3.

Table 4.3. The pull-out and shear fracture forces of polyamide monofilaments of different diameters for 1-meter length

Diameter (mm)	Pull-out Force (kN/m)	Shear Fracture Force (kN/m)	Diameter (mm)	Pull-out Force (kN/m)	Shear Fracture Force (kN/m)
0.1	0.035	10.996	0.6	0.207	65.973
0.2	0.069	21.991	0.7	0.242	76.969
0.3	0.104	32.987	0.8	0.276	87.965
0.4	0.138	43.982	0.9	0.311	98.960
0.5	0.173	54.978	1.0	0.346	109.956

4.1.2. Selection of the Way of Channel Wall Coating

In the literature studies, the healing agent and catalyst are kept in separate channels in liquid form within the structure. In other words, only when the crack is propagated along two separate channels, does the agent and catalyst get mixed and trigger the self-healing mechanism on the crack zone (Patrick et al., 2014, Therriault et al., 2003).

In this thesis work, the catalyst added to the epoxy polymer matrix is distributed uniformly inside the composite laminate and located on the channel walls. The healing agent is injected inside the microvascular channels and all channels are filled with the agent and stored.

During the initial trials, the healing agent reacted immediately with the catalyst presented on the channel walls when it was injected into channels. As a result of this, microvascular channels have been fully closed off or partially blocked. To remedy this issue, the walls of the channels were then coated with different coating (wax and epoxy) materials. To evaluate the effect and performance of these coatings around the channel walls, small cross-sections were taken from the prepared samples and analysed with SEM. In Figure 4.1(c), the epoxy layer can be seen on the walls of epoxy-coated channels. However, as shown in Figure 4.1(b), there is clearly no layer around the periphery of the wax-coated channel wall.

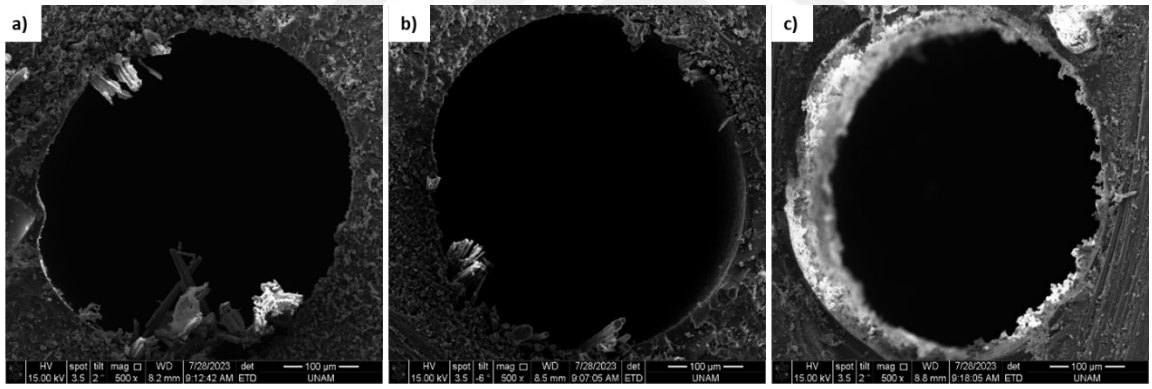


Figure 4.1. SEM images of a) uncoated b) wax-coated and c) epoxy-coated microvascular channels

The observations by using SEM, as shown in Figure 4.2, were made on the specimens to investigate, whether the 5E2N agent injected into the channels reacted with the composite structure containing Grubbs' catalyst. In samples containing uncoated and wax-coated channel walls, polymerization reactions took place between the Grubbs' catalyst and the healing agent. Then, the microvascular channels were filled up with polymer as shown in Figure 4.2(a and b). On the other hand, it is seen that there is no polymerization reaction in the epoxy-coated channels and the channels remain fully clear and open as seen in Figure 4.2(c).

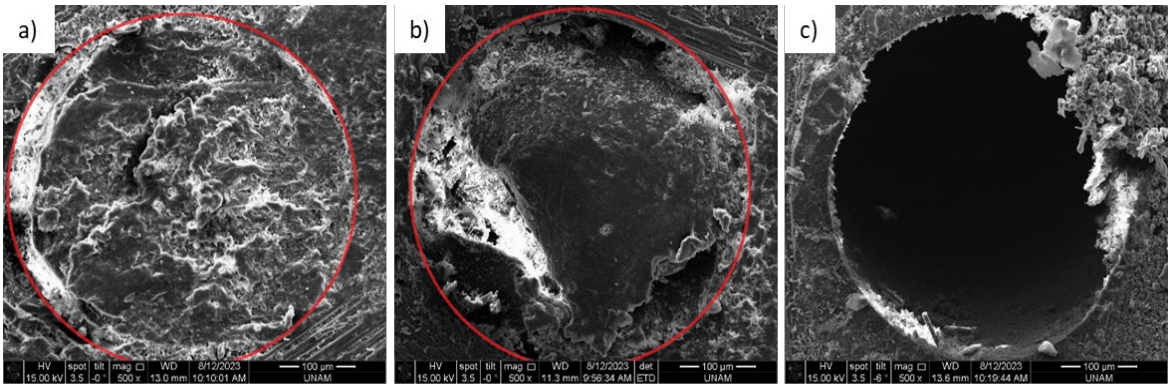


Figure 4.2. SEM images of a) uncoated b) wax-coated and c) epoxy-coated microvascular channels after 5E2N agent injected into channels

As a result of the SEM analysis, epoxy coating provided a barrier around the microvascular channel walls and prevented self-healing before crack formation. This is because there was not any unexpected reaction that occurred with the Grubbs' catalyst and 5E2N healing agent.

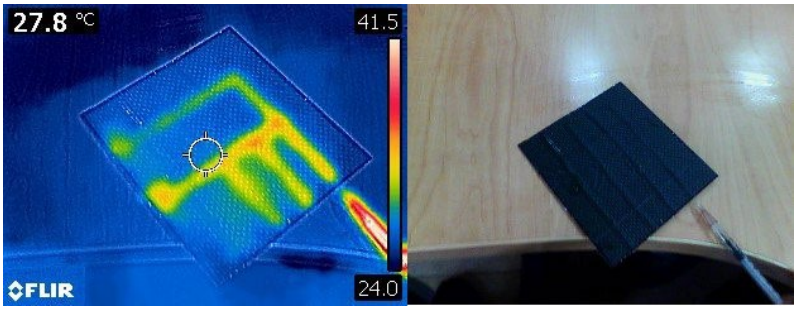
4.2. Inspection of Channel Structure Inside Composite Laminate

It is necessary to observe whether the microvascular channels created during the channel formation process are completely open and whether there is any structural deterioration. Various methods have been applied to obtain images or examine the presence and shape of microvascular channels within the composite structure, such as by using a thermal camera and scanning with micro-computed tomography (μCT). Both methods were used as discussed below.

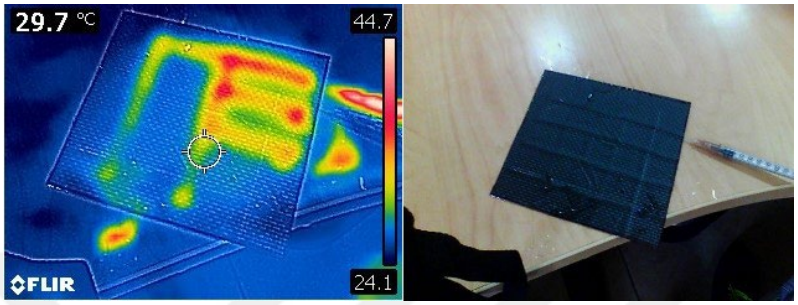
4.2.1. Inspection via Thermal Camera

This method can be considered as a crude approach to visually examine the formation of microvascular channels inside the CFRP composite laminate. Initial investigations were carried out by injecting water at room temperature through the channels to test whether there was any disruption such as clogging of the channels during the channel creation process and whether the connection between the channels was successful. It was observed that water reached all channels and exited from the other end of each channel. This means that the interconnection between channels is successfully established and there is no blockage in the microvascular channels.

In order to visualize the success of the channel creation process, hot water was injected into a few channels in a laminate with interconnected microvascular channels. Then, the change in heat distribution during water flow in the channels was recorded with a thermal camera. It is observed that hot water was distributed successfully to other interconnected channels. Pictures showing the flow of hot water inside the connected channels were captured and shown in Figure 4.3.



(a)



(b)

Figure 4.3. Thermal camera images of hot water injected composite laminates containing interconnected microvascular channels

Inspection with a thermal camera offers the opportunity to make practical observations on the successful creation of microvascular channels without the need for high-technology visualization techniques. As a results of this, it is proven that channels were created successfully and the connection between channels was easily achieved by the use of the novel microvascular channel formation method developed in this study.

4.2.2. Micro CT Inspection

Micro CT is a high-resolution imaging technique that enables non-destructive 3D examination of different densities within the solid structure. The clearance and state of the microvascular channels inside the composite structures were easily detected by µCT as shown in Figure 4.4. The black areas in the X-ray scans indicate the clearances and voids, dark grey areas in the X-ray scans indicate the dense epoxy and polymer matrix, and the light grey areas in the X-ray scans indicate the carbon fabric in the composite laminate.

From the µCT X-ray scans it is seen that the microvascular channels are built successfully by the novel channel formation technique. Microvascular channels are clean and wide open through the composite laminate as indicated in Figure 4.4(d and f) showing the results of X-ray scanning. Also, the scan in Figure 4.4(h) for the microvascular channels that are uncoated and the 5E2N healing agent injected inside shows that the agent undergoes a ring-opening polymerization reaction with catalyst resulting in the closure of the channels.

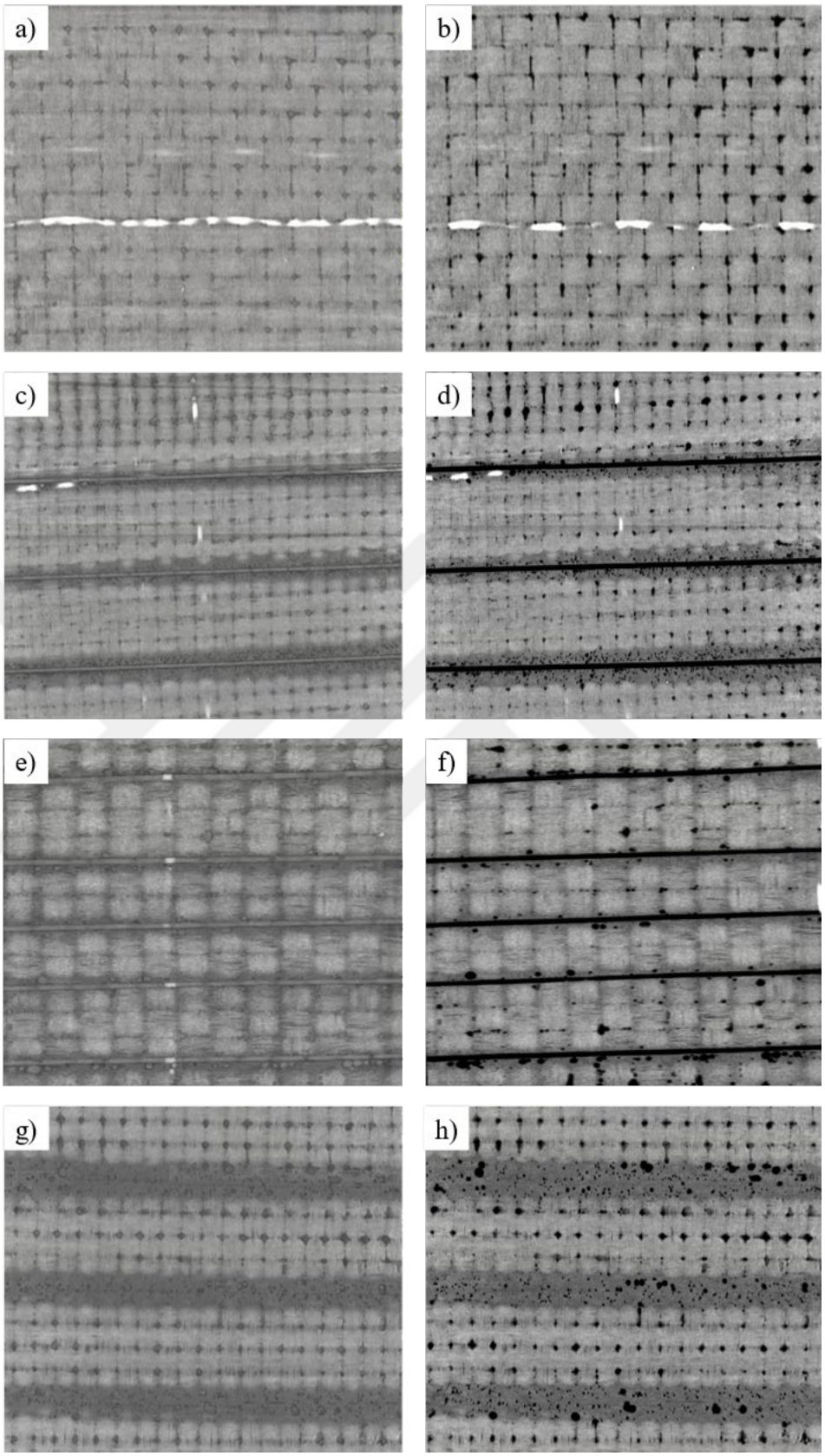


Figure 4.4. 3D scanned images obtained from μCT inspection of specimens including a) no channels, c) three channels, e) five channels, g) uncoated channels which are healed after 5E2N is injected. X-ray scan images obtained from μCT inspection of specimens including b) no channels, d) three channels, f) five channels, h) uncoated channels which are healed after 5E2N is injected

4.3. Mechanical Performance of Composites Including Microvascular Channels

It was investigated whether the channels, created to provide self-healing properties within the composite structure, had a negative impact on the strength of the structure. To be able to determine the impact of microvascular channels on the mechanical characteristics of composite structures, specimens in various channel configurations were subjected to 3-point bending tests. The force-displacement curves of each test result for each configuration are plotted as indicated in figures from Figure 4.5 to Figure 4.10.

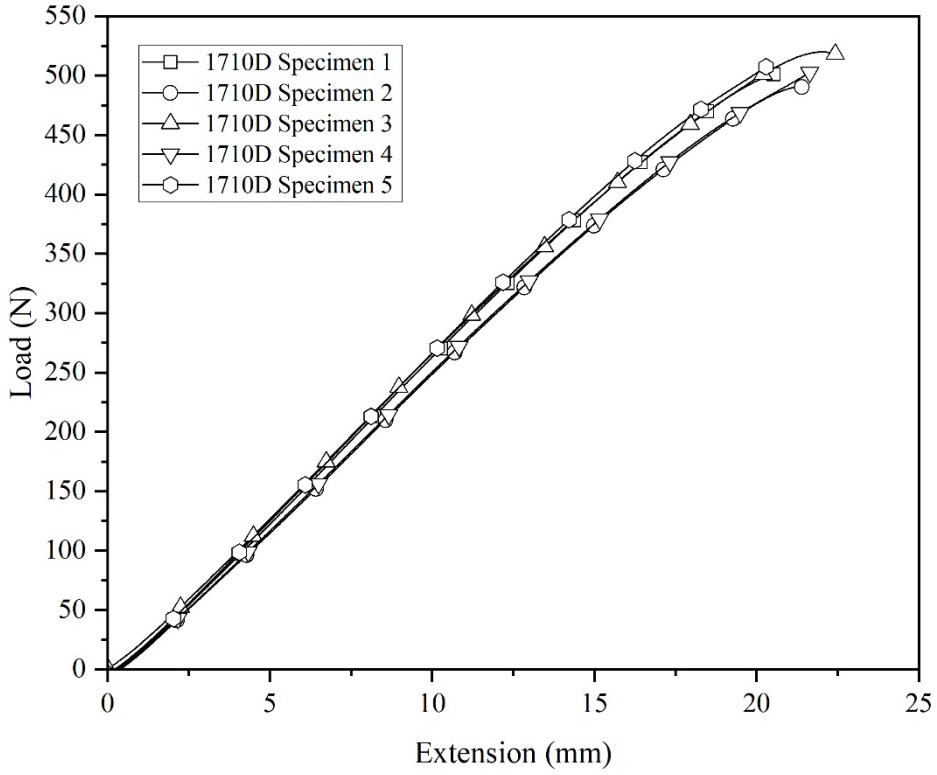


Figure 4.5. Load–extension curves as a result of 3-point bending tests conducted for specimens in E00 configuration

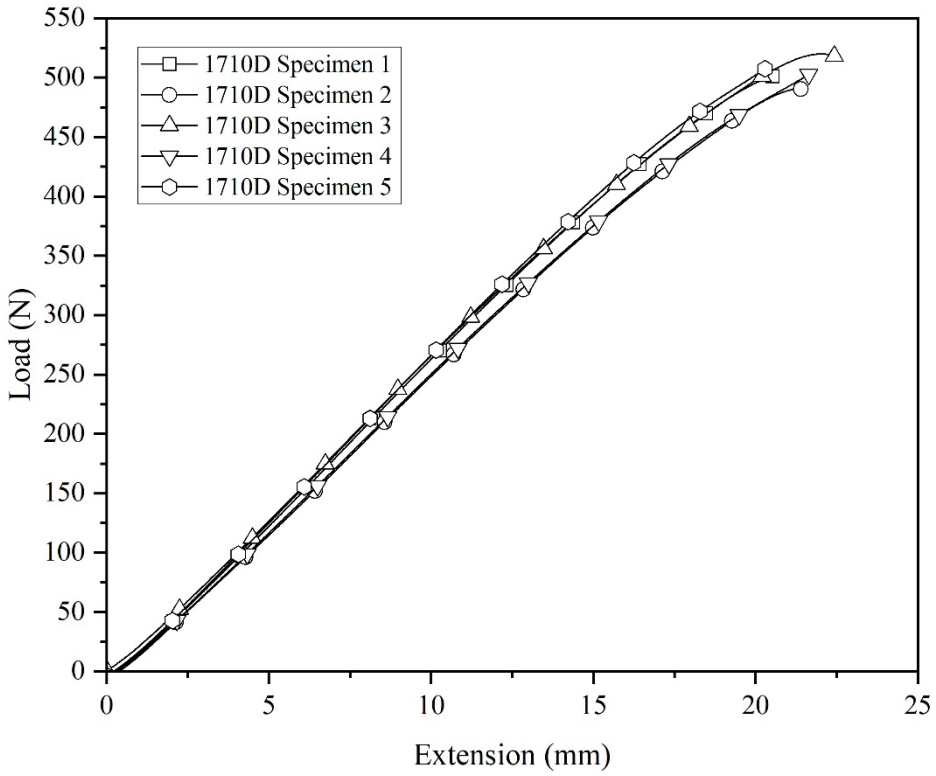


Figure 4.6. Load–extension curves as a result of 3-point bending tests conducted for specimens in 1710D configuration

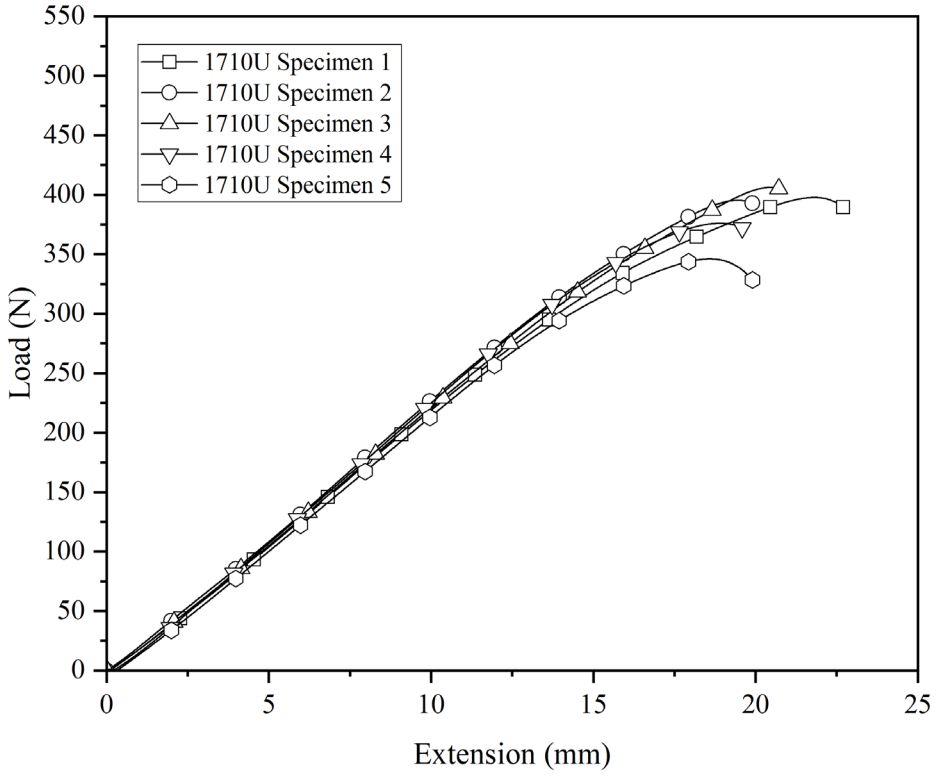


Figure 4.7. Load–extension curves as a result of 3-point bending tests conducted for specimens in 1710U configuration

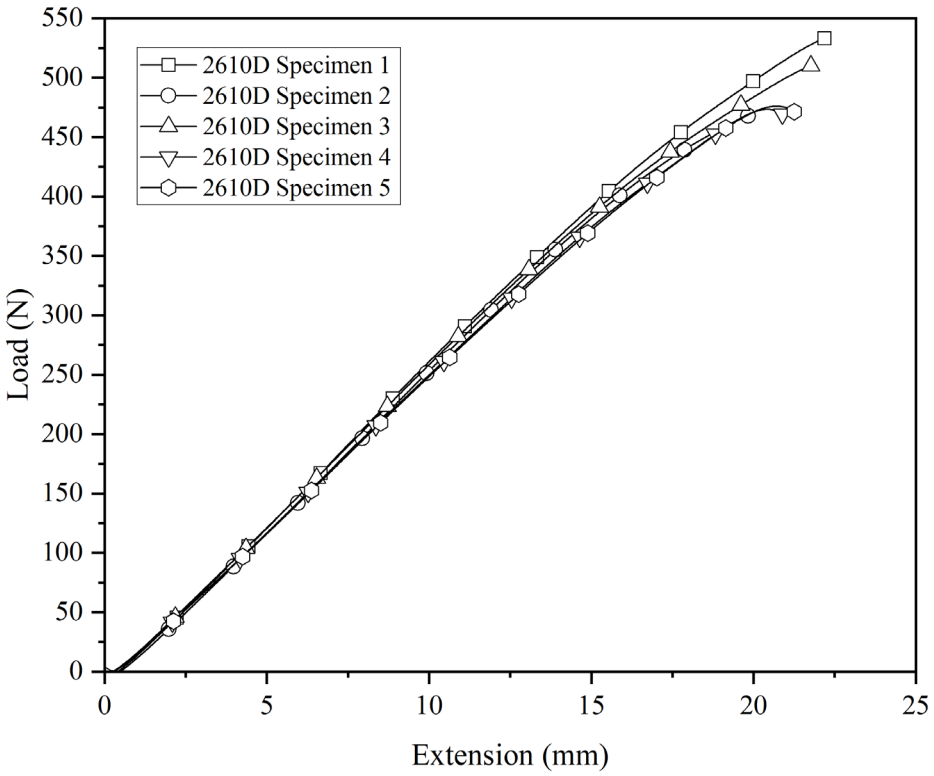


Figure 4.8. Load–extension curves as a result of 3-point bending tests conducted for specimens in 2610D configuration

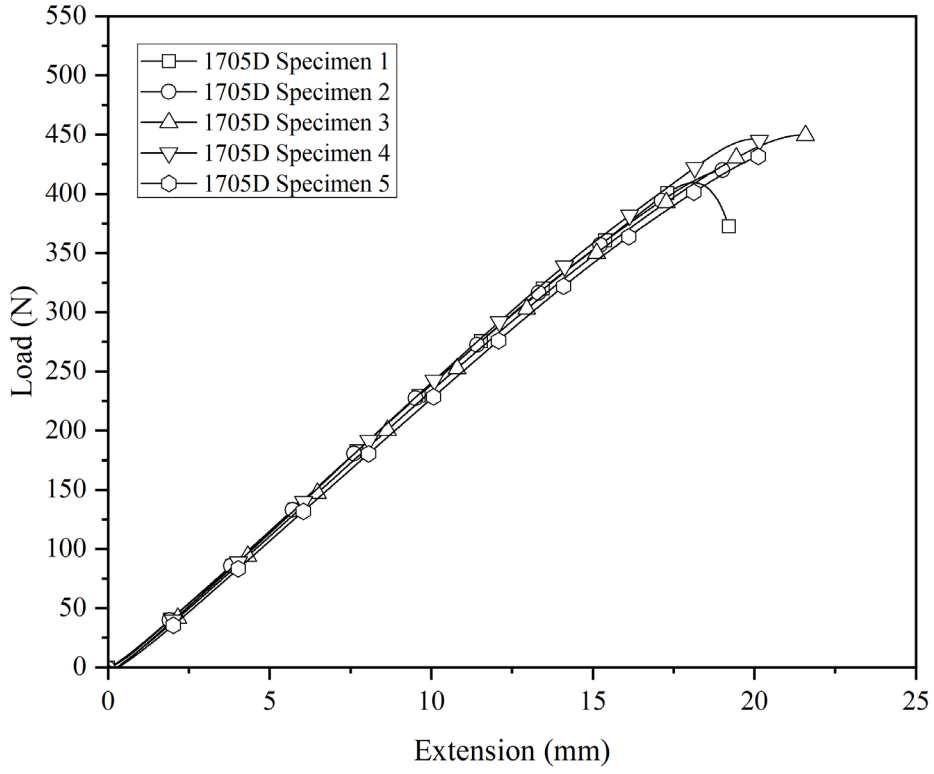


Figure 4.9. Load–extension curves as a result of 3-point bending tests conducted for specimens in 1705D configuration

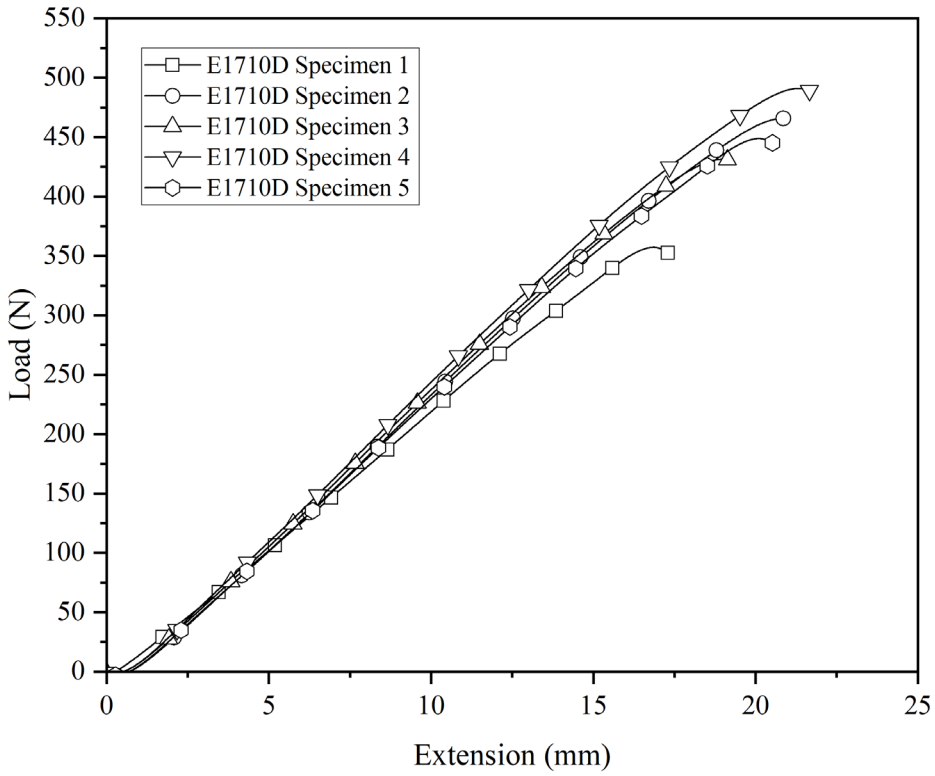
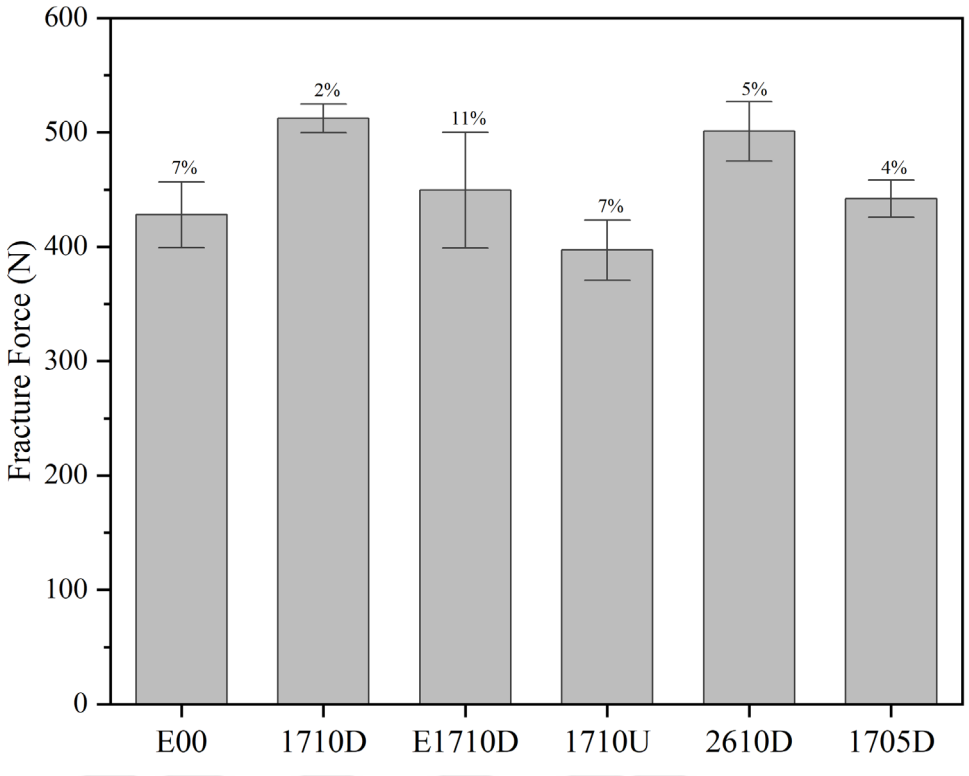


Figure 4.10. Load–extension curves as a result of 3-point bending tests conducted for specimens in E1710D configuration

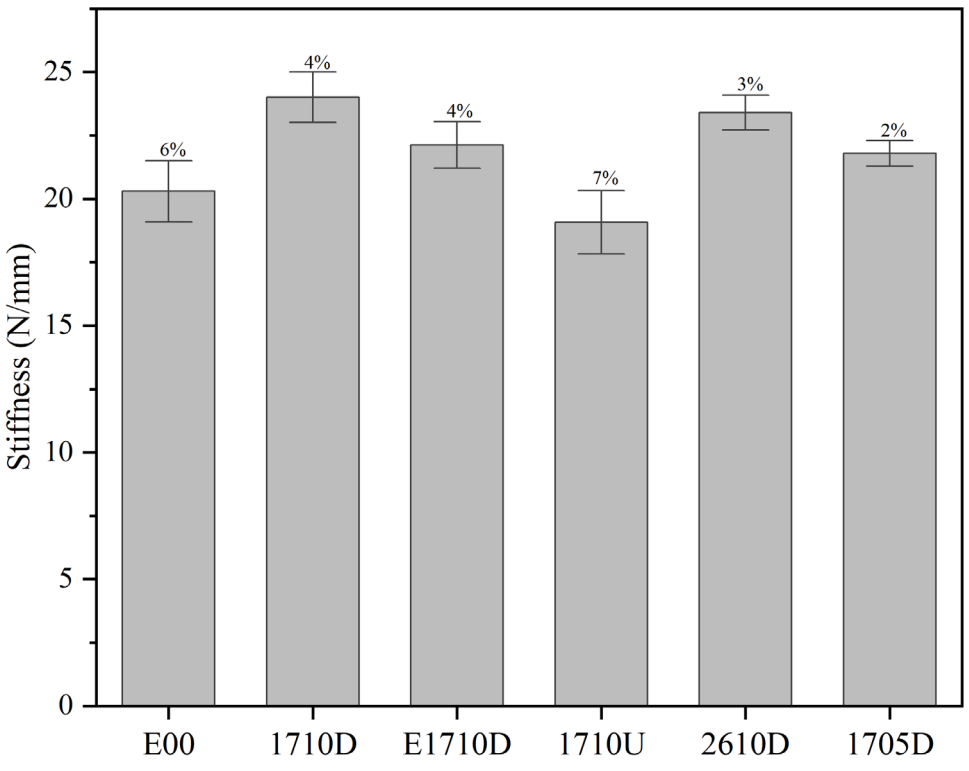
According to the experimental results obtained from 3-point bending tests, fracture forces and stiffness values for specimens in various configurations are compared with each other by plotting them on the bar charts including standard deviations as indicated in Figure 4.11 and average values of the results were tabulated in Table 4.4. The stiffness values are obtained by using Equation 3.7.

Table 4.4. Averages of fracture force, deflection and stiffness values of specimens in different configurations and their standard deviation values

Configuration	Average Fracture Force (N)	Standard Deviation (N)	Relative Standard Deviation	Average Extension (mm)	Standard Deviation (mm)	Relative Standard Deviation	Average Stiffness (N/mm)	Standard Deviation (N/mm)	Relative Standard Deviation
E00	427.96	28.77	7%	21.13	1.82	9%	20.30	1.20	6%
1710D	512.34	12.51	2%	21.37	0.92	4%	24.01	1.00	4%
E1710D	449.54	50.57	11%	20.27	1.59	8%	22.13	0.92	4%
1710U	397.13	26.28	7%	20.85	1.25	6%	19.07	1.24	7%
2610D	501.01	26.05	5%	21.40	0.79	4%	23.41	0.69	3%
1705D	442.08	16.40	4%	20.30	1.01	5%	21.79	0.51	2%



(a)



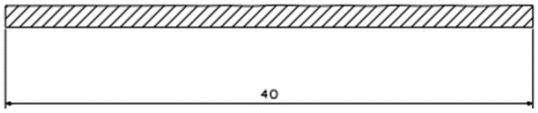
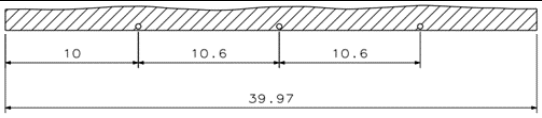
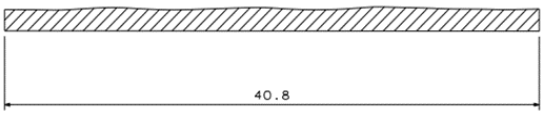
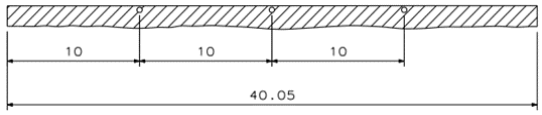
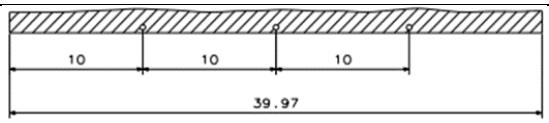
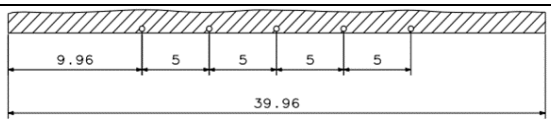
(b)

Figure 4.11. Bar charts of a) fracture forces and b) stiffness values in different configurations based on 3-point bending test results

According to these comparison results, it is observed that the strength and stiffness values of composite specimens with 1710A and 2610A channel configurations are approximately 20% better than those of specimens without channels. However, the main reason in this case is that composite structures with different channel configurations do not have the same cross-sectional area and the corrugations that occur on the upper surfaces of composite structures with microvascular channels create a shape factor effect in the structure. Due to this effect, the results cannot be evaluated directly and compared appropriately.

In order to make more appropriate comparisons, shape factors are determined for each configuration with reference to the solid shape, which is the E00 configuration, as explained in section 3.2.3. First of all, the second moment of area (*I*) values, which is necessary to calculate the microscopic shape factor, are obtained from the 3D scanning as shown in the Table 4.5 and shape factor values are calculated as indicated in Equation 3.2 by using these inertia values.

Table 4.5. Scanned cross-sections and second moment of area (I) values of each configuration

Configuration	**Scanned Cross-Section**	**Max. - Min. Thickness (mm)**	**Second Moment of Area I_x (mm^4)**
E00		1.67-1.59	14.29
1710D		1.89-1.53	16.62
E1710D		1.78-1.57	15.11
1710U		1.74-1.47	12.94
2610D		1.78-1.51	13.77
1705D		1.65-1.46	11.95

Normally, the second moment of area values of samples having microvascular channels are expected to be lower than those of sample having no channel because, there are gaps causing

subtraction in the cross-sectional area due to the channel (Budynas et al., 2011). However, the reason why the second moment of area value is higher for the sample in the 1710D configuration, which has microvascular channels, is that its thickness is approximately 0.2 mm thicker than the E00 configuration. These thickness values are available in Table 4.6.

After obtaining the microscopic shape factors for each configuration, the fracture force and stiffness values according to the 3-point bending test results are modified based on Equation 3.7 and Equation 3.8 in order to eliminate the shape factor effect of the corrugated top surfaces on the composite laminate. The specific force (F*) and specific stiffness (S*) values irrespective of the shape factor effect are obtained as a result of this modification. The average values of specific force, specific stiffness and shape factor values are tabulated in Table 4.6 and the bar charts including standard deviations to make a comparison irrespective of the effect of shape factor are plotted as shown in Figure 4.12. As a result of this comparison, the effect of channels on the mechanical properties of the composite structure is evaluated according to the channel quantity and location within the composite laminate.

Table 4.6. Averages of specific fracture force, specific stiffness and shape factor values of specimens in different configurations

Configuration	Max. - Min. Thickness (mm)	Second Moment of Area I_x (mm^4)	Average Shape Factor ($\Psi^e_{B_{xx}}$)	Average Specific Fracture Force (N)	Standard Deviation (N)	Relative Standard Deviation	Average Specific Stiffness (N/mm)	Standard Deviation (N/mm)	Relative Standard Deviation
E00	1.67-1.59	14.29	1.00	427.96	28.77	7%	20.30	1.20	6%
1710D	1.89-1.53	16.62	1.20	426.46	7.68	2%	19.99	0.88	4%
E1710D	1.78-1.57	15.11	1.12	402.31	29.75	7%	19.86	0.65	3%
1710U	1.74-1.47	12.94	1.01	394.82	23.07	6%	18.96	1.02	5%
2610D	1.78-1.51	13.77	1.19	420.87	18.18	4%	19.67	0.49	2%
1705D	1.65-1.46	11.95	1.09	406.01	13.98	3%	20.02	0.79	4%

While considering the standard deviations of the results which are obtained by eliminating the effect of the microscopic shape factor from the 3-point bending test results, it is observed that microvascular channels with created configurations do not exhibit a substantial effect on the strength of the composite structure. When the channel configurations were compared among themselves, it was observed that there was a slight reduction in the strength and stiffness values compared to the reference structure which is the E00 configuration. Saeed et al. (2016) is explained the reason of this reduction as to be generation of resin-rich regions and reduction in fiber volume fraction. In this study, no significant change in the values was observed when standard deviations were considered.

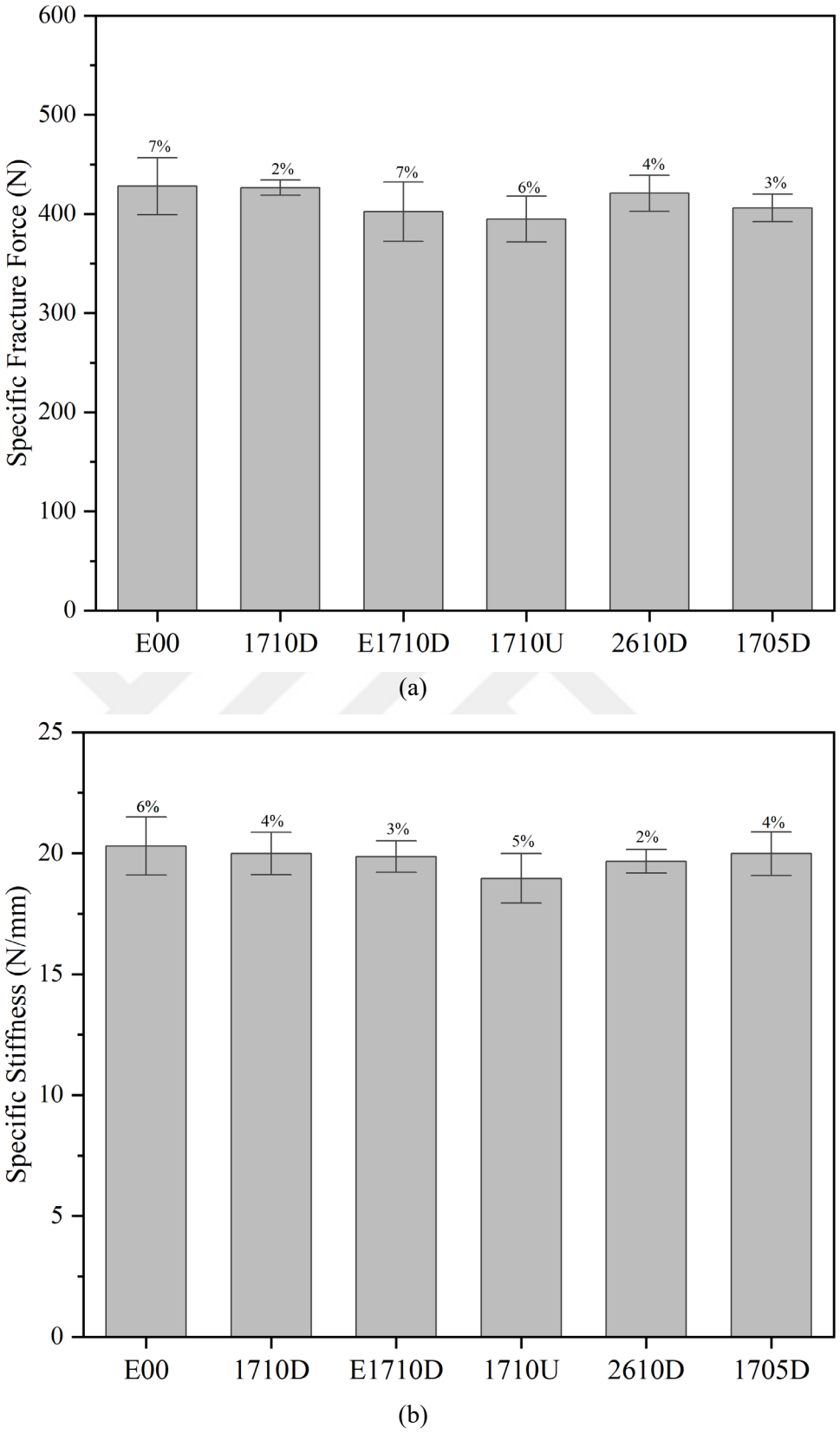


Figure 4.12. Bar charts of a) specific fracture forces and b) specific stiffness values in different configurations irrespective of the shape factor effect

4.4. Uniformity of Catalyst in Composite Laminate

In this study 2% wt. Grubbs' catalyst is integrated into composite laminates by mixing it into the epoxy polymer. 3 Roll Mill machine is used to mix the catalyst with epoxy polymer homogeneously. The distribution of catalyst inside the composite structure is investigated with the SEM-EDS analyses to the cross-sectional surface of specimens cut out from the composite laminate. It is observed that the epoxy-catalyst mixture achieved to be homogeneous as visualized in Figure 4.13. The green points represent the ruthenium (Ru) atoms contained in the Grubbs' catalyst. It is observed that Grubbs' catalyst is successfully distributed homogeneously within the composite structure.

As a result of this analysis, the homogenization of additive (in this case catalyst) within the epoxy polymer matrix was successfully accomplished using a 3 Roll Mill machine and catalyst was distributed into the carbon fiber reinforced composite uniformly.

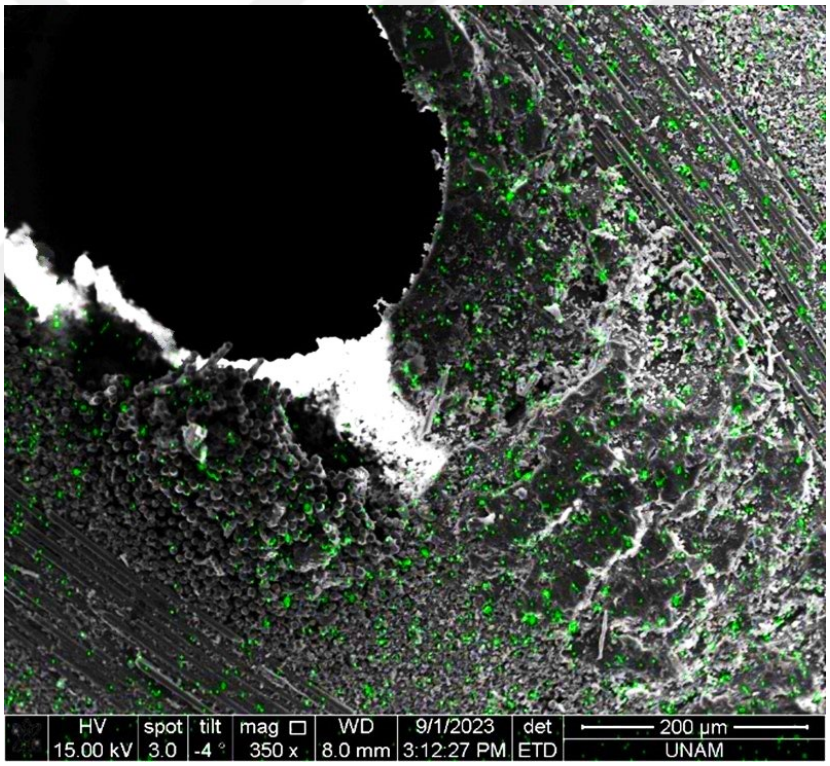


Figure 4.13. Visualization of the distribution of Ru atoms with EDS analyses in a cross-sectional area of 800µm x 650µm taken from the composite structure

4.5. Self-Healing of Composite

In order to observe the fracture properties and healing behaviour before and after the application of self-healing mechanism, compact tension tests are applied in predefined approaches to the specimens produced based on ASTM D5045 standards. In this test, the force was applied to the specimens and crack tip opening displacement (CTOD) values were measured to see the effect of the healing agent as the crack propagates. During the tests, two approaches were followed, and

the tests were conducted with different groups of specimens at different healing times. Since it was observed that the ring-opening polymerization reaction began after the first 30 minutes, the tests were conducted for healing times of 30, 60, 120 and 150 minutes. The situation inside the structure during the compact tension tests was visualized in relation to the Force-CTOD curve as depicted in Figure 4.14. It was noted that, during the tests were conducted, room temperature was approximately 18 °C.

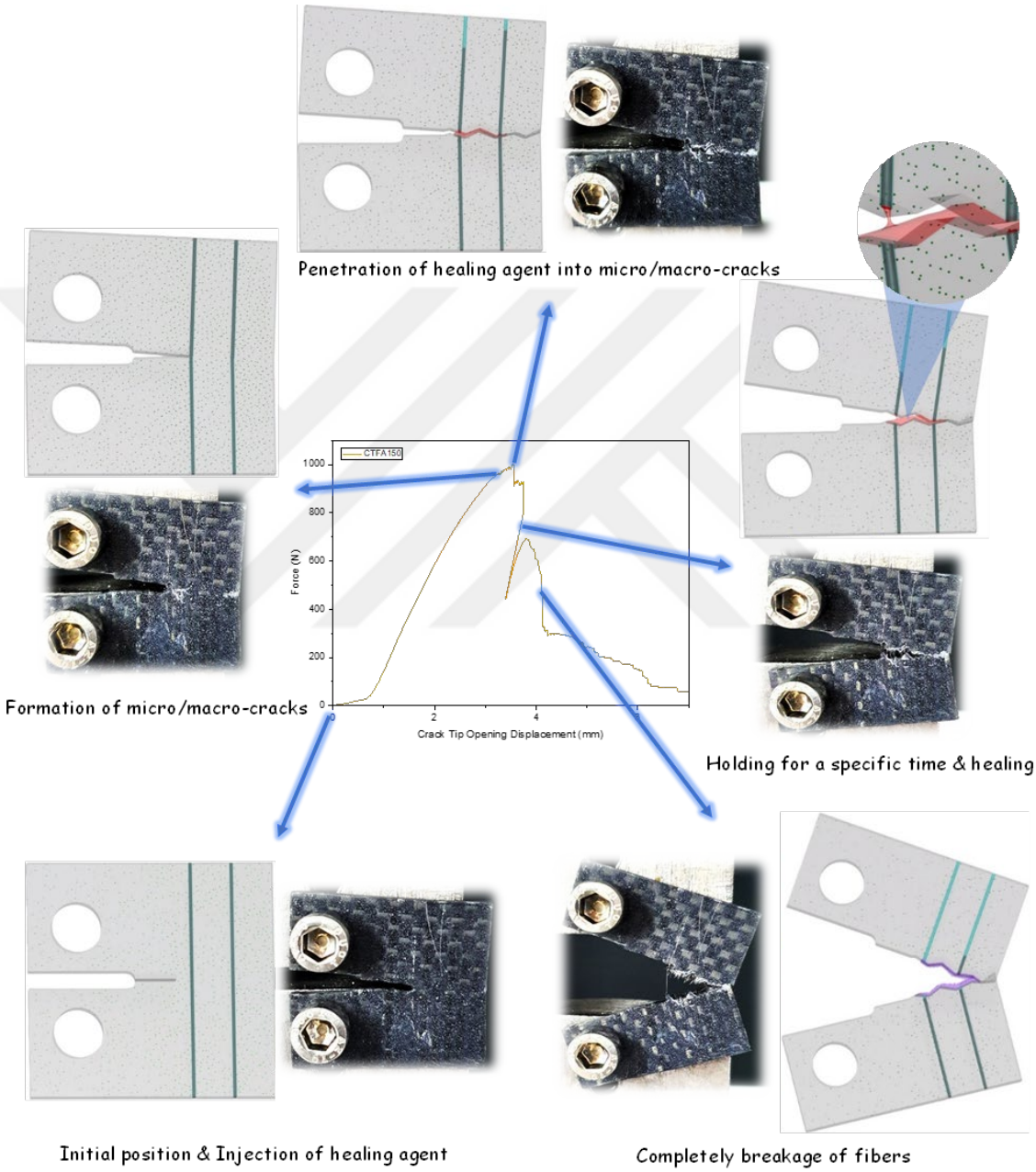


Figure 4.14. Schematically visualization of situation inside the structure during the compact tension tests in relation to the Force-CTOD curve

The results of each approach are compared to each other, as plotted in Figure 4.15 and Figure 4.16, to observe the effect of the self-healing mechanism on the mechanical properties of composite structures. It is observed from the figures below that the maximum force values of the virgin

specimen with empty microvascular channels (CTE) are slightly higher (9%) than that of the specimen without channels (CTS). The main reason for this situation is that the channels, round in shape, in the structure increases triaxiality (Wang et al., 2021; LI et al., 2020) which cause increase in strain at that location. The crack tip energy released during the crack propagation is distributed over a wider area when the crack reaches the channel edge because of the blunting effect of channels in circular shape (Kousourakis et al., 2006). So, the maximum force to initiate the crack is increased.

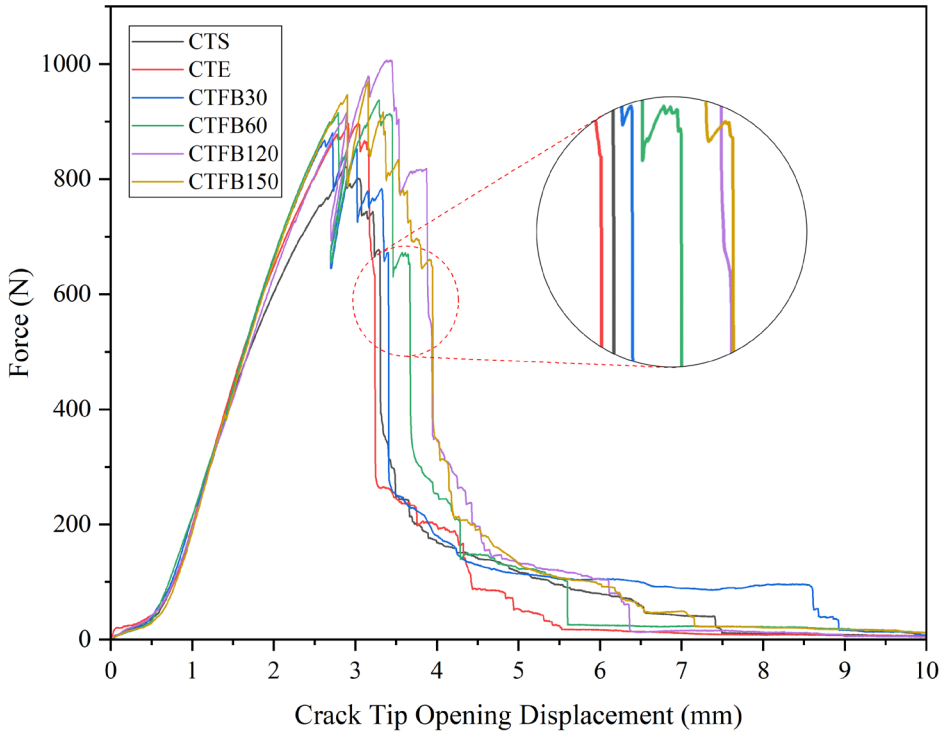


Figure 4.15. Force – CTOD curves of the solid, virgin and self-healing agent injected specimens according to Approach 1

The microvascular channels were filled with healing agent and the Force–CTOD measurements were plotted as a result of tests conducted according to Approach 1, as shown in Figure 4.15. An increment was observed in crack opening displacements, compared to virgin specimens, as the effect of the healing agent. This means that there is healing for micro-cracks in the polymer matrix under the applied load.

The Force–CTOD measurements were plotted as a result of tests conducted according to Approach 2, as shown in Figure 4.16. During the tests for Approach 2, the microvascular channels were fed with healing agent continuously to fill the crack zone because the load was released after the fracture occurs at the crack zone in the macroscale. So, there was a considerably higher volume of agents needed at the crack zone in this approach.

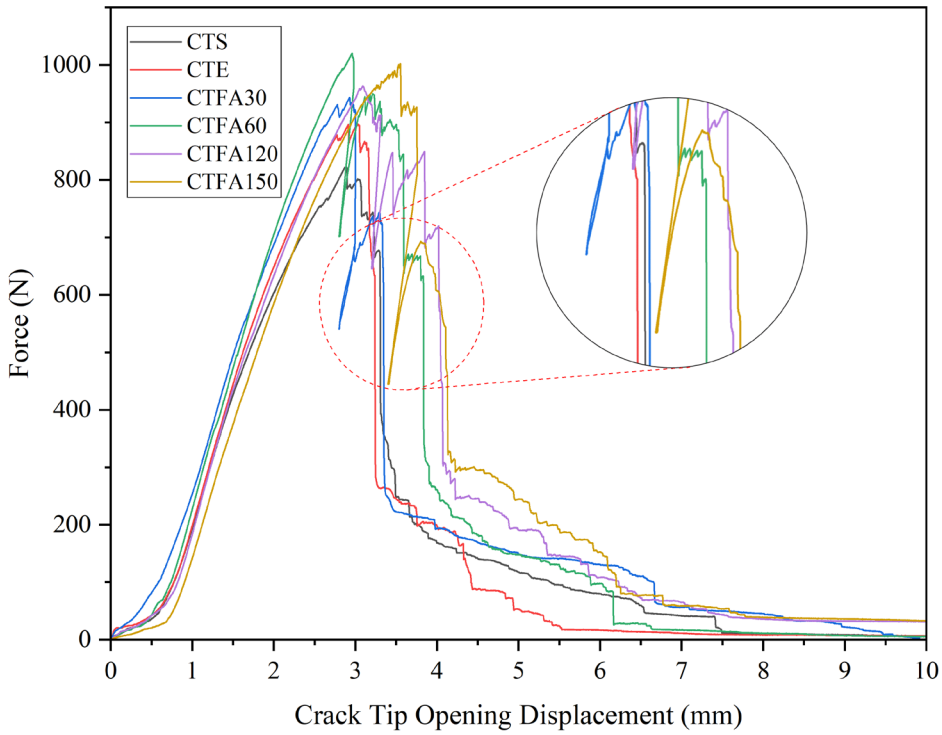


Figure 4.16. Force – CTOD curves of the solid, virgin and self-healing agent injected specimens according to Approach 2

Similar to the results of the Approach 1, an increment was observed in crack opening displacements, compared to virgin specimens, as the effect of the healing agent. So, healing for macro-cracks in the polymer matrix under the applied load was also observed in the Approach 2.

Table 4.7. Averages of force, strain energy and healing efficiency values of specimens in different scenarios for both Approach 1 and Approach 2

Configuration	**Average Ultimate Force (N)**	**Average Fracture Force (N)**	**Average CTOD at Fracture (mm)**	**ΔU (J)**	**Standard Deviation (J)**	**Healing Efficiency**	**Relative Standard Deviation**
CTS	821.67	622.91	3.30	1.935	0.070	-	4%
CTE	897.03	603.44	3.24	1.853	0.059	-	3%
CTFB30	880.31	668.53	3.40	2.243	0.108	121.0 %	5%
CTFB60	937.97	650.56	3.67	2.287	0.146	123.4 %	6%
CTFB120	1006.75	590.93	3.89	2.517	0.073	135.8 %	3%
CTFB150	969.63	647.63	3.95	2.511	0.095	135.5 %	4%
CTFA30	942.94	611.22	3.35	2.320	0.088	125.1 %	4%
CTFA60	1020.56	608.75	3.84	2.534	0.081	136.7 %	3%
CTFA120	963.56	615.81	4.02	2.709	0.133	146.2 %	5%
CTFA150	1002.39	581.34	4.05	2.756	0.102	148.7 %	4%

The average ultimate force, fracture force, CTOD values at fracture point, change in strain energy (area under the load-displacement curve, ΔU) and healing efficiency values compared to virgin specimens were tabulated as shown in Table 4.7.

The healing efficiency values were evaluated based on calculations of Mode-I strain release rate (G_I) which is a measure of resistance to crack propagation where the crack faces move apart normal to the crack plane. For the same crack area, the efficiency was defined as the ratio of area under the load-displacement curve of healed specimen (ΔU_{healed}) to area under the load-displacement curve of virgin specimen (ΔU_{virgin}), which is named as CTE, as indicated in equation 3.11.

The evaluated healing efficiency values were compared based on virgin specimen and plotted as shown in Figure 4.17 and Figure 4.18 for both Approach 1 and Approach 2.

For Approach 1, the healing efficiencies were observed as approximately 121%, 123%, 136% and 136% for the healing times of 30, 60, 120 and 150 minutes, respectively. Based on these results, a significant resistance on crack propagation was observed up to healing time of 120 minutes and there is a slight difference in efficiency values, after healing time of 120 minutes. In the case that the tensile load was interrupted when the micro-cracks was occurred, the healing agent penetrated into the micro-cracks arising near the channels. Hence, a healing was achieved as a result of triggering the self-healing mechanism.

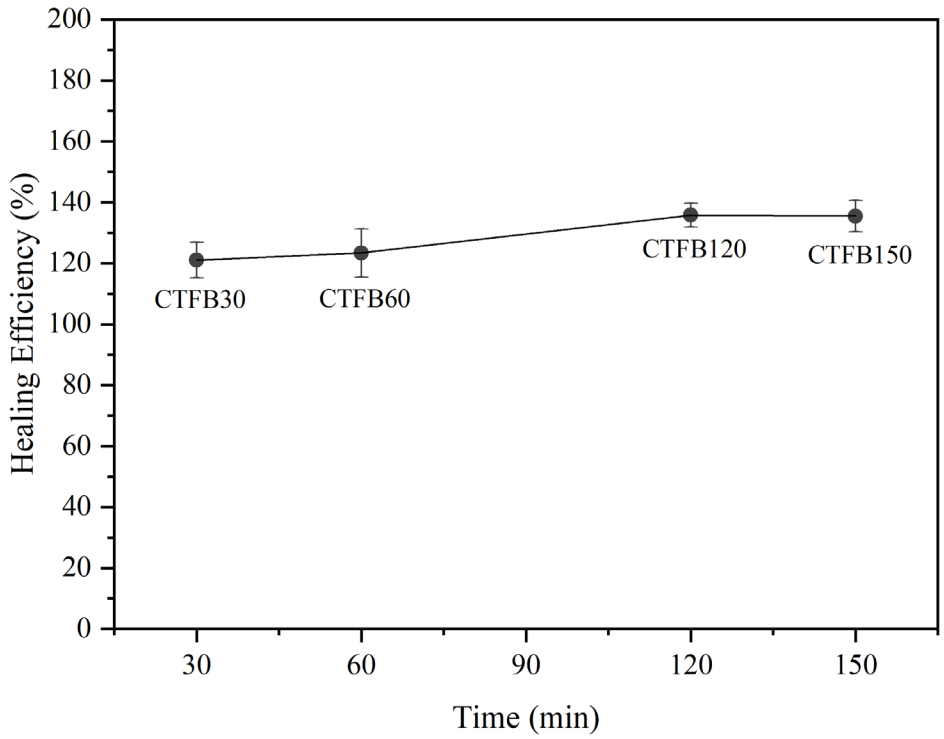


Figure 4.17. Development of healing efficiency over time according to Approach 1

For Approach 2, the healing efficiencies were observed as approximately 125%, 137%, 146% and 149% for the healing times of 30, 60, 120 and 150 minutes, respectively. Based on these results, a significant resistance on crack propagation was observed up to healing time of 120 minutes and there is a slight difference in efficiency values, after healing time of 120 minutes. The self-healing mechanism was certainly triggered after the fracture of fibers initiated along the crack propagation zone and a healing was achieved.

As a result, the use of the healing mechanism through microvascular channels created with the novel method was found to be successful. It was observed that healing was achieved for structures where the healing agent can be stored in microvascular channels with Approach 1. For example, structures may be small and multi-structural parts such as, rib, stringer, brackets etc. in an aircraft. Also, with Approach 2 healing was achieved for the large structural parts such as, skin, spar, panel etc. in an aircraft where the channels can be fed continuously with healing agent.

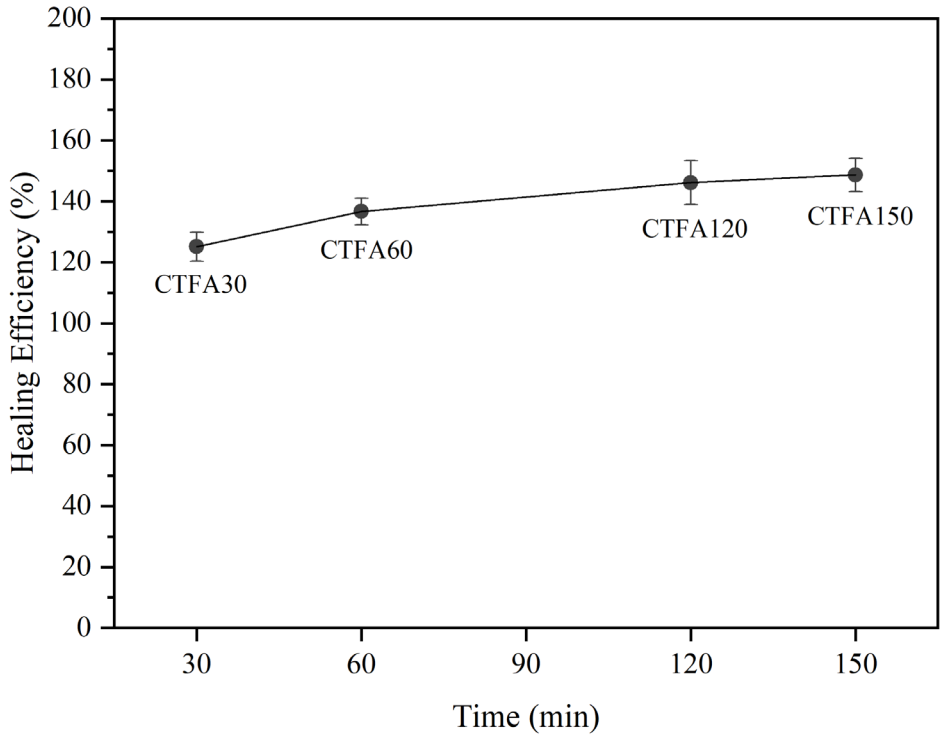


Figure 4.18. Development of healing efficiency over time according to Approach 2

In addition, images of the crack zone were observed using a stereo microscope, as shown in Figure 4.19. In these images, crack zones where the agent was not injected, and where the agent was injected were examined closely. It is seen that in the crack area where the agent has been continuously injected into the channel from the back of it during the propagation, the crack is filled by the agent. As a result, polymerization occurs instantaneously as shown in Figure 4.19(c and d).

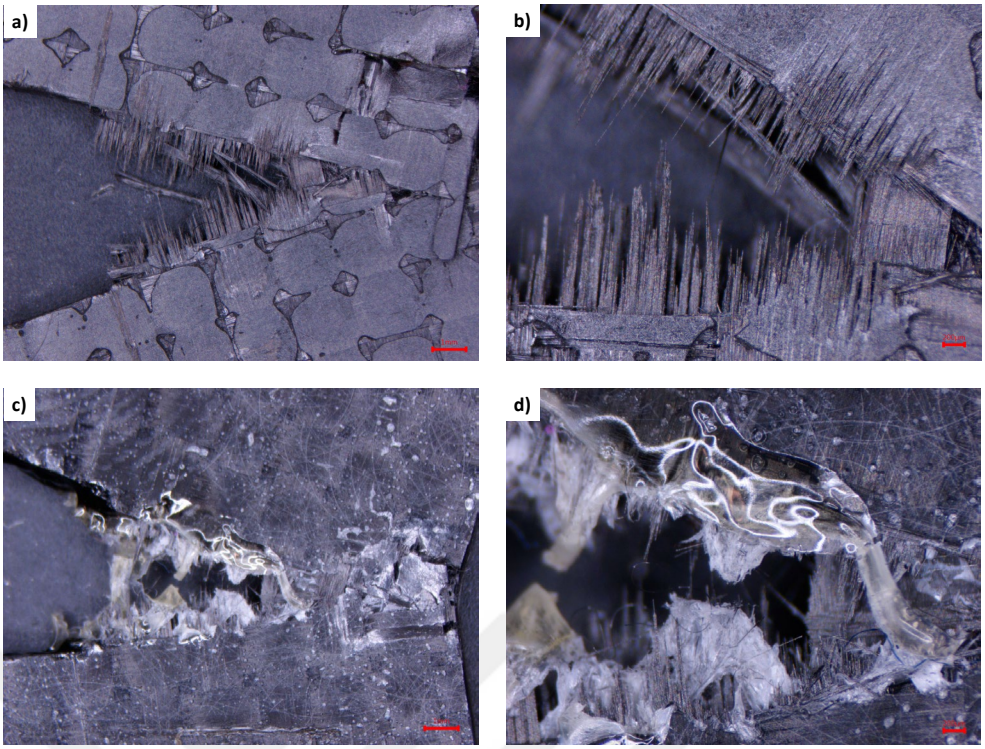


Figure 4.19. a) Distant view and b) close-up images of the crack zone where the agent was not injected, c) distant view and d) close-up images of the crack zone where the agent was injected

5. CONCLUSION

In this study, carbon fiber reinforced polymer structures having microvascular channels were produced and self-healing features via these microvascular channels of composite structures were experienced. Unlike the present channel formation methods, a novel microvascular channel production method was developed and introduced to the literature. In the literature studies, the pre- and post-processes required to create microvascular channels within the composite structure are time-consuming and not suitable for rapid and large-scale production. With the novel method developed within this study, polyamide monofilaments are used as core to obtain cavities as they are removed from the structure. The selected core material of polyamide monofilaments allowed easy removal in a short time, and microvascular channels were created without any collapse or deterioration. With this method, production time is shortened, and production becomes easier due to its simple application compared to the available methods such as the use of sacrificial material etc. Therefore, a reduction in the production cost of composites having microvascular channels was achieved. In addition to all these, polyamide monofilaments used to create channels are commercially available, cheap and available in various diameters. Also, monofilaments can be reused because they do not break or deteriorate after the process.

In the literature, since the healing agent and catalyst are located in two separate channels within the structure, the crack can only heal after reaching each separate channel. This situation negatively affects the strength of the structure and limits the number of channels that can be created. However, a novel coating method applied to the microvascular channel walls in this study, allowed the catalyst to be distributed into the matrix in solid form and the healing agent to be preserved in the channel without any undesired reaction. Since the catalyst is distributed into the structure in solid powder form, there is no need for a separate channel for the catalyst. Thus, healing can begin immediately whenever the crack contacts any of the channels before it grows further, and the number of microvascular channels that can be placed within the structure can be increased.

In order to create isolated microvascular channel networks, there are lots of methods available in the literature (Bleay et al., 2001; Lima et al., 2013; Norris et al., 2012; Norris et al., 2011; Pang and Bond, 2005a; Phillips and Baur, 2013; Trask and Bond, 2010; H. R. Williams et al., 2007; Wu et al., 2012; Zainuddin et al., 2014). Since isolated microvascular channels do not enable to supply a sufficient volume of healing agents continuously for their repeated damage-healing cycles, the creation of interconnected microvascular channels becomes more important. Because the mechanism, which consists of networks connected to each other by alternative channel pathways, reaches the damage even if a part of the channel is blocked, allowing the agent to reach the damaged area. This mechanism provides repeated healing cycles. However, the methods available in the literature for creation of the interconnected microvascular channel networks require time-consuming pre- and post-processes (Coppola et al., 2014; Dong et al., 2012; Esser-Kahn et al., 2011; Patrick et

al., 2014). With the novel method developed in this study, it is possible to create microvascular channels more easily and in a shorter time by weaving or locating the monofilaments, used to create channels, into the fabric in an appropriate sequence and applying them to the structure to form interconnected channels.

As a catalyst material, Grubbs' Catalyst was successfully distributed into the matrix material of composite structure homogeneously by using a three-roll mill machine and as a healing agent, 5E2N was injected and stored in microvascular channels successfully in this study. Compared to other available agents, the healing reaction was achieved in a shorter time by using 5E2N & Grubbs' catalyst duo. Additionally, since the self-healing agent can remain liquid between -80°C and 148°C, it allows damages that occurred in aircraft structures to be healed during operation.

The effect of microvascular channels on the flexural strength of composite material was investigated by 3-point bending tests. It was also observed that the corrugated top surfaces of the laminates created a microscopic shape factor which affects the flexural properties because the height of the laminate layers above the channel plane is not adequate to eliminate the corrugation. This is because the thickness of the laminate is not thick enough to compensate corrugation. The test results were modified to eliminate the effect of the shape factor and there was no significant reduction observed in the strength and stiffness values compared to the reference specimen when the standard deviations were considered. This means that microvascular channels with a diameter of 450 μm had negligible negative effects on the structure of the samples tested in the specified configurations.

The healing behaviour of the mechanism was investigated during crack propagation by compact tension test. Tests were conducted for two different approaches, one to observe the healing of microcracks and the other to observe the healing of macrocracks when fractures were detected. The tests were repeated for different healing times of 30, 60, 120 and 150 minutes to investigate the effect of the healing reaction over time. According to the results obtained from compact tension tests, healing abilities for both approaches and different healing times were evaluated in terms of healing efficiency. As a result, the efficiency increases as the healing time increases and a slight increase was also observed in efficiency values after healing time of 120 minutes for both approaches. The main reason for this is that the healing reaction is approximately completed after this period.

Also, in the approach where the healing of microcracks was observed, healing efficiency reached up to 136% and in the approach where the healing of macro cracks was observed, healing efficiency reached up to 149%. The main reason for this difference is that as the crack grew to the macro scale due to the fracture, a larger volume of healing agent was required and continuously injected into the channels. As a result of these tests, it was observed that healing was achieved via microvascular channels created by the method developed in this study. On the other hand, 5E2N provides more flexibility to this healing process since it reacts over a wide temperature range and in a short time.

With this success, the easy integration of the self-healing feature into composite structural parts contributes to ensuring structural durability, operational safety, and operational continuity by automatically repairing minor damages, depending on the platform on which it is used. In addition, maintenance and repair costs will decrease and downtime will be minimized due to the self-healing features.

Nowadays, interest in smart materials and composites is increasing and the self-healing composite market is growing with ongoing research and development. Technological advancements and industry recognition will drive further growth. Cost, scalability, and regulatory considerations will determine widespread adoption. The self-healing polymer market is expected to grow from USD 0.9 billion to USD 69.93 billion by 2032, with a compound rate of growth (CAGR) of 62.2% (Self-Healing Polymer Market Size, Share, Growth | Report, 2030). This shows the potential of this study for the future works.

However, catalysts and healing agents used for self-healing mechanisms are quite expensive compared to polymer composite materials used in the market. Therefore, it is more suitable for use in sectors where the cost is of secondary importance, such as the space and aviation industry. The positive impact of self-healing on critical factors such as enhanced safety, reliability, operational continuity, improving efficiency and gaining competitive advantages in these sectors makes this technology a worthwhile investment. However, as the use of self-healing composites increases, the cost of ingredient catalysts and healing agent materials may decrease further.

Future Studies

In this study, 2% wt. Grubbs' catalyst was mixed into the matrix. However, the effect of the amount of catalyst on the self-healing mechanism should be investigated in future studies.

Also, the samples tested in this study contain isolated channels. In future studies, test samples containing interconnected channels should be produced and the tests should be repeated for these samples as well. Thus, the effect of a continuous supply of healing agents, which is providing repeated, healing cycles can be examined for the interconnected channels. In addition, the effects of the channel diameter should also be investigated.

One of the most important parameters for self-healing composites is interlaminar shear strength (ILSS). ILSS is known to be highly sensitive to interlaminar voids, cavities, or defects, which can be formed during composite production or intentionally created (Goodwin et al., 1997). Similarly, microchannels in CFRP composites act as interlaminar cavities and significantly lower their ILSS. The interlaminar shear strength tests should be conducted to investigate and determine the effects of microvascular channels on this parameter.

On the other hand, most structures are subjected to various repetitive loads during their lifetime. This situation causes damage due to the fatigue of the material. So, the effects of

microvascular channels and healing cycles via these channels should be investigated under alternating loads in future studies.

Additionally, the healing agent used in this study (5E2N) enables healing over a wide range of temperatures, between -80°C and 148°C, tests should be repeated at these extreme temperatures to examine the effect of temperature on the healing process in fiber reinforced polymer structures.

REFERENCES

Agarwal, B. D., Broutman, L. J., & Chandrashekhara, K. (2006). Analysis and performance of fiber composites. John Wiley. https://books.google.com/books/about/Analysis_and_Performance_of_Fiber_Compos.html?hl=tr&id=T1CtwL9uK5MC

Aïssa, B., Nechache, R., Haddad, E., Jamroz, W., Merle, P. G., & Rosei, F. (2012). Ruthenium Grubbs' catalyst nanostructures grown by UV-excimer-laser ablation for self-healing applications. Applied Surface Science, 258(24), 9800–9804. https://doi.org/10.1016/j.apsusc.2012.06.032

Aïssa, B., Tagziria, K., Haddad, E., Jamroz, W., Loiseau, J., Higgins, A., Asgar-Khan, M., Hoa, S. V., Merle, P. G., Therriault, D., & Rosei, F. (2012). The Self-Healing Capability of Carbon Fibre Composite Structures Subjected to Hypervelocity Impacts Simulating Orbital Space Debris. ISRN Nanomaterials, 2012, 1–16. https://doi.org/10.5402/2012/351205

Altenbach, H., Altenbach, J., & Kissing, W. (2004). Mechanics of Composite Structural Elements. In Mechanics of Composite Structural Elements. Springer Berlin Heidelberg. https://doi.org/10.1007/978-3-662-08589-9

ANSYS Inc., Ansys® Granta Selector Software (2016). Retrieved from http://www.grantadesign.com/products/ces/

Ashby, M. F. (1989). Overview No. 80: On the engineering properties of materials. Acta Metallurgica, 37(5), 1273–1293. https://doi.org/10.1016/0001-6160(89)90158-2

Ashby, M. F. (2011a). Chapter 4- Material Property Charts. In M. F. Ashby (Ed.), Materials Selection in Mechanical Design (Fourth Edition, pp. 57–96). Butterworth-Heinemann. https://doi.org/https://doi.org/10.1016/B978-1-85617-663-7.00004-7

Ashby, M. F. (2011b). Chapter 9- Selection of Material and Shape. In M. F. Ashby (Ed.), Materials Selection in Mechanical Design (Fourth Edition, pp. 243–276). Butterworth-Heinemann. https://doi.org/https://doi.org/10.1016/B978-1-85617-6637.00009-6

Bekas, D. G., Baltzis, D., & Paipetis, A. S. (2017). Nano-reinforced polymeric healing agents for vascular self-repairing composites. Materials & Design, 116, 538–544. https://doi.org/10.1016/J.MATDES.2016.12.049

Bellan, L. L., Kniazeva, T., Kim, E. E., Epshteyn, A. A., Cropek, D. D., Langer, R., & Borenstein, J. J. (2012). Fabrication of a Hybrid Microfluidic System Incorporating both Lithographically Patterned Microchannels and a 3D Fiber-Formed Microfluidic Network. Advanced Healthcare Materials, 1(2), 164–167. https://doi.org/10.1002/ADHM.201100052

Bellan, L. M., Singh, S. P., Henderson, P. W., Porri, T. J., Craighead, H. G., & Spector, J. A. (2009). Fabrication of an artificial 3-dimensional vascular network using sacrificial sugar structures. Soft Matter, 5(7), 1354–1357. https://doi.org/10.1039/B819905A

Bergman, S. D., & Wudl, F. (2007). Mendable polymers. Journal of Materials Chemistry, 18(1), 41–62. https://doi.org/10.1039/B713953P

Blaiszik, B. J., Kramer, S. L. B., Olugebefola, S. C., Moore, J. S., Sottos, N. R., & White, S. R. (2010). Self-Healing Polymers and Composites, Annual Review of Materials Research, 40, 179–211. https://doi.org/10.1146/annurev-matsci-070909-104532

Bleay, S. M., Loader, C. B., Hawyes, V. J., Humberstone, L., & Curtis, P. T. (2001). A smart repair system for polymer matrix composites. Composites Part A: Applied Science and Manufacturing, 32(12), 1767–1776. https://doi.org/10.1016/S1359-835X(01)00020-3

Bond, I. P., Trask, R. S., & Williams, H. R. (2008). Self-healing fiber- reinforced polymer composites. MRS Bulletin, 33(8), 770–774. https://doi.org/10.1557/MRS2008.164

Boroujeni, A. Y., Tehrani, M., Nelson, A. J., & Al-Haik, M. (2014). Hybrid carbon nanotube–carbon fiber composites with improved in-plane mechanical properties. Composites Part B: Engineering, 66, 475–483. https://doi.org/10.1016/J.COMPOSITESB.2014.06.010

Brown, E. N., Sottos, N. R., & White, S. R. (2002). Fracture testing of a self-healing polymer composite. Experimental Mechanics 2002 42:4, 42(4), 372–379. https://doi.org/10.1007/BF02412141

Budynas, R. G. (Richard G., Nisbett, J. Keith., & Shigley, J. Edward. (2011). Shigley's mechanical engineering design. McGraw-Hill.

Colquhoun, H., & Klumperman, B. (2013). Self-healing polymers. Polymer Chemistry, 4(18), 4832–4833. https://doi.org/10.1039/C3PY90046K

Coope, T. S., Wass, D. F., Trask, R. S., & Bond, I. P. (2014). Metal Triflates as Catalytic Curing Agents in Self-Healing Fibre Reinforced Polymer Composite Materials. Macromolecular Materials and Engineering, 299(2), 208–218. https://doi.org/10.1002/MAME.201300026

Coppola, A. M., Thakre, P. R., Sottos, N. R., & White, S. R. (2014). Tensile properties and damage evolution in vascular 3D woven glass/epoxy composites. Composites PartA:Applied Science and Manufacturing, 59, 9–17. https://doi.org/10.1016/J.COMPOSITESA.2013.12.006

Daniel, I. M., & Mccormick, R. R. (2007). Failure of Composite Materials. Strain, 43(1), 4–12. https://doi.org/10.1111/J.1475-1305.2007.00302.X

Das, R., Melchior, C., & Karumbaiah, K. M. (2016). Self-healing composites for aerospace applications. Advanced Composite Materials for Aerospace Engineering, 333–364. https://doi.org/10.1016/B978-0-08-100037-3.00011-0

Ding, W. (1999). Delamination analysis of composite laminates.

Dong, H., Esser-Kahn, A. P., Thakre, P. R., Patrick, J. F., Sottos, N. R., White, S. R., & Moore, J. S. (2012). Chemical treatment of poly(lactic acid) fibers to enhance the rate of thermal depolymerization. ACS Applied Materials and Interfaces, 4(2), 503–509. https://doi.org/10.1021/AM2010042

Dry, C. (1994). Matrix cracking repair and filling using active and passive modes for smart timed release of chemicals from fibers into cement matrices. Smart Materials and Structures, 3(2), 118. https://doi.org/10.1088/0964-1726/3/2/006

Dry, C. M., & Sottos, N. R. (1993). Passive smart self-repair in polymer matrix composite materials. Https://Doi.Org/10.1117/12.148501, 1916, 438–444. https://doi.org/10.1117/12.148501

Ekeocha, J., Ellingford, C., Pan, M., Wemyss, A. M., Bowen, C., & Wan, C. (2021). Challenges and Opportunities of Self-Healing Polymers and Devices for Extreme and Hostile Environments. Advanced Materials, 33(33), 2008052. https://doi.org/10.1002/ADMA.202008052

Elias, A. J. (2008). Molecule matters. Resonance, 13(5), 456–467. https://doi.org/10.1007/S12045-008-0052-7

Esser-Kahn, A. P., Thakre, P. R., Dong, H., Patrick, J. F., Vlasko-Vlasov, V. K., Sottos, N. R., Moore, J. S., & White, S. R. (2011). Three-dimensional microvascular fiber-reinforced composites. Advanced Materials, 23(32), 3654–3658. https://doi.org/10.1002/adma.201100933

Garrett, J. D. (2016). Experimentation of Mode I and Mode II Fracture of Uni-Directional Composites and Finite Element Analysis of Mode I Fracture Using Cohesive Contact. Master's Theses. https://doi.org/10.15368/theses.2016.142

Gdoutos, E. E., Pilakoutas, K., & Rodopoulos, C. A. (2000). Failure analysis of industrial composite materials. McGraw-Hill. https://books.google.com/books/about/Failure_Analysis_of_ Industrial_Composite.html?hl=tr&id=Bo4BsB85PY0C

Gergely, R. C. R., Santa Cruz, W. A., Krull, B. P., Pruitt, E. L., Wang, J., Sottos, N. R., & White, S. R. (2018). Restoration of Impact Damage in Polymers via a Hybrid Microcapsule–Microvascular Self-Healing System. Advanced Functional Materials, 28(2), 1704197. https://doi.org/10.1002/ADFM.201704197

Golden, A. P., & Tien, J. (2007). Fabrication of microfluidic hydrogels using molded gelatin as a sacrificial element. Lab on a Chip, 7(6), 720–725. https://doi.org/10.1039/B618409J

González, A., Norambuena-Contreras, J., Storey, L., & Schlangen, E. (2018). Effect of RAP and fibers addition on asphalt mixtures with self-healing properties gained by microwave radiation heating. Construction and Building Materials, 159, 164–174. https://doi.org/10.1016/J.CONBUILDMAT.2017.10.070

Goodwin, A. A., Howe, C. A., & Paton, R. J. (1997). The Role of Voids in Reducing the Interlaminar Shear Strength of RTM Laminates. 11.

Guadagno, L., Longo, P., Raimondo, M., Naddeo, C., Mariconda, A., Sorrentino, A., Vittoria, V., Iannuzzo, G., & Russo, S. (2010). Cure behavior and mechanical properties of structural self-

healing epoxy resins. Journal of Polymer Science Part B: Polymer Physics, 48(23), 2413–2423. https://doi.org/10.1002/POLB.22139

Gualandi, C., Zucchelli, A., Fernández Osorio, M., Belcari, J., & Focarete, M. L. (2013). Nanovascularization of polymer matrix: Generation of nanochannels and nanotubes by sacrificial electrospun fibers. Nano Letters, 13(11), 5385–5390. https://doi.org/10.1021/NL402930X

Habault, D., Zhang, H., & Zhao, Y. (2013). Light-triggered self-healing and shape-memory polymers. Chemical Society Reviews, 42(17), 7244–7256. https://doi.org/10.1039/C3CS35489J

Hager, M. D., Greil, P., Leyens, C., van der Zwaag, S., & Schubert, U. S. (2010). Self-healing materials. Advanced Materials (Deerfield Beach, Fla.), 22(47), 5424–5430. https://doi.org/10.1002/ADMA.201003036

Hansen, C. J., Saksena, R., Kolesky, D. B., Vericella, J. J., Kranz, S. J., Muldowney, G. P., Christensen, K. T., & Lewis, J. A. (2013). High-Throughput Printing via Microvascular Multinozzle Arrays. Advanced Materials, 25(1), 96–102. https://doi.org/10.1002/ADMA.201203321

Hansen, C. J., Wu, W., Toohey, K. S., Sottos, N. R., White, S. R., & Lewis, J. A. (2009). Self-Healing Materials with Interpenetrating Microvascular Networks. Advanced Materials, 21(41), 4143–4147. https://doi.org/10.1002/ADMA.200900588

Hashemi, S., Kinloch, A. J., & Williams, J. G. (1990). The Analysis of Interlaminar Fracture in Uniaxial Fibre-Polymer Composites. RSPSA, 427(1872), 173–199. https://doi.org/10.1098/RSPA.1990.0007

He, J., Mao, M., Liu, Y., Shao, J., Jin, Z., & Li, D. (2013). Fabrication of Nature-Inspired Microfluidic Network for Perfusable Tissue Constructs. Advanced Healthcare Materials, 2(8), 1108–1113. https://doi.org/10.1002/ADHM.201200404

Herbst, F., Döhler, D., Michael, P., & Binder, W. H. (2013). Self-Healing Polymers via Supramolecular Forces. Macromolecular Rapid Communications, 34(3), 203–220. https://doi.org/10.1002/MARC.201200675

Hu, Z., Shao, Q., Huang, Y., Yu, L., Zhang, D., Xu, X., Lin, J., Liu, H., & Guo, Z. (2018). Light triggered interfacial damage self-healing of poly(p-phenylene benzobisoxazole) fiber composites. Nanotechnology, 29(18), 185602. https://doi.org/10.1088/1361-6528/AAB010

Huang, J. H., Kim, J., Agrawal, N., Sudarsan, A. P., Maxim, J. E., Jayaraman, A., & Ugaz, V. M. (2009). Rapid Fabrication of Bio-inspired 3D Microfluidic Vascular Networks. Advanced Materials, 21(35), 3567–3571. https://doi.org/10.1002/ADMA.200900584

Ibrahim, M. E. (2014). Nondestructive evaluation of thick-section composites and sandwich structures: A review. Composites Part A: Applied Science and Manufacturing, 64, 36–48. https://doi.org/10.1016/J.COMPOSITESA.2014.04.010

Jacobsen, A. J., Barvosa-Carter, W., & Nutt, S. (2007). Micro-scale Truss Structures formed from Self-Propagating Photopolymer Waveguides. Advanced Materials, 19(22), 3892–3896. https://doi.org/10.1002/ADMA.200700797

Joven, R., Das, R., Ahmed, A., Roozbehjavan, P., & Minaie, B. (2012). Thermal properties of carbon fiber/epoxy composites with different fabric weaves. SAMPE International Symposium Proceedings. Charleston, SC. https://www.researchgate.net/publication/262007032

Kahar, N. N. F. N. M. N., Osman, A. F., Alosime, E., Arsat, N., Azman, N. A. M., Syamsir, A., Itam, Z., & Hamid, Z. A. A. (2021). The Versatility of Polymeric Materials as Self-Healing Agents for Various Types of Applications: A Review. Polymers 2021, Vol. 13, Page 1194, 13(8), 1194. https://doi.org/10.3390/POLYM13081194

Kaw, A. K. (2006). Mechanics of composite materials. Taylor & Francis.

Keller, M. W., & Crall, M. D. (2018). 6.15 Self-Healing Composite Materials. Comprehensive Composite Materials II, 431–453. https://doi.org/10.1016/B978-0-12-803581-8.10026-8

Kim, J. T., Kim, B. K., Kim, E. Y., Kwon, S. H., & Jeong, H. M. (2013). Synthesis and properties of near IR induced self-healable polyurethane/graphene nanocomposites. European Polymer Journal, 49(12), 3889–3896. https://doi.org/10.1016/J.EURPOLYMJ.2013.10.009

Kousourakis, A., & Mouritz, A. P. (2010). The effect of self-healing hollow fibres on the mechanical properties of polymer composites. Smart Materials and Structures, 19(8), 085021. https://doi.org/10.1088/0964-1726/19/8/085021

Kousourakis, A., Mouritz, A. P., & Bannister, M. K. (2006). Interlaminar properties of polymer laminates containing internal sensor cavities. Composite Structures, 75(1–4), 610–618. https://doi.org/10.1016/J.COMPSTRUCT.2006.04.086

Kumar, R., Rajesh Jesudoss Hynes, N., Senthamaraikannan, P., Khan, A., Rangappa, S. M., Siengchin, S., Sundara Bharathi, S. R., Asiri, A. M., & Khan, I. (2019). Self-repairing fiber polymer composites: Mechanisms and properties. Self-Healing Composite Materials: From Design to Applications, 71–85. https://doi.org/10.1016/B978-0-12-817354-1.00005-3

Lanzara, G., Yoon, Y., Liu, H., Peng, S., & Lee, W. I. (2009). Carbon nanotube reservoirs for self-healing materials. Nanotechnology, 20(33), 335704. https://doi.org/10.1088/0957-4484/20/33/335704

LeCompte, T. (anonymous 1). How Things Work: Self-Healing Airplanes | Air & Space Magazine| Smithsonian Magazine. Retrieved 29 January 2024, from https://www.smithsonianmag.com /air-space-magazine/how-things-work-self-healing-airplanes-35558146/

Lessard, L. B., Nemes, J. A., & Lizotte, P. L. (1995). Utilization of FEA in the design of composite bicycle frames. Composites, 26(1), 72–74. https://www.academia.edu/31327393/Utilization_of_FEA_in_the_design_of_composite_bicycle_frames

Lewis, J. A., & Gratson, G. M. (2004). Direct writing in three dimensions. Materials Today, 7(7–8), 32–39. https://doi.org/10.1016/S1369-7021(04)00344-X

Li, R., Zhan, M., Zheng, Z., Zhang, H., Cui, X., Lv, W., & Lei, Y. (2020). A constitutive model coupling damage and material anisotropy for wide stress triaxiality. Chinese Journal of Aeronautics, 33(12), 3509–3525. https://doi.org/10.1016/J.CJA.2020.09.018

Lim, D., Kamotani, Y., Cho, B., Mazumder, J., & Takayama, S. (2003). Fabrication of microfluidic mixers and artificial vasculatures using a high-brightness diode-pumped Nd:YAG laser direct write method. Lab on a Chip, 3(4), 318–323. https://doi.org/10.1039/B308452C

Lima, M. S. F., Sakamoto, J. M. S., Simoes, J. G. A., & Riva, R. (2013). Laser Processing of Carbon Fiber Reinforced Polymer Composite for Optical Fiber Guidelines. Physics Procedia, 41, 572–580. https://doi.org/10.1016/J.PHPRO.2013.03.118

Malinskii, Y. M., Prokopenko, V. v., Ivanova, N. A., & Kargin, V. S. (1970). Investigation of self-healing of cracks in polymers. Polymer Mechanics 1973 6:3, 6(3), 382–384. https://doi.org/10.1007/BF00858197

Maria, M. (2013). Advanced composite materials of the future in aerospace industry. Incas Bulletın, 5(3), 139–150. https://doi.org/10.13111/2066-8201.2013.5.3.14

Mauldin, T. C., & Kessler, M. R. (2013). Self-healing polymers and composites. 55(6), 317–346. https://doi.org/10.1179/095066010X12646898728408

Mijovic, J. (1995). Handbook of polymer–fibre composites, F. R. Jones, ed. Longman Group, UK (1994), ISBN 0582 065 542, 418 pp. Polymers for Advanced Technologies, 6(8), 591–591. https://doi.org/10.1002/PAT.1995.220060807

Mobaraki, M., Ghaffari, M., & Mozafari, M. (2020a). Basics of self-healing composite materials. Self-Healing Composite Materials: From Design to Applications, 15–31. https://doi.org/10.1016/B978-0-12-817354-1.00002-8

Mobaraki, M., Ghaffari, M., & Mozafari, M. (2020b). Self-healing polymers for composite structural applications. Self-Healing Composite Materials: From Design to Applications, 33–51. https://doi.org/10.1016/B978-0-12-817354-1.00003-X

Mohapatra, C. (2009). Revealing of Failure Modes of FRP Composites by Microscopic Technique.

Neil, D. (2004). VISION Our Driving Conundrum Change is coming. POPULAR SCIENCE TA - TT -, 265(3), 61–70. https://worldcat.org/title/199006954

Norris, C. J., Bond, I. P., & Trask, R. S. (2011). Interactions between propagating cracks and bioinspired self-healing vascules embedded in glass fibre reinforced composites. Composites Science and Technology, 71(6), 847–853. https://doi.org/10.1016/j.compscitech.2011.01.027

Norris, C. J., Meadway, G. J., O'Sullivan, M. J., Bond, I. P., & Trask, R. S. (2011). Self-Healing Fibre Reinforced Composites via a Bioinspired Vasculature. Advanced Functional Materials, 21(19), 3624–3633. https://doi.org/10.1002/ADFM.201101100

Norris, C. J., White, J. A. P., McCombe, G., Chatterjee, P., Bond, I. P., & Trask, R. S. (2012). Autonomous stimulus triggered self-healing in smart structural composites. Smart Materials and Structures, 21(9), 094027. https://doi.org/10.1088/0964-1726/21/9/094027

Olugebefola, S. C., Hamilton, A. R., Fairfield, D. J., Sottos, N. R., & White, S. R. (2013). Structural reinforcement of microvascular networks using electrostatic layer-by-layer assembly with halloysite nanotubes. Soft Matter, 10(4), 544–548. https://doi.org/10.1039/C3SM52288A

Pang, J. W. C., & Bond, I. P. (2005a). A hollow fibre reinforced polymer composite encompassing self-healing and enhanced damage visibility. Composites Science and Technology, 65(11–12), 1791–1799. https://doi.org/10.1016/J.COMPSCITECH.2005.03.008

Pang, J. W. C., & Bond, I. P. (2005b). 'Bleeding composites'—damage detection and self-repair using a biomimetic approach. Composites Part A: Applied Science and Manufacturing, 36(2), 183–188. https://doi.org/10.1016/J.COMPOSITESA.2004.06.016

Patrick, J. F., Hart, K. R., Krull, B. P., Diesendruck, C. E., Moore, J. S., White, S. R., & Sottos, N. R. (2014). Continuous Self-Healing Life Cycle in Vascularized Structural Composites. Advanced Materials, 26(25), 4302–4308. https://doi.org/10.1002/ADMA.201400248

Phillips, D. M., & Baur, J. W. (2013). A microvascular method for thermal activation and deactivation of shape memory polymers. Http://Dx.Doi.Org/10.1177/1045389X12471907, 24(10), 1233–1244. https://doi.org/10.1177/1045389X12471907

Ponnamma, D., Sadasivuni, K. K., Cabibihan, J.-J., & Al-Maadeed, M. A.-A. (2017). Smart polymer nanocomposites: Energy harvesting, self-healing and shape memory applications. Springer.

Pruez, J., Shoukry, S., Williams, G., & Shoukry, M. (2013). Lightweight Composite Materials for Heavy Duty Vehicles. https://doi.org/10.2172/1116021

Ramesh, M., Arun Ramnath, R., Khan, A., Khan, A. A. P., & Asiri, A. M. (2020). Electrically conductive self-healing materials: preparation, properties, and applications. Self-Healing Composite Materials: From Design to Applications, 1–13. https://doi.org/10.1016/B978-0-12-817354-1.00001-6

Roper, C. S., Schubert, R. C., Maloney, K. J., Page, D., Ro, C. J., Yang, S. S., & Jacobsen, A. J. (2015). Scalable 3D Bicontinuous Fluid Networks: Polymer Heat Exchangers Toward Artificial Organs. Advanced Materials, 27(15), 2479–2484. https://doi.org/10.1002/ADMA.201403549

Russell, A. J., & Street, K. N. (1987). The effect of matrix toughness on delamination: static and fatigue fracture under mode II shear loading of graphite fibre composites. ASTM Special Technical Publication, 275–294. https://doi.org/10.1520/STP24383S

Saeed, M. U., Li, B. Bin, & Chen, Z. F. (2016). Mechanical effects of microchannels on fiber-reinforced composite structure. Composite Structures, 154, 129–141. https://doi.org/10.1016/J.COMPSTRUCT.2016.07.057

Saeed, M. U., Li, B. Bin, Chen, Z. F., & Khan, Z. M. (2016). A novel processing approach to produce microchannel embedded carbon-epoxy composites. Journal of Manufacturing Processes, 22, 26–33. https://doi.org/10.1016/J.JMAPRO.2016.01.007

Saini, S., & Jain, D. (2017). The effect of healing time on the self-healing efficiency of carbon fibre reinforced polymer composites. Materials Today: Proceedings, 4(2), 2903–2909. https://doi.org/10.1016/J.MATPR.2017.02.171

Scelsi, L., Bonner, M., Hodzic, A., Soutis, C., Wilson, C., Scaife, R., & Ridgway, K. (2011). Potential emissions savings of lightweight composite aircraft components evaluated through life cycle assessment. Express Polymer Letters, 5(3), 209–217. https://doi.org/10.3144/EXPRESSPOLYMLETT.2011.20

Schaedler, T. A., Jacobsen, A. J., Torrents, A., Sorensen, A. E., Lian, J., Greer, J. R., Valdevit, L., & Carter, W. B. (2011). Ultralight metallic microlattices. Science, 334(6058), 962–965. https://doi.org/10.1126/SCIENCE.1211649

Scheiner, M., Dickens, T. J., & Okoli, O. (2016). Progress towards self-healing polymers for composite structural applications. Polymer, 83, 260–282. https://doi.org/10.1016/J.POLYMER.2015.11.008

Schwartz, M. M. (1984). Composite materials handbook. 651. https://search.worldcat.org/title/9017647

Self-Healing Polymer Market Size, Share, Growth | Report, 2030. (anonymous 2). Retrieved 21 January 2024, from https://www.marketresearchfuture.com/reports/self-healing-polymer-market-4135.

Siddique, A., Abid, S., Shafiq, F., Nawab, Y., Wang, H., Shi, B., Saleemi, S., & Sun, B. (2021). Mode I fracture toughness of fiber-reinforced polymer composites: A review. Journal of Industrial Textiles, 50(8), 1165–1192. https://doi.org/10.1177/1528083719858767

Smith, F. (2013). The Use of composites in aerospace: Past, present and future challenges.

Sun, C. (1995). Vibration damping of structural elements. 372. https://search.worldcat.org/title/31754445

Sun, D., Sun, G., Zhu, X., Ye, F., & Xu, J. (2018). Intrinsic temperature sensitive self-healing character of asphalt binders based on molecular dynamics simulations. Fuel, 211, 609–620. https://doi.org/10.1016/J.FUEL.2017.09.089

Takeda, N. (2002). Characterization of microscopic damage in composite laminates and real-time monitoring by embedded optical fiber sensors. International Journal of Fatigue, 24(2–4), 281–289. https://doi.org/10.1016/S0142-1123(01)00083-4

Tan, W. C. K., Kiew, J. C., Siow, K. Y., Sim, Z. R., Poh, H. S., & Taufiq, M. D. (2008). Self Healing of Epoxy Composite for Aircraft's Structural Applications. Solid State Phenomena, 136, 39–44. https://doi.org/10.4028/WWW.SCIENTIFIC.NET/SSP.136.39

Tan, Y., Wu, G., Suh, S. S., Yang, J. M., & Hahn, H. T. (2008). Damage tolerance and durability of selectively stitched stiffened composite structures. International Journal of Fatigue, 30(3), 483–492. https://doi.org/10.1016/J.IJFATIGUE.2007.04.008

Teoh, S. H., Chia, H. Y., Lee, M. S., Nasyitah, A. J. N., Luqman, H. B. S. M., Nurhidayah, S., & Tan, W. C. K. (2012). Self Healing Composite for Aircraft's Structural Application, 24(1–2), 157–163. https://doi.org/10.1142/S0217979210064083

Therriault, D., White, S. R., & Lewis, J. A. (2003). Chaotic mixing in three-dimensional microvascular networks fabricated by direct-write assembly. Nature Materials, 2(4), 265–271. https://doi.org/10.1038/nmat863

Thostenson, E. T., & Chou, T. W. (2006). Carbon Nanotube Networks: Sensing of Distributed Strain and Damage for Life Prediction and Self Healing. Advanced Materials, 18(21), 2837–2841. https://doi.org/10.1002/ADMA.200600977

Toohey, K. S., Sottos, N. R., Lewis, J. A., Moore, J. S., & White, S. R. (2007). Self-healing materials with microvascular networks. Nature Materials 2007 6:8, 6(8), 581–585. https://doi.org/10.1038/nmat1934

Trask, R. S., & Bond, I. P. (2006). Biomimetic self-healing of advanced composite structures using hollow glass fibres. Smart Materials and Structures, 15(3), 704. https://doi.org/10.1088/0964-1726/15/3/005

Trask, R. S., & Bond, I. P. (2010). Bioinspired engineering study of Plantae vascules for self-healing composite structures. Journal of The Royal Society Interface, 7(47), 921–931. https://doi.org/10.1098/RSIF.2009.0420

Trask, R. S., Williams, H. R., & Bond, I. P. (2007). Self-healing polymer composites: mimicking nature to enhance performance. Bioinspiration & Biomimetics, 2(1). https://doi.org/10.1088/1748-3182/2/1/P01

Trilaksono, A., Watanabe, N., Kondo, A., Hoshi, H., & Iwahori, Y. (2014). Automatic Damage Detection and Monitoring of a Stitch Laminate System Using a Fiber Bragg Grating Strain Sensor. Open Journal of Composite Materials, 04(01), 47–60. https://doi.org/10.4236/OJCM.2014.41006

Vacuum Systems for Composite Manufacturing. (anonymous 3). Retrieved 7 September 2023, from https://vacaero.com/information-resources/vac-aero-training/180484-vacuum-systems-for-composite-manufacturing.html.

Vaiyapuri, R., Greenland, B. W., Colquhoun, H. M., Elliott, J. M., & Hayes, W. (2013). Molecular recognition between functionalized gold nanoparticles and healable, supramolecular polymer blends – a route to property enhancement. Polymer Chemistry, 4(18), 4902–4909. https://doi.org/10.1039/C3PY00086A

Van Tittelboom, K., De Belie, N., Van Loo, D., & Jacobs, P. (2011). Self-healing efficiency of cementitious materials containing tubular capsules filled with healing agent. Cement and Concrete Composites, 33(4), 497–505. https://doi.org/10.1016/J.CEMCONCOMP.2011.01.004

Wang, H., Ogin, S. L., Thorne, A. M., & Reed, G. T. (2006). Interaction between optical fibre sensors and matrix cracks in cross-ply GFRP laminates. Part 2: Crack detection. Composites Science and Technology, 66(13), 2367–2378. https://doi.org/10.1016/J.COMPSCITECH.2005.10.021

Wang, Y., Mohamed, O., Dunn, K., Sui, T., Bashir, M., Cooper, P., Lukenskas, A., Wu, G., & Gorley, M. (2021). Effects of stress triaxiality and strain rate on the fracture of a CuCrZr alloy. Journal of Nuclear Materials, 543, 152546. https://doi.org/10.1016/J.JNUCMAT.2020.152546

Wang, Y., Pham, D. T., & Ji, C. (2015). Self-healing composites: A review. Cogent Engineering, 2(1), 1075686. https://doi.org/10.1080/23311916.2015.1075686

White, S. R., Sottos, N. R., Geubelle, P. H., Moore, J. S., Kessler, M. R., Sriram, S. R., Brown, E. N., & Viswanathan, S. (2001). Autonomic healing of polymer composites. Nature 2001 409:6822, 409(6822), 794–797. https://doi.org/10.1038/35057232

Williams, G., Trask, R., & Bond, I. (2007). A self-healing carbon fibre reinforced polymer for aerospace applications. Composites Part A: Applied Science and Manufacturing, 38(6), 1525–1532. https://doi.org/10.1016/J.COMPOSITESA.2007.01.013

Williams, H. R., Trask, R. S., & Bond, I. P. (2007). Self-healing composite sandwich structures. Smart Materials and Structures, 16(4), 1198. https://doi.org/10.1088/0964-1726/16/4/031

Williams, J. G., & Pavan, A. (2000). Fracture of polymers, composites, and adhesives. Elsevier Science B.V.

Wool, R. P. (1980). Crack healing in semicrystalline polymers, block copolymers and filled elastomers. Polymer Science and Technology, 12 A, 341–362. https://doi.org/10.1007/978-1-4613-3093-6_22

Wool, R. P. (2008). Self-healing materials: a review. Soft Matter, 4(3), 400–418. https://doi.org/10.1039/B711716G

Wool, R. P., & O'Connor, K. M. (1981). A theory crack healing in polymers. Journal of Applied Physics, 52(10), 5953–5963. https://doi.org/10.1063/1.328526

Wu, A. S., Coppola, A. M., Sinnott, M. J., Chou, T. W., Thostenson, E. T., Byun, J. H., & Kim, B. S. (2012). Sensing of damage and healing in three-dimensional braided composites with

vascular channels. Composites Science and Technology, 72(13), 1618–1626. https://doi.org/10.1016/J.COMPSCITECH.2012.06.012

Wu, D. Y., Meure, S., & Solomon, D. (2008). Self-healing polymeric materials: A review of recent developments. Undefined, 33(5), 479–522. https://doi.org/10.1016/J.PROGPOLYMSCI.2008.02.001

Wu, W., Deconinck, A., & Lewis, J. A. (2011). Omnidirectional Printing of 3D Microvascular Networks. Advanced Materials, 23(24), H178–H183. https://doi.org/10.1002/ADMA.201004625

Wu, X. F., Rahman, A., Zhou, Z., Pelot, D. D., Sinha-Ray, S., Chen, B., Payne, S., & Yarin, A. L. (2013). Electrospinning core-shell nanofibers for interfacial toughening and self-healing of carbon-fiber/epoxy composites. Journal of Applied Polymer Science, 129(3), 1383–1393. https://doi.org/10.1002/APP.38838

Xue, C., Li, W., Li, J., Tam, V. W. Y., & Ye, G. (2019). A review study on encapsulation-based self-healing for cementitious materials. Structural Concrete, 20(1), 198–212. https://doi.org/10.1002/SUCO.201800177

Yang, Q., Wang, P., Zhao, C., Wang, W., Yang, J., & Liu, Q. (2017). Light-Switchable Self-Healing Hydrogel Based on Host–Guest Macro-Crosslinking. Macromolecular Rapid Communications, 38(6), 1600741. https://doi.org/10.1002/MARC.201600741

Youngblood, J. P., & Sottos, N. R. (2008). Bioinspired Materials for Self-Cleaning and Self-Healing. MRS Bulletin, 33(8), 732–741. https://doi.org/10.1557/MRS2008.158

Zainuddin, S., Arefin, T., Fahim, A., Hosur, M. V., Tyson, J. D., Kumar, A., Trovillion, J., & Jeelani, S. (2014). Recovery and improvement in low-velocity impact properties of e-glass/epoxy composites through novel self-healing technique. Composite Structures, 108(1), 277–286. https://doi.org/10.1016/J.COMPSTRUCT.2013.09.023

Zechel, S., Geitner, R., Abend, M., Siegmann, M., Enke, M., Kuhl, N., Klein, M., Vitz, J., Gräfe, S., & Dietzek, B. (2017). Intrinsic self-healing polymers with a high E-modulus based on dynamic reversible urea bonds, NPG Asia Materials, 9 (2017) e420. https://doi.org/10.1038/am.2017.125

Zhao, Y., Zhang, W., Liao, L. P., Wang, H. M., & Li, W. J. (2011). The self-healing composite anticorrosion coating. Physics Procedia, 18, 216–221. https://doi.org/10.1016/J.PHPRO.2011.06.084

Zhu, D. Y., Rong, M. Z., & Zhang, M. Q. (2013). Preparation and characterization of multilayered microcapsule-like microreactor for self-healing polymers. Polymer, 54(16), 4227–4236. https://doi.org/10.1016/J.POLYMER.2013.06.014

Zhu, D. Y., Rong, M. Z., & Zhang, M. Q. (2015). Self-healing polymeric materials based on microencapsulated healing agents: From design to preparation. Progress in Polymer Science, 49–50, 175–220. https://doi.org/10.1016/J.PROGPOLYMSCI.2015.07.002

CURRICCULUM VIATE

Eray KOŞTUR